1-1-2013

Creation of a Computational Simulation of Maternal Trauma in Motor Vehicle Accident

Benjamin C. Weed

Creation of a computational simulation of maternal trauma in motor vehicle accident

By

Benjamin C. Weed

A Dissertation
Submitted to the Faculty of
Mississippi State University
in Partial Fulfillment of the Requirements
for the Degree of Doctor of Philosophy
in Biomedical Engineering
in the Department of Agricultural and Biological Engineering

Mississippi State, Mississippi

May 2013

Creation of a computational simulation of maternal trauma in motor vehicle accident

By

Benjamin C. Weed

Approved:

Jun Liao Assistant Professor of Agricultural and Biological Engineering Committee Chair	Lakiesha N. Williams Assistant Professor of Agricultural and Biological Engineering Committee Member
Steven H. Elder Professor and Graduate Coordinator of Biomedical Engineering Committee Member	Raj Prahbu Assistant Research Professor of Agricultural and Biological Engineering Committee Member
David Christiansen Assistant Clinical Professor of Pathobiology/Population Medicine Committee Member	Sarah A. Rajala Dean of the Bagley College of Engineering

Name: Benjamin C. Weed

Date of Degree: May 10, 2013

Institution: Mississippi State University

Major Field: Biomedical Engineering

Major Professor: Jun Liao

Title of Study: Creation of a computational simulation of maternal trauma in motor vehicle accident

Pages in Study: 146

Candidate for Degree of Doctor of Philosophy

Maternal trauma is the leading non-obstetric cause of maternal and fetal death. Because the anatomy of a pregnancy is distinct, and highly transient, the pregnant woman and her fetus are both susceptible to injuries which are not seen in the typical trauma patient. The pregnant uterus, the placenta, and the fetus are all relatively poorly supported, as compared with non-transient abdominal or thoracic organs, which can lead to injuries such as uterine rupture, placental abruption, and fetal trauma or death.

The leading cause of maternal trauma is automotive collision, and other common causes include violence, falls, and other accidents. Automotive collision is often researched with more traditional physical experiments such as post-mortem crash testing, but this form of study is exceedingly difficult with the pregnant subject due to ethical and logistical issues. Computational simulations of automotive collisions have received much attention as a method of performing experiments without the use of physical specimens, and have been successful in modeling trauma. These simulations benefit from constitutive relationships which effectively describe the biomechanical and structural behaviors of biological tissues. Internal state variable models driven by microstructural

data offer the potential for capturing a myriad of material behaviors intrinsic to many biological tissues.

The studies presented include many advances in the existing research of maternal trauma. These studies include advanced biomechanical and microstructural characterization of the placenta, the organ commonly injured in maternal trauma, to capture stress state and strain rate dependencies, as well as microstructural evolution across stress states. The studies also describe the construction of a finite element mesh of a near-term pregnant woman and fetus from medical images. This finite element mesh was implemented in a simulation of maternal trauma based on one of the only post mortem studies of pregnant cadavers ever reported in the literature. The results are a significant advancement for trauma simulation research.

DEDICATION

I dedicate this work to my family, friends, teachers, coaches, band directors, counselors, scoutmasters, professors, and anyone else who ever gave their time to give me a better opportunity. I could have never achieved anything without your support.

ACKNOWLEDGEMENTS

I would like to acknowledge the contributions of my committee: Jun Liao, Raj Prabhu, Lakiesha Williams, Steve Elder, David Christiansen, and the Mississippi State Agricultural and Biological Engineering Department and its faculty, the Labor and Delivery department at Oktibbeha County Hospital, the College of Veterinary Medicine, The Center for Advanced Vehicular Systems, The Electron Microscope Center, Bill Monroe, Amanda Lawrence, Giselle Thibedeau, Peter Ryan, Mark Horstemeyer, Ali Borazjani, Sourav Patnaik, Ryan Gilbrech, Scott Metzler, Robbin Bertucci, Bryn Brazile,

TABLE OF CONTENTS

LIST OF TABLES

LIST OF FIGURES

CHAPTER I

INTRODUCTION

Overview

Maternal trauma is a serious source of mortality and morbidity for both pregnant mothers, and their fetuses. Maternal trauma occurs through several modes: accidents such as falls, violence, and most frequently automotive. The most common pathologies are placental abruption, where the placenta is prematurely separated from the uterus, fetal skeletal injuries, which can include fractures of the neck and skull, and fetal organ injuries, such as brain damage and injury to abdominal organs. Maternal trauma is relatively difficult to study due to ethical and logistical issues inherent to obtaining samples and performing experiments. Computational methods, such as finite element simulations, are very promising for simulating maternal trauma. Such computational tools require certain major components to perform: geometry to represent the simulated system, material data for the simulated materials, and loading conditions to drive the simulation. The goal for this study was to contribute to the state of the art in each of these major areas. There is a need for study of mechanical data concerning tissues of pregnancy, including placenta which is highly related to abruption. Placenta had previously only been evaluated in tension, and there was a clear need for study of the stress state dependency of placenta to add understanding of shear and compressive mechanical responses in this tissue. Furthermore, internal state variable modeling

techniques, particularly those driven by damage correlated structure property relationships, have shown great promise in modeling properties such as stress state and strain rate sensitivities, damage, and other complex phenomena. There has been great success in implementing realistic geometries in human modeling by translating medical images to anatomically accurate models. To our knowledge, there has not been a publish model of maternal trauma which uses an anatomically derived model. Our model was derived from an MRI scan of a 36 week pregnancy, and includes the majority of relevant anatomy. Our simulation is based on acceleration profiles from a post mortem crash experiment where 3 pregnant post mortem subjects were evaluated under 20 kilometer per hour crashes and acceleration data for fetal and maternal anatomical features was recorded. This data was used to derive velocity boundary conditions for implementation in our chosen finite element software, Abaqus 6.10-2. Abaqus simulations were carried out by applying an initial predefined velocity field of 20 kilometers per hour, followed by our derived velocity boundary condition, which slowed and reversed our model as though the body was coming to rest and recoiling. Our simulations showed the viability of two different implementations of the derived velocities, and a mesh refinement study for 3 different levels of element size.

Specific Aim 1- Stress State and Strain Rate Dependence of the Human Placenta

The first aim of this study is to characterize material properties of human placenta more thoroughly than the current available literature. The goals for the biomechanical study of placenta will include the understanding of failure mechanics, structure-property relationships, stress state dependency, strain rate dependency, and sub-failure mechanical performance. Experiments will include mechanical tests in uniaxial tension, uniaxial

compression, and simple shear to fully understand the effects of multi-axial loading in placenta. These three testing modes will each be evaluated at three different strain-rates to simultaneously evaluate the stress-state dependency and strain-rate dependency of human placenta. There will be 9 separate loading protocols with a minimum of n=4 samples per protocol. Furthermore, we will analyze the structure property relationships related to the microstructural evolution due to external loading by conducting interruption tests of at two loading levels per stress state, as well as under no load, to fix and observe the tissue microstructure under load. These samples were be prepared through traditional histological methods including paraffin embedding, sectioning, and stained using H&E, and then observed by light microscopy. The data from mechanical tests and image analysis of micrographs will form the basis for material models to be used in computational simulations.

Specific Aim 2 – Stress-State Dependent Structure Property Relationships in Human Placenta

The second aim of this study is to evaluate the structure property relationships of human placenta based on the micrographs of interruption tests collected in Specific Aim 1, as this data can be very valuable in the creation of advanced material models. The micrographs of interrupted mechanical tests will be processed and analyzed for relevant morphological details and quantification of structure property evolution through the use of image analysis tools. Values to be quantified will target particle morphology or spacing under various loading states and will include: area, perimeter, area fraction, nearest neighbor distance, aspect ratio, major/minor axis orientation, circularity, roundness and solidity. These values will be examined, in conjunction with stress-strain

curves, to identify correlating trends and the hardening rules for microstructural features. Values which correlate well to stress-strain trends will be identified and selected for future incorporation to internal state variable (ISV) models based on structure property data. Constitutive relationships based on these structure-property relationships will have the potential to include damage, failure, strain rate and stress state dependencies. Similar approaches to material modeling have been successful in several metal alloy studies, and recently liver and brain have been modeled using an ISV template. The ultimate goal of this study will be the use of its data in this modeling template, to create a powerful and valuable tool for use in simulation.

Specific Aim 3 – Anatomically Derived Simulation of Maternal Trauma in Motor Vehicle Accident

The third aim of this study was to create and evaluate a computational simulation for the study of maternal trauma. This simulation was based on finite element analysis of an Maternal trauma is a serious source of mortality and morbidity for both pregnant mothers, and their fetuses. Maternal trauma occurs through several modes: accidents such as falls, violence, and most frequently automotive. The most common pathologies are placental abruption, where the placenta is prematurely separated from the uterus, fetal skeletal injuries, which can include fractures of the neck and skull, and fetal organ injuries, such as brain damage and injury to abdominal organs. Maternal trauma is relatively difficult to study due to ethical and logistical issues inherent to obtaining samples and performing experiments. Computational methods, such as finite element simulations, are very promising for simulating maternal trauma. Such computational tools require certain major components to perform: geometry to represent the simulated

system, material data for the simulated materials, and loading conditions to drive the simulation. The goal for this study was to contribute to the state of the art in each of these major areas. There is a need for study of mechanical data concerning tissues of pregnancy, including placenta which is highly related to abruption. Placenta had previously only been evaluated in tension, and there was a clear need for study of the stress state dependency of placenta to add understanding of shear and compressive mechanical responses in this tissue. Furthermore, internal state variable modeling techniques, particularly those driven by damage correlated structure property relationships, have shown great promise in modeling properties such as stress state and strain rate sensitivities, damage, and other complex phenomena. There has been great success in implementing realistic geometries in human modeling by translating medical images to anatomically accurate models. To our knowledge, there has not been a publish model of maternal trauma which uses an anatomically derived model. Our model was derived from an MRI scan of a 36 week pregnancy, and includes the majority of relevant anatomy. Our simulation is based on acceleration profiles from a post mortem crash experiment where 3 pregnant post mortem subjects were evaluated under 20 kilometer per hour crashes and acceleration data for fetal and maternal anatomical features was recorded. This data was used to derive velocity boundary conditions for implementation in our chosen finite element software, Abaqus 6.10-2. Abaqus simulations were carried out by applying an initial predefined velocity field of 20 kilometers per hour, followed by our derived velocity boundary condition, which slowed and reversed our model as though the body was coming to rest and recoiling. Our simulations showed the viability of two

different implementations of the derived velocities, and a mesh refinement study for 3 different levels of element size.

Background

Maternal trauma in car crash is a significant source of injury, morbidity, and mortality for both mothers and fetuses. Motor vehicle related mortality in pregnant women is highest in USA and account annually for about 93,000 cases [1]. Additionally, the number of fetal deaths since four decades has increased as much as seven time the mortality of infant deaths [2]. The primary maternal pathology associated with maternal trauma is placental abruption where the placenta detaches, partially or completely, from the uterus. This results in serious complications such as hemorrhaging and termination of pregnancy. The stability of the pregnancy and the successful transfer of nutrients from the mother to the fetus can also be affected, even under minor levels of abruption. Beyond the placental aspects of trauma, the fetus can also be directly injured. These injuries frequently result in death, and have been associated with cognitive and developmental deficits in surviving individuals.

Maternal trauma is difficult to study with traditional experiments, because of many logistical and ethical issues. A very small number of studies have succeeded in using post mortem subjects to create some very valuable data sets, but the availability of pregnant human cadaveric subjects or tissues is very low or negligible. There is also not a suitable animal surrogate for use in these studies as only primates are even remotely similar for crash testing, and chimpanzee research in automotive collisions was ceased during the 1970s due to ethical concerns balanced against the relatively poor scientific value caused by anatomical differences.

Computational simulations have shown great promise in recreating biological experiments *in silico* without physical specimens, through the use of finite element simulations. Finite element simulations of trauma has been studied in various tissues and organ systems, including brain, liver, and pregnancy. These simulations are based on constitutive relationships which must capture the mechanical properties of these biological materials. The material properties can display very complex mechanical behavior, include simultaneous occurrence of complex phenomena such as hyperelasticity, viscoelasticity, stress state dependency, damage accumulation, anisotropy, and other ultrastructural effects, all while sustaining extremely large deformations. The creation of material models capable of capturing such trends requires appropriate experimental data and analysis, before mathematical incorporation in the constitutive relationships. In addition to material properties, finite element analysis requires three-dimensional geometric meshes which are deformed during simulations. These geometries can be created using traditional tools for three-dimensional design such as computer aided design tools, which are essentially basic approximations. It has recently become more common to use meshes derived from real anatomy, through the use of meshing tools which convert scans from medical imaging technologies such as MRI or CT scanning into three-dimensional meshes for direct use in finite element software packages. The final major component required for a finite element simulation is the set of loading conditions which will drive the simulation. This study will endeavor to create a computational simulation of maternal trauma based on medical image derived anatomical meshes, and material models based on advanced mechanical testing.

Maternal Trauma (MT) affects 5-8% of all pregnancies and is the leading non-obstetric cause of maternal death in the United States [3-7]. It is also a source of serious injury and mortality for the unborn fetus with many life-long consequences caused by both explicit trauma and emergency preterm delivery.[4, 8-11] The most common cause of trauma is automotive collisions, with other major causes including violence and falls [4, 10, 12, 13]. Pregnant drivers involved in vehicular collision can suffer from abruptio placentae [14-19], placental separation [20], uterine contraction[21], uterine rupture [16, 22, 23], abdominal pain or injuries [18, 24, 25], preterm labor [15, 18, 26], pelvic fracture [27], fetomaternal hemorrhage [16, 28, 29], vaginal bleeding, maternal tachycardia [18], "seat belt" injury [29], chest injury, head injury [18], extremity injury, etc. Other complications include preterm delivery [14, 18], increased risk of fetal hypoxia [30], fetal skull fracture [31], fetal prematurity [15, 30], abnormal fetal heart beat or rate [18, 21], lower fetal weight [7, 30], fetal growth restriction [15] etc. Risk factors such as improper restraints or no seat belt use [7, 14, 32-38], vehicular speed of more than 30 mph [14, 21] and absence of airbags [1, 35, 39, 40], are few of the several reasons for the cause the pathologies mentioned above. The most commonly associated pathology is abruptio placentae (AP), detachment of the placenta from uterus.[7, 41, 42] AP affects approximately 1% of all pregnancies, and leads to hemorrhaging and reduction of blood flow to the fetus, as well as maternal complications including disseminated intravascular coagulation and renal failure.[4, 41, 43, 44] automotive collisions during pregnancy are particularly troubling to the clinician, because it is difficult to predict the outcome for the mother and fetus, and therefore are difficult to effectively treat.[4, 6, 10, 11, 45] automotive collisions can also cause additional less common pathologies not associated

with AP such as amniotic fluid embolism, uterine rupture, maternal or fetal fractures, and other traumatic fetal injuries.[4, 9, 31, 46-48] Despite these issues, there has been relatively little research conduted to investigate maternal trauma in automotive collisions or other traumatic events. Some groups have evaluated the epidemiological side of maternal trauma, elucidating many interesting trends and increasing our awareness of this problem [4, 10, 12]. Recently, groups have used computational simulations to study trauma, including maternal trauma [49, 50]. Research has included experimental studies to evaluate real-world loading conditions and evaluation of tissue material properties [51-56].

Anatomy of Maternal Trauma

The placenta is a transient vascular organ that develops during pregnancy [41, 43, 44]. It attaches by microvilli to the uterine decidua and acts, along with the umbilicus, as a nutritional and respiratory conduit between the mother and fetus. During pregnancy the uterus increases greatly in size and the placenta and membranes form to protect and nourish the fetus.

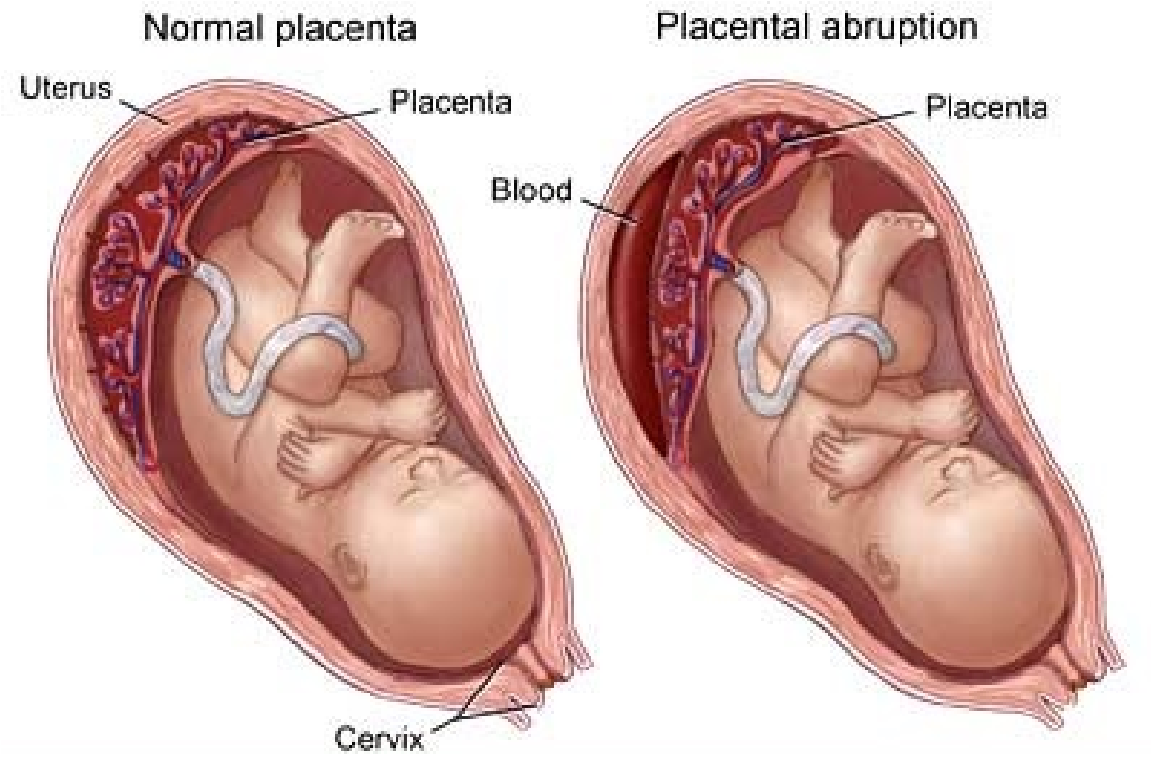

Figure 1 Anatomical diagram of placental abruption

The placenta is attached to the inner surface uterus and does not receive direct support from any boney or ligamentous tissues. This presents an interesting anatomical situation when it comes to trauma. The transient organs of pregnancy, in particular the utero-placental junction is not well supported or protected particularly susceptible to separation, or placental abruption[46, 52]. Figure 1 shows the pregnant uterus and indicates a common type of placental abruption. This separation can occur due to physiological complications such as chemical or molecular induced changes in cardiovascular tissues, or it can occur due to traumatic loading with tears the placenta away from the uterus[41, 43]. In either event, the damage is not repaired, and there is at least some loss of blood flow between the mother and fetus. Figure 2 indicates a large

clotted area in the placenta. This would not contribute blood flow to the fetus and would most likely result in fetal morbidity. If the damage is large enough this can result in termination of the pregnancy and life-threatening maternal hemorrhaging [4, 43].

Figure 2 Placenta showing infarct regions due to abruption

In addition to placental abruption, much other pathology has been reported in the literature. These include fetal fractures, such as skull and craniofacial damage [31, 57]. There is also the possibility associated traumatic brain injury and potential for central nervous system damage [48, 58, 59]. Because the fetus, similar to the placenta, is not directly supported with respect to the bones and other maternal structures, these injuries can occur even with relatively few maternal symptoms and minor trauma, often causing

delays in proper clinical interventions due to a lack of indications of fetal morbidities [58, 59].

The head and brain associated trauma is believed to be influenced by the tight fit of the head in the pelvis during the advanced stages of pregnancy, where the proximity to bony structures in the pelvis allows the skull to impact with potentially deleterious results. Even when these traumatic events do not result in fetal death, there is still a risk for lifelong complications including developmental and cognitive deficits indicative of traumatic brain injuries.

Issues Facing this Field of Research

MT is difficult to study since *in vitro* or *in vivo* testing of physical specimens carries many logistical and ethical issues. There is not a suitable animal surrogate for human trauma in automotive collision, because there is not another animal with sufficiently similar anatomy. Even apes such as chimpanzees are not believed to provide enough scientific value to this area of research to offset the ethical issues related to primate research. The availability of suitable pregnant human specimens, including tissue samples or cadavers obtained through surgeries or post-mortem subjects, is extremely limited. Despite these difficulties, it is important to have methods for understanding maternal trauma to provide clinicians and scientists with better information about how these pathologies occur, and to allow manufacturers of automotive safety equipment to create safer restraints for pregnant passengers [8, 52]. Computational simulations have been used with great promise in traumatic injury prediction, especially in traumatic brain injury which is a potentially serious outcome in almost all automotive collisions, as well as sports and other common trauma modalities such as accident and violence [60-66].

Previous finite element simulations of pregnant patients has shown promise in helping to understand the complex injury mechanisms involved in maternal injuries (Figure 3) including a validation of the advice that pregnant women and their unborn fetus are safer while wearing a seat belt, which is often disputed among the lay community due to a belief that the seatbelt poses a greater danger to the fetus [49-51, 67, 68].

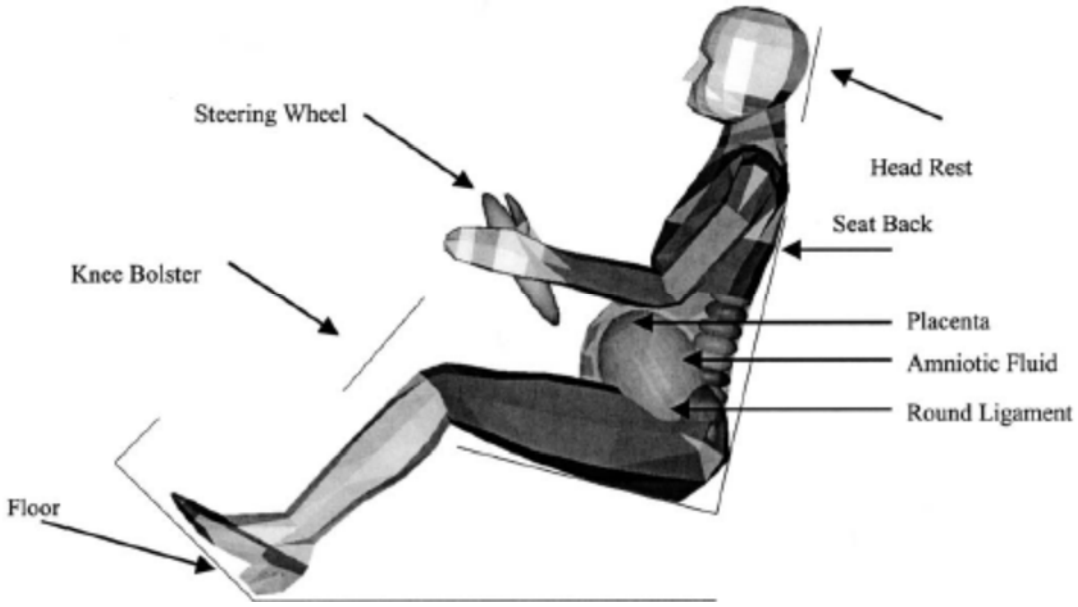

Figure 3 Simulation of maternal vehicular collision by Moorcroft et al. (2003)

Finite element simulations such as these generally require three major components: a three-dimensional mesh representing the system to be simulated, the constitutive relationships which describe the material behaviors which occur within the simulation, and a means of recreating real world loading conditions within the simulation. The goal of this study is to advance the current state of pregnant trauma simulation by advancing the research in these simulation components. The ultimate outcome will be the

creation of a new simulation that is not only and advancement of the current standard, but also includes the framework and experimental material property data necessary for future improvements and refinements, especially as simulation and modeling technologies and techniques continue to rapidly improve.

Major Components of Study

Mechanical and Structural Characterization of Placenta

The first major area of this study was the evaluation of the biomechanical and microstructural properties of human placenta. This is a vital part in the modeling process, as the biomechanical experiments provide the data necessary to create the constitutive relationships which describe material behavior and allow finite element simulations to operate. Previous MT simulations have used material models based on tensile loading, and have accounted for the rate dependency of human placenta [49, 53, 54, 56, 68]. It has been shown in non-biological materials that the loading state and strain rate can affect the material properties, but relatively little has been done in the biological world to examine this phenomenon [66, 69-71]. Previous efforts in maternal trauma have not considered the stress-state dependence of tissue components, which can be a limiting factor in the accuracy of these simulations since loading is usually complicated and multi-axial [49, 53, 54, 56, 68]. Our studies into the biomechanics of human placenta included evaluation in tension, compression, and shear, each at three strain rates to simultaneously assess the rate dependency and stress state dependency of the mechanical response. The microstructural characteristics of placenta were also investigated through an interrupted mechanical testing approach, where tissue samples were chemically fixed under load to capture the changes in morphology due to load. These interrupted samples were then

processed by sectioning and histological staining for light microscopy. Light micrographs were further analyzed for qualitative trends.

Modern modeling techniques allow for many complex material properties to be simultaneously recreated, allowing for realistic modeling and simulation of biological tissues at an unprecedented level of accuracy. These models have the potential to account for anisotropy, multi-axial loading, stress-state and strain-rate dependency, viscoelasticity, and other complex loading scenarios through internal state variables based on structure properties. These models offer many useful and powerful advantages over more traditional modeling approaches such as polynomial equations. These structure property models require information about way in which the microstructure of the material responds to loading. Microstructure features change under deformation and their morphology can be, and is often directly, related to the stress-strain status of the material. With regards to this sort of morphological evolution, placenta has a particularly interesting microstructure. Since it is comprised primarily of blood vessels of varying sizes, blood, and connective tissue supporting the blood vessel network, there is a considerable amount of ultra-structural detail to consider. The blood vessels are inherently random in orientation, size, and distribution. In general, larger vessels feed individual lobes, and the entire system of vessels connects to three large vessels in the umbilicus. This network of vessels accommodates a large volume of blood which shifts around by cardiovascular pumping under normal circumstances, but is highly susceptible to traumatic loading.

The micrographs obtained during our mechanical and microstructural characterization were measured with image particle analysis tools for quantitative

changes in tissue morphology. These particle derived parameters are known structure property relationships and will be used with the stress state dependent mechanical analysis to develop advanced constitutive models of placenta material behaviors. Our interruption tests showed the microstructure of placenta behaved in different ways under each of the different stress states. Compressive loading was characterized by a long shallow toe-in region, during which blood vessels compacted and fluid was pushed out of collapsing vessels. As loading increased there was an abrupt transition to stiffer material response, at which point the blood vessels had mostly collapsed and the loading was dominated by compression of compacted vascular tissue. Further studies will be necessary to determine the degree of recoverability of this type of loading, as well as the prospects of complete failure of compressive samples. In contrast, tensile loading behaved in a manner similar to many well described collagenous tissues, where a toe-in region characterized by microstructural uncrimping transitions to a linear region of tension and potential damage. There was a noticeable, but not extremely shallow toe-in region, during which the blood vessels were stretched and recruited into alignment and tension followed by a steeper linear region. The linear region was characterized by some vessel recruitment, with a shift towards smaller particles and increased void space indicative of a damaged material due to excessive tension. Shear loading was characterized by a shifting and collapse of vessels along the direction of shear followed by a load state that resembled diagonal tension at higher strains. These observations are useful in understanding the tissue behavior under load, and provide valuable insight into the material phenomena occurring in placental deformation.

Beyond qualitative observations, modern image management and analysis techniques allowed quantification of many different values with important implications for mechanical modeling [62, 66]. Blood vessel elongation and tearing, or collapse and compaction were measured from interrupted mechanical test specimens through a variety of morphological parameters derived from the grouping of pixels within an image. These parameters were then evaluated for correlations to stress-strain phenomenon and ultimately incorporated into ISV based models to effectively capture real-world material behavior. Parameters of interest included those related to spacing and distribution such as Area Fraction and Nearest Neighbor Distance, as these have been correlated to damage and weakening in liver and brain, as well as non-biological materials[62, 66, 69, 70, 72]. Other important parameters were those describing particle shape and alignment such as include aspect ratio, major axis orientation, circularity, and roundness. Parameter whose trends were correlated with mechanical data will be selected as a candidate for ISV modeling. Essentially, the phenomenological trends of one or more structure property parameters is used as a variable in one or more driving terms in a constitutive relationship. This can be advantageous over other sorts of phenomenological models because the structure properties are capable of better capturing the general internal state of a material under complex loading, while many other phenomenological models can only capture uniaxial loading. These models have been used in metal alloy research and FEA engineering studies to optimize automotive parts and other applications [70, 73-75].

As previously stated, maternal trauma is exceedingly difficult to study through direct experimentation because of logistical and ethical issues. While accurate understanding is important, there is no appropriate *in vitro* surrogate which can address

all of the important research questions. Human cadavers are difficult to obtain and will have significantly altered material properties due to post mortem effects. The use of animal surrogates is unlikely to be feasible. The anatomy of placentation differs greatly among species, perhaps more than any other organ [76]. Humans have a discoid hematochorial placenta which is found primarily in primates, and only the large primate species have anatomy that could even theoretically accommodate an automobile. Since primate research is arguably more difficult and costly than human research, this is unreasonable pursue. Other species available for research simply do not have enough anatomical similarity to warrant involvement in an automotive trauma experiment. Because of these difficulties, the prospects of computational simulation of trauma are especially promising for maternal trauma research. With relatively few physical specimens required, a plethora of questions regarding maternal and fetal injuries and susceptibility can be addressed. Previous groups have studied maternal trauma using finite element simulations. Moorcroft showed that pregnant passengers are safer and less likely to experience placental abruption while wearing a safety belt, as compared to not wearing a safety belt [49]. This study used a simplified geometry and linear elastic material properties. They also did not include a fetus, assuming the hydrodynamic forces of the amniotic fluid dominated placental loading during trauma. While the study does make considerable simplifications, it effectively validates the safety belt for pregnant occupants. Our goal was to continue this research approach using anatomically derived meshes based on medical images, and to include the fetus in our simulation to allow study of both maternal and fetal trauma.

Creation of Mesh for Finite Element Simulation

The next major aspect of this study was the creation of an advanced finite element mesh for use in simulation. The primary goal with creating this geometry was to include as much relevant anatomy as possible, and to do so in such a way that more complex anatomy or improvements to the geometry can be made in future iterations of this simulation. The ScanIP software package facilitates this by allowing for selection of desired anatomy and progressive increase of additional layers of detail and refinement. In order to ensure anatomical accuracy of our model, we obtained MRI images of a 36 week pregnancy from University of Cape Town Medical School (UCT). Images were obtained in accordance with the UCT Human Ethics and Rights Committee, which is substantially similar to our IRB. Existing image data from pregnant MRIs were reviewed by gynecological clinicians, and images from late-term pregnancies with little or no pathologies were sanitized of all identifying information. Images were then transferred to MSU facilities to be processed and incorporated into an FEA mesh. Scans consisted of 38 slices obtained at 4mm spacing. These scans (see Figure 4 for select slices) included all major abdominal anatomy from navel to spine and from the lower ribcage to the pelvis.

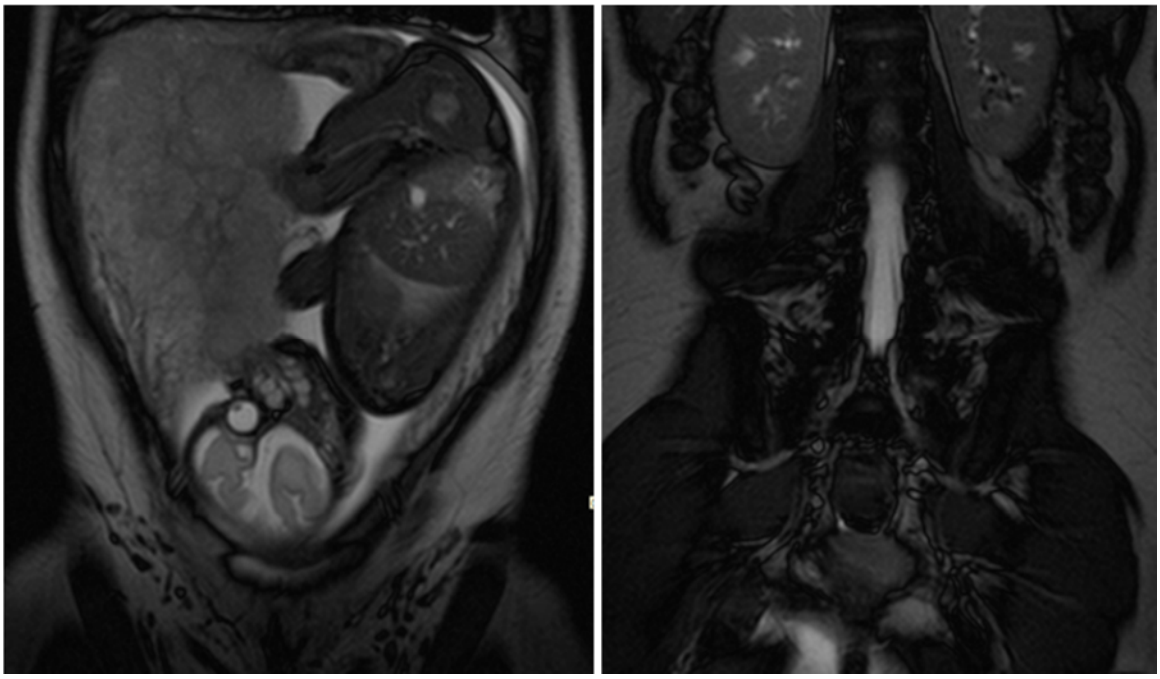

Figure 4 MRI images from 36 week pregnancy

Once obtained, meshes were assembled using the ScanIP software suite (SimpleWare, UK). ScanIP allows the user to select relevant anatomical features from 2-dimensional images obtained in a serial stack, and then project those images into a 3-dimensional mask which can be imported into different CAD programs, or meshed and imported into FEA programs. MRIs were reviewed and processed to indicate important anatomical features including skin, muscle, uterus, placenta, umbilicus, fetus, bones, and spinal cord. Each image slice was manually traced for these anatomical features forming a set of masters from which further processing necessary for mesh refinement could be completed. Three dimensional representations of these two dimensional tracings are shown in Figure 5.

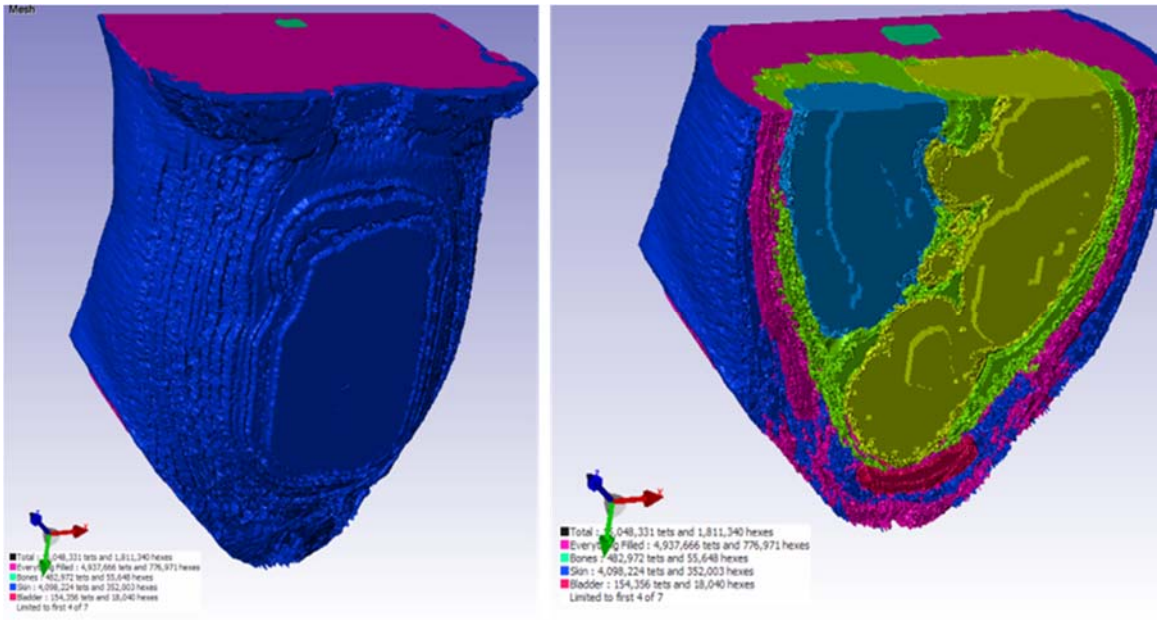

Figure 5 Mask geometry of pregnant woman created by ScanIP software suite

In order to form a mesh, ScanIP must resample available images in order to be mesh to a given approximate element size. Resampled images are again manually edited to address any artifacts related to the resampling process. ScanIP creates a mesh for export to FEA software packages. Examples of exported meshes are shown in Figure 6.

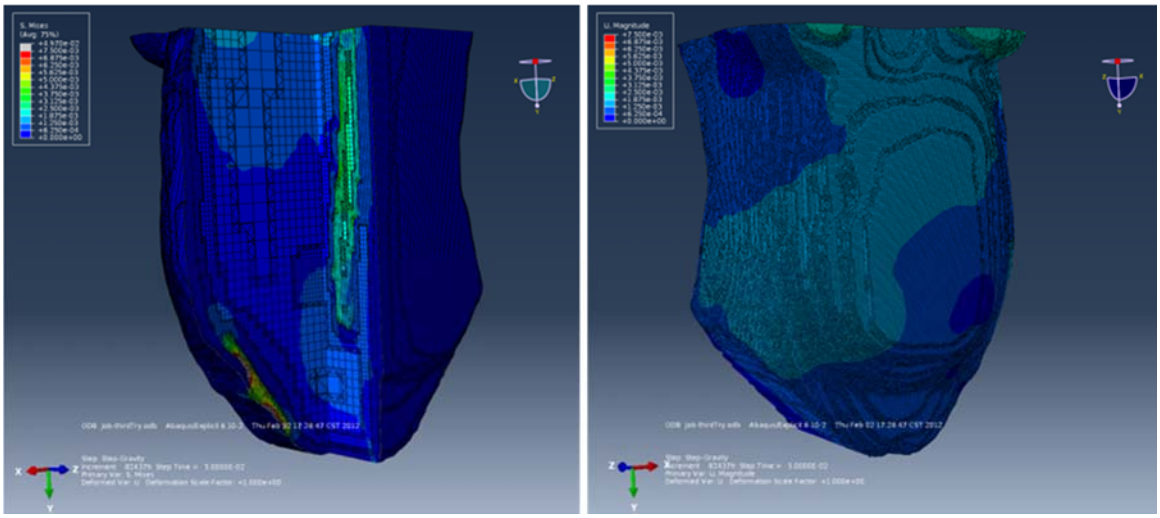

Figure 6 Finite element results from simple gravitational loading

Implementation of Post-Mortem Crash Test Subject Data

The final major component necessary for simulation was a set of loading conditions suitable for recreating trauma. A previous study used post-mortem pregnant test subjects to evaluate accelerations during a 20 kilometer per hour crash [51]. This study obtained 3 post-mortem subjects in the 3rd trimester of pregnancy. Preparation for crash testing included removal of the uterus and creation of a mold, which was then used to make a ballistics gel cast of the uterus. The uterus cast was loaded with a baby doll and water to simulate amniotic fluid and fetus. The baby doll was seeded with accelerometers at the vertex, top of the head, and the buttocks. The wing of the maternal iliac was also seeded with an accelerometer. The prepared test subject was then placed in a mid-sized automobile and crashed on a test rail at 20 km/h. The recorded acceleration profiles from these tests were published and, they form the basis for our finite element boundary conditions. Acceleration profiles from the fetal vertex and buttocks were digitized using

the DigiData profile digitization software (Thunderhead Engineering, Manhattan KS). These acceleration profiles were then kinematically integrated to their corresponding velocity profiles. These velocity profiles were normed, allowing for easy implementation in Abaqus simulations as a boundary condition with adjustable amplitude.

Finite Element Simulation Using Collected Data

The anatomically derived mesh created through Scan IP was imported into Abaqus 6.10 FEA software. The model was assigned basic material properties of linear elasticity, Poisson's Ratio, and density, and the interfaces between anatomical features were joined with a Tie Constraint, which effectively matches the interface between the surfaces so no movement or friction occurs. A predefined velocity field of twenty kilometers per hour was applied to the entire model, so as to simulate the beginning of the published crash profiles at full speed. Two sets of nodes along the front side of the abdomen were used to approximate seat belts for the implementation of velocity boundary conditions to serve as the loading criteria for these simulations. The velocity profiles previously created were applied to the seat belt regions with initial amplitude of twenty kilometers per hour. The restriction of these nodes along the front of the abdomen to a crash profile effectively recreated a front impact crash. Two different sets of velocity profiles were applied to three different levels of mesh refinement to validate the level of meshing detail in our geometry. Data was mined using a custom Python script for exporting kinematic and stress-strain data from Abaqus output databases, and then analyzed using Microsoft Excel to understand the dominant trends in material response under load, and to verify the level of detail and refinement. This analysis completed the verification that our meshing and loading conditions approach can simulate a pregnant

automotive collision. This simulation can now serve as a valuable template for studying maternal trauma, and retains the potential for improvement and additional layering of anatomical and material complexity. .

The studies that follow represent a strong basis for a computational simulation of maternal trauma in motor vehicle accident. The mechanical tests performed evaluate new and relevant material properties and provide insight not otherwise available in the literature. The stress-state dependency and microstructural information will aid future researchers in understanding the complex issue of placental abruption. The MRI derived mesh and Abaqus implementation are an excellent beginning to an extremely flexible and powerful tool for studying an otherwise inaccessible research topic. While the current implementations use simpler material properties, the model can accommodate future material models based on the structure-property data paired to the mechanical tests. This project provides the foundation for the implementation of a modern *in silico* experiment of realistic geometries, loading conditions, and material properties.

CHAPTER II

BIOMECHANICAL AND MICROSTRUCTURAL ANALYSIS OF HUMAN PLACENTA

Overview of Mechanical Testing in Maternal Trauma

To fully understand and simulate AP from MT, the mechanical properties of the pregnant uterus, the placenta, and the interface between the two need to be known. The easiest of these tissues to study, primarily for reasons related to the procurement of the tissues, is placenta. Pregnant uterus is difficult to get, and non-pregnant uteruses available following most hysterectomies are extremely different in size and morphology. Understanding the mechanical properties of the utero-placental junction may prove to be the most difficult part to understand since intact human samples are not ethically plausible. Non-human primates have similar placentation, but carry their own significant ethical barriers. Rodents may represent the best animal model for studying the utero-placental junction since they share a discoid hematochorial placenta, but they do have different physiology and bear litters which may introduce complications. Our studies focused on human placentas, which are readily available and obtained from the Oktibbeha County Hospital (Starkville, MS) in accordance with the Mississippi State University Institutional Review Board (IRB) and Institutional Biosafety Committee (IBC) policies and approvals. Previously published experimental biomechanics studies have investigated the material properties of human placentas.[53, 54, 56, 77, 78] These

studies have used tensile testing to evaluate and describe complex biomechanical properties of placentas including hyperelasticity, strain rate dependence, and viscoelasticity. To our knowledge, no study has directly investigated the effects of different loading states (tension, compression, and shear) on a human placenta although studies have shown that the mechanical behavior of biological materials might vary under different loading modes [66, 71, 79-81]. Furthermore, we do not know of any studies which evaluate the microstructure of placenta as it relates to loading or mechanical response. Our mechanical studies are supplemented with extensive histological and morphological data including histology of interrupted mechanical tests and scanning electron microscopy (SEM). This data is important in elucidating the mechanisms underlying tissue response, and can be incorporated into structure property derived constitutive relationships which offer many advantages over other phenomenological modeling methods [60, 66, 69, 70, 72, 73, 82].

In this study, we specifically investigated the mechanical behavior of human placentas under various stress states and strain rates. The stress state dependence of human placentas was evaluated by mechanical testing in the tensile, shear, and compressive loading states. Interrupted mechanical tests were also conducted and placenta microstructures were analyzed to reveal the intrinsic mechanisms of tissue behavior under different stress states. The data presented in this study will be used to develop stress-state dependent constitutive models for use in finite element simulations of pregnant females in automotive collision or other situations of interest (e.g., pregnant woman falling). A computational simulation built on thorough and accurate

microstructure characterizations will yield better predictions, provide in-depth understanding of injury mechanisms, and assist in corresponding safety designs.

Methods

Mechanical Testing

Sample Preparation

Human placentas from eleven donors were used in this study. All samples were obtained from uncomplicated singleton vaginal deliveries at Oktibbeha County Hospital in accordance with the Mississippi State University (MSU) Institutional Review Board (#08-275). Donating patients were screened for the presence of sexually transmitted diseases (including HIV, HBV, and HCV) and unclear perinatal history. Samples were placed in 4 °C Ringers lactate buffered saline (LBS) immediately after delivery and were transported immediately to MSU Biological Engineering facilities where all tests were performed in a BSL2 certified laboratory. All tests were performed within 24 hours of delivery. Note that vaginally delivered placentas were used because placentas obtained by caesarean delivery are pulled from the uterine wall and are usually already mechanically damaged by this process. Due to the size limit of the placenta tissue, we were not able to perform tests for each strain-rate and stress-state condition within a single donor. However, donor placentas were randomly assigned to loading modalities (tension, compression, and shear). Within a loading modality, there were between three and four donors, each donor placenta contributed at least one test to each strain rate.

Specimens were rinsed in LBS and dissected in preparation for mechanical testing. All samples were prepared such that each specimen was dissected from within a single placental lobe as previously described.[56, 78] This prevents issues with

underestimation of placental strength due to the thinner or weaker regions between lobes. Specimens were dissected to their appropriate shape by scalpel dissection using a guiding stencil to allow consistent shape. No specimens were frozen prior to testing since we found that the placenta tissue properties changed greatly after freezing and thaw procedures. Furthermore, it was observed that specimens quickly degraded after more than 24 hours so all tests needed to be performed as early as possible. Specimens were mechanically tested using the Mach 1 Micromechanical Testing System (Biomomentum, Laval, Quebec, Canada) shown in Figure 7A. Tension, compression, and shear mechanical tests were performed under three different strain rates to investigate the stress state dependence of placenta tissue. Each donor was tested in a single stress-state and contributed at least one test to each strain-rate. All mechanical tests were conducted in a water bath containing LBS. All tensile and compression tests included a preloading of 1 gram, preconditioning of 10 cycles, and a re-preload of 1 gram upon completion of preconditioning.

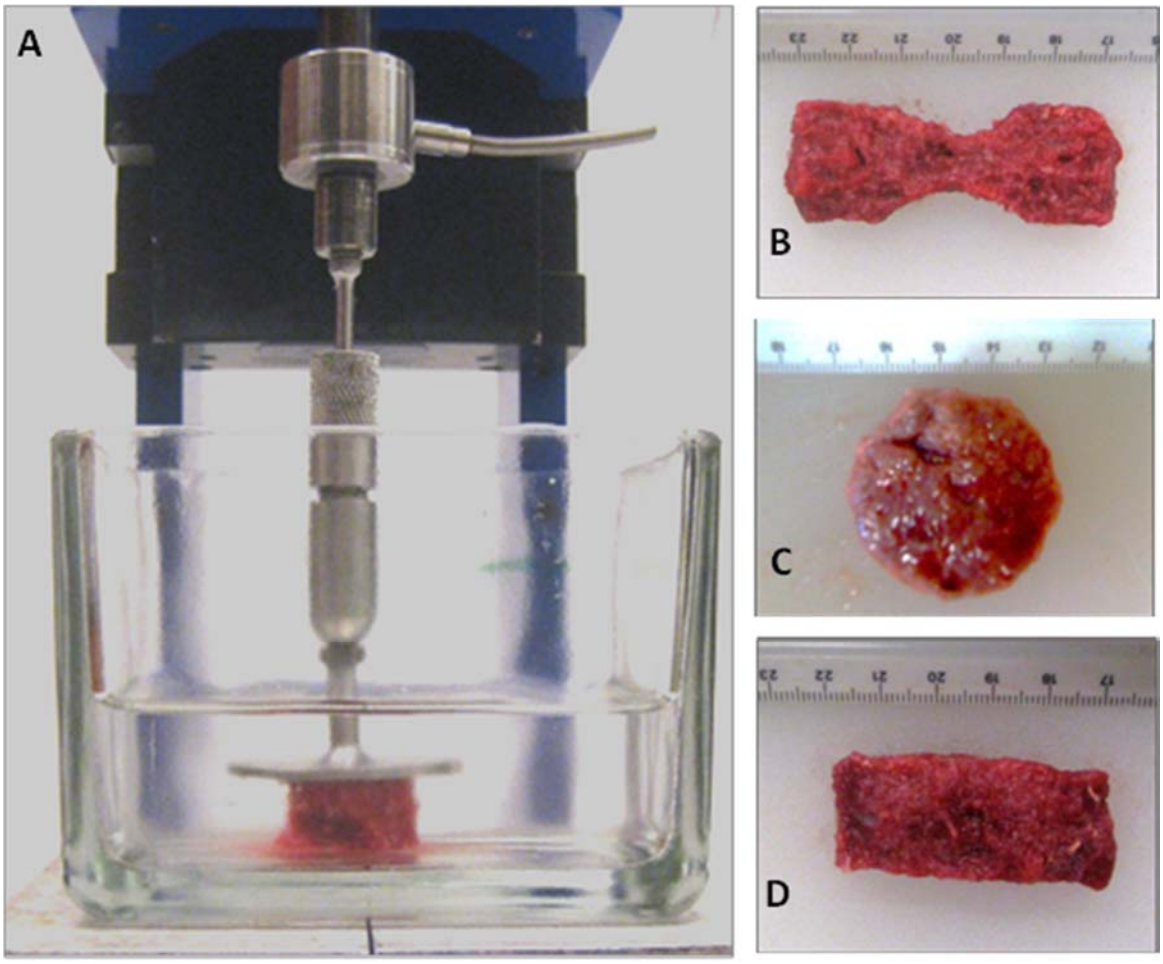

Figure 7 Mechanical Testing Configuration

Tensile Testing

Dogbone shaped samples (Figure 7B) were prepared with a grip-to-grip length of 40 mm, a width of 10 mm at the center of the dogbone, and a thickness of 5 mm. Dogbone samples were found to be necessary in achieving appropriate sample failure; rectangular samples tended to fail at the clamps. Samples were preloaded to 1 gram, subjected to 10 cycles of 5 grams preconditioning, preloaded to 1 gram, and then pulled to failure. The majority of the ends of the dogbone specimens were within the grips to

minimize distortion of strain uniformity, and all tensile specimens failed in the middle region of the dogbone indicating that the specimen shape served its intended purpose. The small amount of dogbone shape outside the clamp does limit our uniform strain state assumption, but was necessary to achieve our desired failure results. Local deformation tracking could be used to mitigate this issue in future studies. The tensile failure tests were conducted at rates of 40, 400, and 4000 μm/s (N = 4+ for each rate). In tensile testing, the displacement rates of 40, 400, and 4000 μm/s correspond to strain rates of 0.001, 0.01, and 0.1 /s, respectively.

Unconfined Compression Testing

Cylindrical samples (Figure 7C) were prepared with a grip-to-grip length of 16 mm and a radius of 19 mm. Specimens were mounted and secured with a small dot of PermaBond cyanoacrylate ester adhesive (Permabond, Pottstown PA) to prevent slipping from the compression head. The very small amount of glue did not prevent the specimens from deforming as unconfined compression. Specimens were preloaded to 1 gram, preconditioned to 15 grams for 10 cycles, re-preloaded to 1 gram, and then loaded to 3000 grams. Tests were conducted at rates of 40, 400, 4000 μm/s (N = 5+ for each rate). In compression testing, the displacement rates of 40, 400, and 4000 μm/s correspond to strain rates of 0.0025, 0.025, and 0.25 /s, respectively.

Shear Testing

Rectangular samples (Fig. 7D) were prepared to have a width of 20 mm, length of 50 mm, and thickness of 10 mm. All samples were prepared such that the shear loading aligned parallel to the uterine wall. These samples were glued to the shear test setup (two

parallel tissue mounting plates) using a minimal amount of PermaBond adhesive. Compressive load between the parallel shear loading surfaces was limited to the minimum necessary to secure the samples with glue. Samples were sheared to 100 grams in the positive and negative directions for 10 cycles. The data from the final cycles were used for analysis, as that data represents the tissue behavior after preconditioning. Tests were conducted at rates of 40, 400, 4000 μm/s (N=5+ for each rate). In shear testing, the displacement rates of 40, 400, and 4000 μm/s correspond to strain rates of 0.004, 0.04, and 0.4 /s, respectively. Data was recorded at sampling rate of 100 /s. All data was processed for further comparison using a custom software tool [66, 71].

Mechanical Data Analyses

Raw data were first analyzed by engineering stress and engineering strain in each stress state at each displacement rate. For tension and compression, the engineering stress was calculated as the loading force over the undeformed cross-sectional area, and the engineering strain was calculated as the displacement divided by the initial grip-to-grip distance (gauge length at 1 gram preload after preconditioning). The engineering stress and engineering strain were then converted to true stress and true strain using the following formulas:

$$\sigma_{true} = \sigma_{eng}(1 + \varepsilon_{eng}) \quad (1)$$

$$\varepsilon_{true} = \ln(1 + \varepsilon_{eng}) \quad (2)$$

Where σ_{eng} and ε_{eng} are the engineering stress and strain, and σ_{true} and ε_{true} are the true stress and strain, respectively. For these formulas, tensile strain is positive, and compressive strain is negative. These formulas also assume material incompressibility.

The incompressibility assumption is limiting because our test setup allows for fluid to flow in and out of the tissue, which will have major implications for compressibility. Further investigation of Poisson's ratio is necessary to better understand this property of placenta.

For shear testing, engineering shear stress was defined as the shear load over the area of contact surface, and engineering shear strain was defined as the change in shear angle (the shear plate displacement over the thickness of sample). In order to accurately compare shear data to compression and tension, an effective stress conversion, based on classical Von Mises stress definitions, was applied to shear stress and strain as follows:

$$\sigma_{true-shear} = \sigma_{12}\sqrt{3}, \quad (4)$$

$$\varepsilon_{true-shear} = \varepsilon_{12}\sqrt{3} \quad (5)$$

This modification to shear can be directly compared to principle stresses such compression and tension, as their converted Von Mises stress is unchanged.Similar to other types of soft tissues,[83, 84] the stress-strain curve of placenta tissues consists of a nonlinear region and a linear region. For each mechanical test, a linear fit was applied in the linear region of the stress-strain curve to determine the slope and x-intercept of the fitted line. The slope of this fitted line represents the tissue's tensile, compressive, or shear modulus in the linear region (large strain elastic modulus) and the x-intercept represents the tissue's extensibility.[84, 85]

Mechanical Data Results

The experimental data were organized by the stress state to assess the strain rate sensitivity of human placenta tissue (Fig. 8). We found that placenta exhibited a strain

rate sensitivity in all three loading states (tension: 0.001, 0.01, and 0.1 /s, Fig. 8A; compression: 0.0025, 0.025, and 0.25 /s, Fig. 8B; shear: 0.004, 0.04, and 0.4 /s, Fig. 8C). The larger applied strain rates incurred stiffer (higher stress) tissue responses.

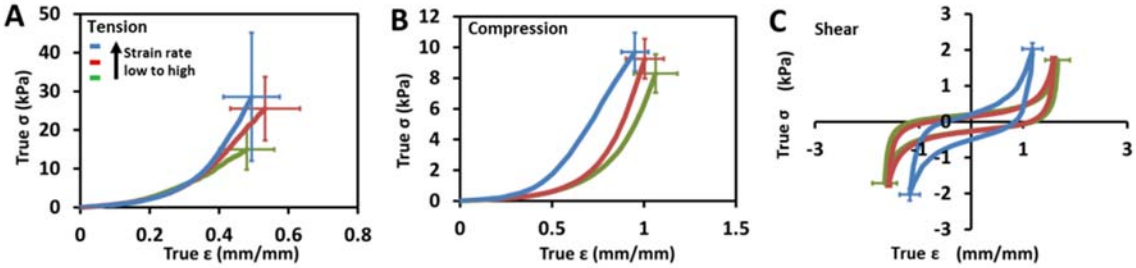

Figure 8 Strain Rate Comparison

To better assess the stress-state dependence of human placenta tissue, the experimental data were further organized by the strain rate domains**.** Significant stress state dependences were exhibited in the placenta for all the examined strain rate domains, i.e., the strain rate domains of 0.001 /s - 0.004 /s (Fig. 9A), 0.01 /s - 0.04 /s (Fig. 9B), and 0.1 /s - 0.4 /s (Fig. 9C).

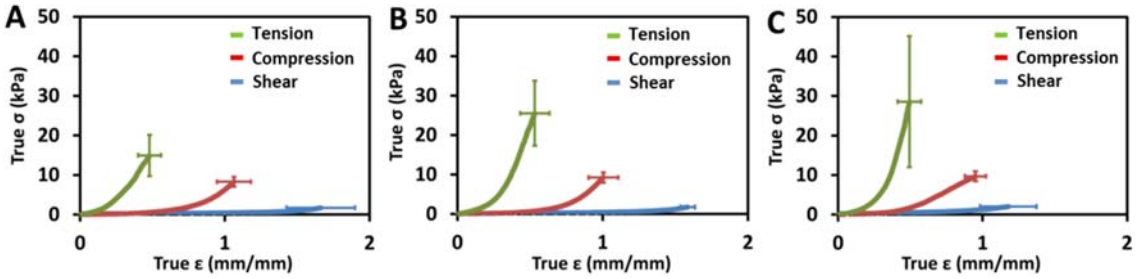

Figure 9 Stress State Comparison

The large strain modulus and extensibility of the placenta tissue were compared among different stress states at various strain rates (Fig. 10). For all three strain rates, the large strain modulus showed an increasing trend in the order of shear, compression, and tension (Fig. 10A), and the extensibility showed a decreasing trend in the order of shear, compression, and tension (Fig. 10B). It is important to note that, while total deformation of tissues was quite large in compression and shear, failures were not always observed. Because of this, the reported large strain moduli of compression and shear were possibly underestimated.

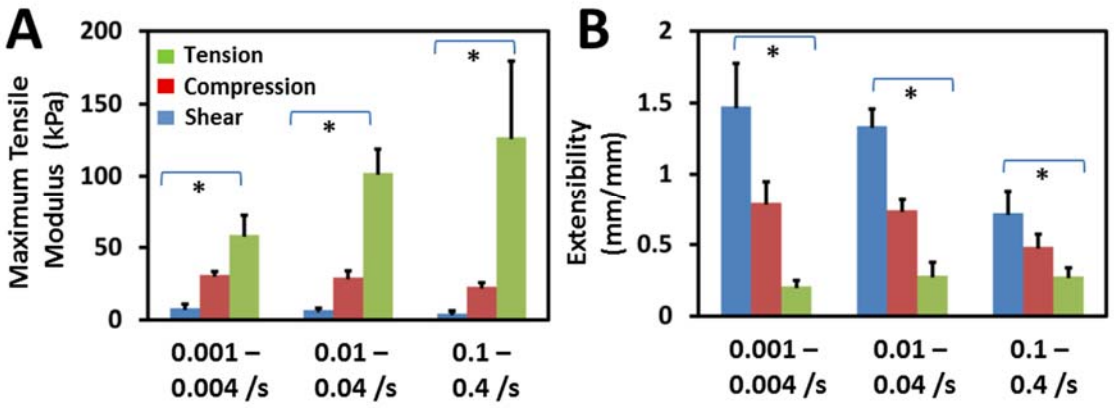

Figure 10 Stress-State and Rate Dependence of Maximum Tensile Elastic Modulus and Extensibility

Statistical Analysis

All experimental data were presented as mean ± standard deviation. One Way Analysis of Variances (ANOVA) was applied for statistical analysis (SigmaStat 3.0, SPSS Inc., Chicago, IL). Comparison among groups was considered significantly different at $p < 0.05$.

Scanning Electron Microscopy

Scanning Electron Microscopy (SEM) was performed to visualize the microstructure of placentas. Samples were prepared by common SEM preparation methods. Briefly, specimens were fixed in Karnovsky's Fixative (2% paraformaldehyde, 2.5% glutaraldehyde, in 0.1M Phosphate Buffer). Samples were further fixed in 1% osmium tetroxide and then dehydrated in a critical point dryer (Polaron E 3000 CPD). Dried samples were sputter coated with gold-palladium and observed using a Zeiss EVO 50 SEM (Zeiss, Thornwood NY) equipped with a LaB6 electron gun and secondary electron detector.

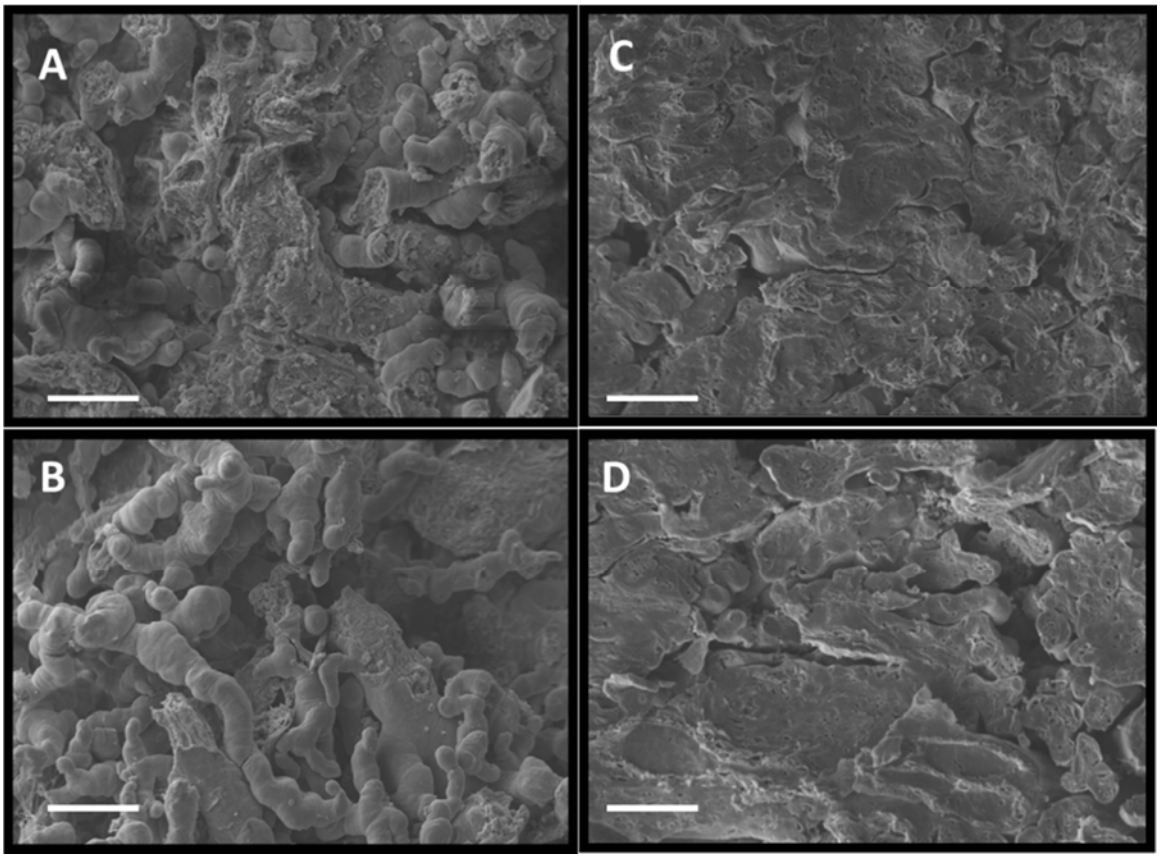

Figure 11 Scanning Electron Microscopy of Human Placenta

SEM micrographs (Fig. 11) of the human placenta showed a highly randomized size and distribution of small blood vessels. These vessels varied greatly in alignment leading to a very tortuous (Fig. 11A, B) and entangled (Fig. 11C, D) network.

Interruption Mechanical Testing and Histology

Interruption mechanical tests were performed to reveal the microstructure evolution of the placenta tissue as the applied load increased. Samples were prepared, as described earlier, for each stress state. After being mounted in the appropriate configuration for their stress state, each sample was deformed to a desired engineering strain value and held at that strain; the water bath was replaced with 10% neutral buffered formalin and the sample was allowed to fix for 24 hours. The interrupted mechanical tests were performed at two strain levels for each stress state, the first near the transitional

region (heel region) of the nonlinear stress-strain curve (22.3%, 35.7%, 39% true strain for tension, compression, and shear, respectively), and the second in the linear region of the stress-strain curve (40.5%, 91.6%, 79% true strain for tension, compression, and shear, respectively).

After fixation, samples were prepared for histology analysis. Samples were embedded in paraffin and cut into 5 μm sections. Samples were then stained with Haematoxylin & Eosin (H&E) and examined by light microscopy (Nikon EC600) to assess internal microstructure changes in response to the external loading, especially the alteration of blood vessel alignment and morphology.

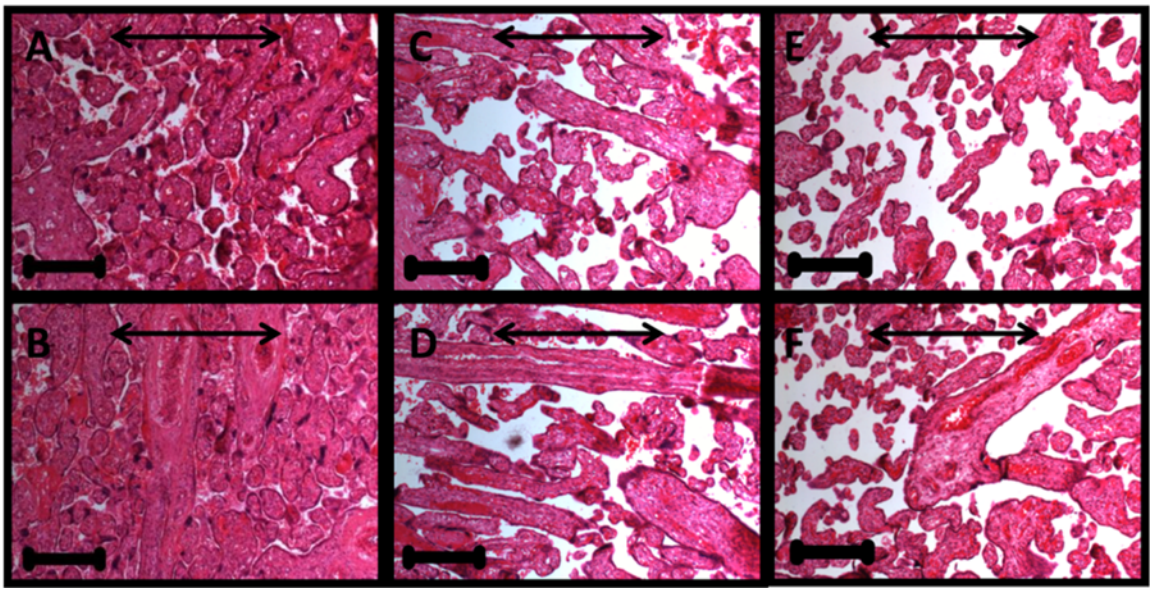

Figure 12 Histology of Interrupted Tension Tests

The interruption mechanical tests (Fig. 12, 13 and 14) showed that the human placenta tissue exhibited various microstructure behaviors in response to different loading states. The undeformed placenta consists of a relatively disordered network of blood vessels of different sizes with little or no preferred direction and the surrounding blood cells (Fig. 12A, 12B). Under tension, as the deformation increased to 22.3% true strain, the blood vessels, especially the larger vessels, were kinematically recruited into tension and align along the primary loading axis (Fig. 12C, 12D) much like texture in synthetic polymers. This motion from an initially isotropic orientation to a preferred orientation is the so-called texture effect in which the kinematics from the loading direction reorients the material (blood vessels). An increase in the appearance of intervascular spaces has also been shown (Fig. 12C, 12D). As the tensile strain neared failure at 40.5% true strain, only the largest vessels were still aligned to the direction of loading, while the smaller vessels appeared to have failed, allowing them to return to a recoiled configuration (Fig. 12E, 12F). At 40.5% true strain, the intervascular spaces further increased (Fig. 12E, 12F).

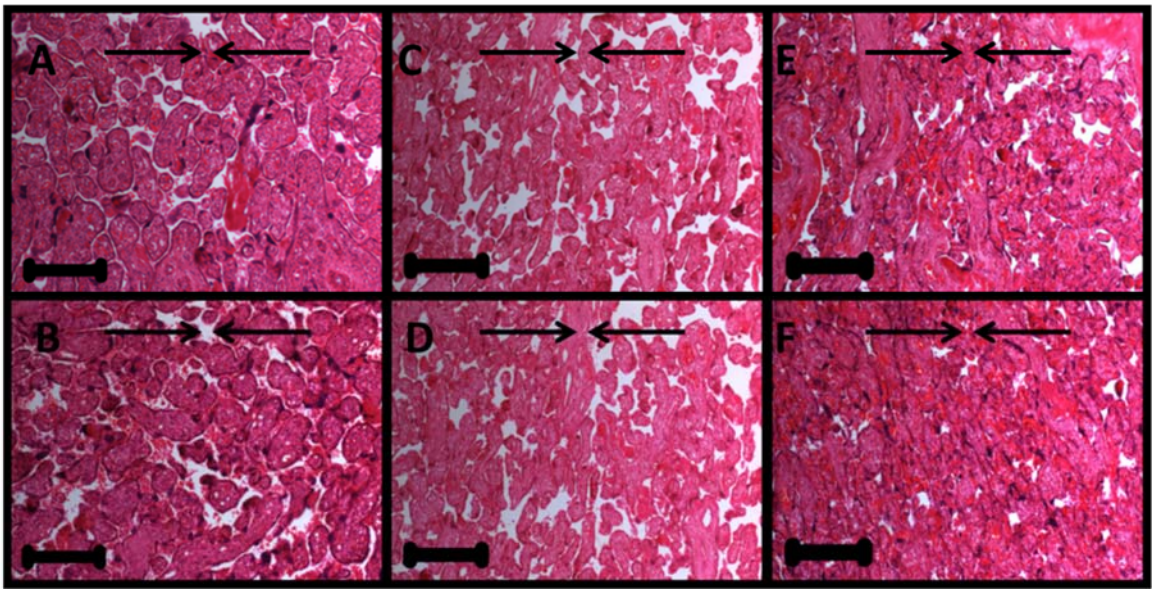

Figure 13 Histology of Interrupted Compression Tests

Placenta microstructure also showed blood vessels to have a relatively circular cross-section in the undeformed state (Fig. 13A, 13B). As the compressive strain increased to 35.7% true strain, the vessels began to collapse, with the vessel cross-sections deformed into elliptical (or elongated) shapes, and the long axes of elliptical (elongated) shapes aligned perpendicular to the loading direction (Fig. 13C, 13D), again following kinematic constraints similar to texture evolution in polymers. At 91.6% compressive true strain, the vessels were highly collapsed and elongated, as well as compacted to the point of having almost no space within or between vessels (Fig. 13E, 13F). The intervascular space was tremendously reduced at 91.6% compressive true strain.

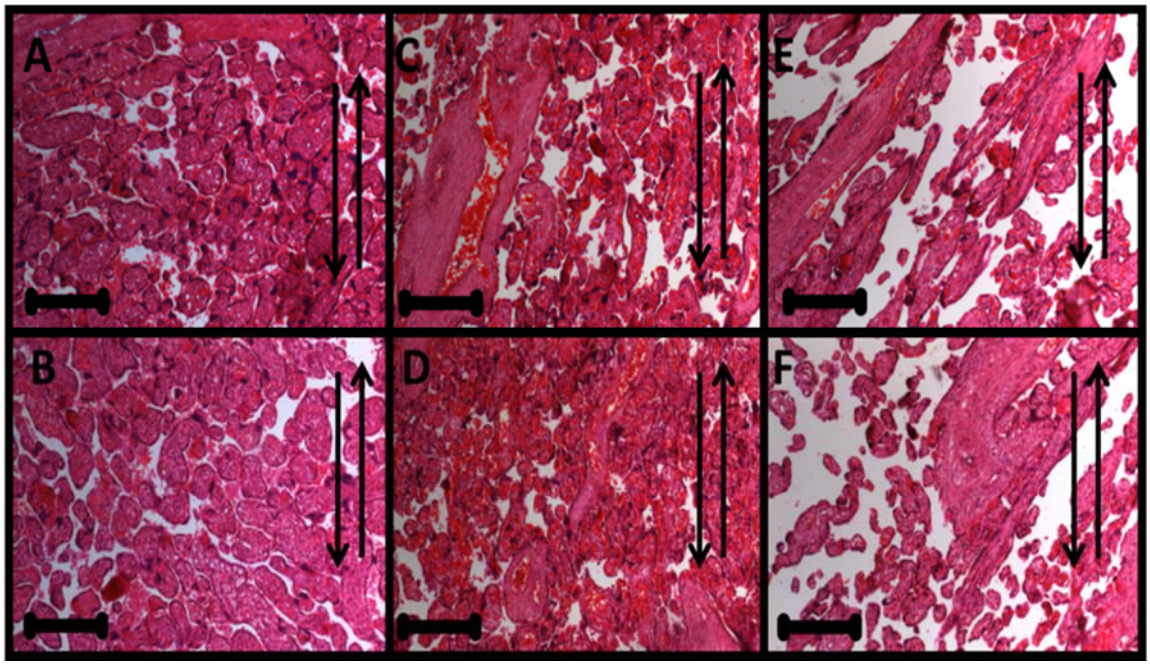

Figure 14 Histology of Interrupted Shear Testing

Microstructure evolution under shear showed a diagonal vessel alignment towards the shearing direction driven by the kinematics, as well as the presence of vessel morphologies similar to that of tensile and compressive microstructure in local regions (Fig. 14). As the shear loading increased to 39% strain, regions of vessel collapse and intervascular space growth were observed (Fig. 14C, 14D). At 79% shear strain, vessels were highly aligned along the diagonal direction of load with significantly larger intervascular spaces (Fig. 14E, 14F).

Conclusions

The data reported here indicates that the mechanical response of placenta is very different among stress states. Placenta is much stiffer in tension than in compression, and compression is much stiffer than shear. Furthermore, the strain rate dependent stiffening

of placenta was shown for all three stress states, and this behavior had only been shown in tension. These differences in mechanical response are motivated by differences in the microstructural evolution, and this manner of phenomenon had never been captured in placenta. This extends the state-of-the-art in placenta biomechanics to include the level of experimental investigation necessary for capturing certain complex effects in constitutive modeling and finite element simulation.

CHAPTER III

IMAGE DERIVED STRUCTURE PROPERTY RELATIONSHIPS OF HUMAN PLACENTA

Background

Finite element analysis is the best option for performing economical experimental analyses for many systems [86-90]. Biological systems such as disease or trauma can take extreme advantage of finite element analysis because of the cost of computation versus the cost of physical experiments which use human tissues or cadavers. This is particularly true in the case of maternal trauma, where the pregnant mother and her fetus are susceptible to injuries not possible in normal human trauma such as fetal trauma, placental abruption, and maternal hemorrhaging [91, 92], are extremely difficult to recreate or study even in physical specimens. Motor vehicle collisions accounts for almost 80% of all maternal trauma cases where the mother is susceptible to all traumas normally associated with motor vehicle collisions, as well pregnancy specific injuries. Motor vehicle collision is also the foremost reason for non-obstetric fetal death [20, 27, 93-102] with injuries potentially involving gastrointestinal, cardiovascular, pulmonary, and neurological systems [39, 92, 103]. An unfortunate fact regarding diagnosis of trauma in pregnancy is that the extent of maternal injury is not a strong indicator of fetal injury; serious fetal injuries may not be identified quickly or appropriately due to an apparent lack of maternal issues [92, 104, 105]. Further understanding of this complex

pathology is important for improving the safety of pregnant passengers, as well as the diagnosis and treatment of injuries following traumatic events in pregnancy. There is very little availability of ethically obtained late term pregnant cadavers for research, and making computational models for understanding and preventing such injuries the most promising option for studying these injuries or developing safety equipment specific to these situations.

These types of computational simulations are still relatively nascent, having many extremely complex behaviors to understand and recreate. Loading conditions in biological systems can be very complex with many multi-axial components [106-124]. Development of constitutive relationships which are capable of capturing the large number of mechanical behaviors seen in biological materials is a major area of research [125-130]. Biological materials display behaviors such as viscoelasticity and rate dependency, which are thought to be dominated by the combination of viscous fluid and elastic solid structural components [131-142]. These biphasic components lead to internal friction and stiffness which varies with strain rate [143-149]. They also display phenomena such as anisotropy and stress-state dependence related to alignment of ultrastructural features such as collagen or elastin fibers, blood vessels, fluids, and other tissue features [150-153]. The native alignment of structural fibers can be highly anisotropic [114, 119, 128, 133, 152, 154-159], which is particularly important given the frequency of multi-axial loading seen in biological systems. Beyond the native alignment, the microstructural response to loading can manifest in many interesting ways such as uncrimping or alignment of disordered fibers in tension, or as compaction and collapse in [112, 119, 145-149]. Beyond the sub-failure behaviors, microstructural and

macrostructural damage are also important to study. All of these behaviors are challenging to describe and require innovative models to recreate.

Interrupted mechanical testing can be used to capture the microstructural behavior of materials under deformation. This method consists of the interrupting of a material under deformation on a mechanical testing machine, and then fixing the microstructure of the material under that deformation (chemically fixed in case of biological tissues) [145-147]. In the case of metals or plastics this is frequently achieved by loading the material into the "plastic region", and then the deformed region is viewed under a desired microscopy method, such as scanning electron microscopy or transmission electron microscopy. In biological materials the material, a specimen of human placenta in this study, is deformed to a desired level and the crosshead on the machine is stopped and held at the same position until removed from the setup. The solution of phosphate buffered saline is removed from the water bath and replaced with a solution of fixative, in our case a 10% formalin mixture, and the tissue is allowed to fix under deformation overnight. The tissue specimen is then removed from the testing apparatus and prepared for microscopy. The type of microscopy preparation is important because different methods reveal different aspect of tissue morphology. Scanning electron micrographs can offer interesting insight into the microstructure, but because the observer sees an exposed face many features end up in somewhat different focal planes. This perspective changes in size which might cause issues in particle analysis. Even when the specimen face is exposed by cryosectioning, the exposed face may not be perfectly perpendicular to the microscope objective. These facts make SEM exceptional for observing microstructure qualitatively, but make quantitative analyses questionable. Transmission electron

microscopy in biological tissues is questionable because of the relative size of the region of interest; individual cells are approximately 10 microns in diameter while relevant structural features such as extracellular matrix fibers can be much larger. Traditional histological sectioning and staining methods are another option for observing microstructure.

We have already established the qualitative microstructural details (qualitative) and stress state dependency of the human placenta tissue in tension, compression and shear in our previous study [146]. As a follow up, in this study, we present the correlation of the obtained mechanical data with morphological and particle spacing quantification via interrupted testing method.

$$Aspect\ Ratio = \frac{(Major\ Axis)}{(Minor\ Axis)}$$
$$Solidity = \frac{(Area)}{(Convex\ Area)}$$
$$Circularity = 4\pi \times \frac{(Area)}{(Perimeter)^2}$$
$$Roundness = 4 \times \frac{(Area)}{\pi \times (Major\ Axis)^2}$$

Table 1 Formulations for ImageJ Shape

The particle analysis tools in such software packages as ImageJ (National Insititute of Health, Bethesda MD) allow for micrographs to be mined for valuable data reflecting microstructure changes, especially the microstructure evolution under mechanical loading. These tools measure the distribution of grouped pixels, which are recognized as particles, and provide important numerical parameters related to the shape and alignment, as well as the spacing, of these particles.

Important parameters will include those which describe shape including aspect ratio, solidity, circularity, and roundness. The mathematical formulations for these shape descriptor parameters are summarized in Table 1. Solidity indicates the amount of concavity in a particle. Aspect ratio, circularity, and roundness all indicate describe a particle's elongation by relating it to such particle measurements as major and minor axis lengths, area, and perimeter. Both roundness and circularity are formulated so that a perfect circle will have a value of 1.0 and as the object is more elongated or has more tortuous features the value decreases, essentially scoring the closeness of a particle to a circle. Aspect ratio is a simple comparison of the long and short axes of an ellipse drawn around a particle and gives an idea of how elongated a particle is. Because external loads can cause particles to collapse and compact under compression or extend stretch out in tension, each of these descriptors can provide important insight into a particle's shape. Beyond the particles' shapes, alignment of microstructural features can change dramatically with external loading. The angle of a particle's major and minor axes can be measured to offer insight into the shifts in features, and the deviation of this across particles can indicate how completely recruited the particles have become. This has interesting potential in biological materials, where a net tissue response is actually the

results of millions features at different ultrastructural levels. In the relatively simple example of tendon, individual microscopic collagen fibers are recruited as the entire tissue structure comes into tension. In the tendon example this fiber recruitment is believed to simultaneously include uncrimping of the least recruited fibers, alignment shifts of the more recruited fibers and the stretch with possibility of failure for the most recruited fibers. We believe a similar, albeit less organized, phenomenon is occurring in placenta and can be quantified through angle measurements taken during particle analysis.

Another aspect of microstructure that is important to consider deals with the spacing of particles, and the change in that spacing due to external loading. This one of the primary approaches for assessing damage in more traditional materials science when particle analysis techniques are used to characterize the microstructure. A customized tool built by our materials science collaborators will be employed for this portion of the particle analysis. Spacing parameters chosen for use in this study will be Number of Objects, Solid Area Fraction, and Nearest Neighbor Distance. Number of objects simply counts the distinct particles in the region of interest and returns the total, which is useful for understanding change in structure but cannot account for size of the particles involved. Solid Area Fraction is the total amount of particle area divided by the total amount of image area, and is often useful for indicating an increase in voids due to tension and shear, or a collapse of voids and cavity structures due to compression. Nearest Neighbor Distance gives the shortest straight-line distance to the centroid of another particle in the image, directly relating to the spacing of particles. Nearest

Neighbor Distance is usually expected to increase with tension and decrease with compression.

The data generated through this process is most valuable for use in constitutive modeling. Traditional constitutive relationships are not suitable for capturing many complex phenomena seen in biological materials, such as viscoelasticity, plasticity, hyperelasticity, strain rate dependency, stress state dependency, and other behaviors driven by the hierarchical ultrastructure of these tissues [160]. Internal state variable (ISV) based models have shown success in modeling many complex material behaviors through a powerful mathematical process which uses partial differential equations to simplify the behaviors to a minimum number of terms by describe behavior through a set of inputs and outputs using state variables, rather than through a large and complex system of equations based solely on inputs and outputs [149, 161]. These models can be configured such that a desired behavior is assigned a vector-based state space and can be considered to move along a corresponding axis in this state space. This vector term is driven by inputs and outputs and allows for related but mathematically non-compatible terms to be combined in order to describe one of these complex material behaviors. Recently, ISV models have been successfully used in the modeling of biological tissues such as artery, heart valve, skin, and growing tissues [138, 152, 162-166]. Several of these studies have incorporated data derived from micrograph studies as ISV terms in their models. The data gathered in this study will be highly valuable in developing these types of models for human placenta.

Methods

Interruption testing

Interrupted mechanical tests (tension, compression and shear) were performed as described in our previous studies [145-147]. Testing was carried out in water bath using 1x phosphate buffered saline (Sigma-Aldrich Co., St. Louis, MO) at 37 °C. Specimens were preloaded to 1 gram, preconditioning of 10 cycles at 10% strain, and a re-preload of 1 gram. Briefly, specimens were loaded to, and held at, desired levels of engineering strain (see Table 2 for details) at a constant deformation rate , using the a 10 kg load cell (with accuracy up to ±0.00005 kg) on the Mach-1™Micromechanical uniaxial testing machine (Biomomentum, Laval, Quebec, Canada).

Stress State	Eng. ε	True ε
Tension	25%	22.3%
	50%	40.5%
Compression	30%	35.7%
	60%	91.6%
Shear	50%	86.6%
	100%	173.2%

Table 2 Strain levels for Interruption Tests

Interrupted mechanical testing of human placenta samples were carried out as per the mentioned strain levels. Samples were fixed using 10% neutral buffered formalin at

the various strain levels and microstructural analysis was performed to calculate various morphological characterizations.

After reaching the desired strain level, the test was stopped and the saline was removed from the water bath. The sample remained intact in the clamps and on the testing machine during this process. The water bath was then refilled with10% neutral buffered formalin (Sigma-Aldrich Co., St. Louis, MO) to fix tissues structures. Specimens were then allowed to fix for twelve hours, and removed from the mechanical testing system and further prepared for histological examination. Specimens were embedded in paraffin, sectioned to 5 μm, and routine Hematoxylin and Eosin staining was performed.

Light Microscopy

As previously described, the sectioned and stained slides were observed using light microscopy [146]. Micrographs were captured at 100x as 12-bit RGB tagged image file (TIF) at a resolution of 2592x1944. Images were then selected based on area of interest, fiber alignment and other characteristic features.

Qualitative Particle Analysis

Images were analyzed qualitatively do identify potential trends in microstructural evolution, which could then be used to identify the best parameters for further quantitative analysis. The primary analysis involves identifying the key tissue features (such as fiber alignment, area fraction etc.) and any aspect of their morphology (e.g. shape change or elongation) which could adversely affect quantitative analysis [167]. In particular, we were interested in the differences in the blood and blood cells as compared

to the blood vessels of the placenta. This is because biphasic (elastic and viscous) nature of human placenta likely plays a major role in its biomechanical properties [146], contributing such phenomena as viscoelasticity [53, 168-170] and stress-state dependence.

The trends being for which we analyzed include, but are not necessarily limited to, changes in the shape, elongation, and alignment of the tissue features, as well as changes in the spacing, compaction, and area fractions of the tissue features. These types of morphology changes are often useful in understanding microstructural evolution. Correlation of these morphological parameters, along the mechanical data will help constitute a leap towards constituting a structure-property relationship, and overall understanding of the internal mechanics of human placenta tissue.

Quantitative analysis of Histological Micrographs

ImageJ software (National Institute of Health, MD) was used for morphological quantitative assessment of the histological images. A custom image analysis tool, CAVS ImageAnalyzer (Center for Advanced Vehicular Systems, Mississippi State University), developed by our collaborators was used for spacing and area fraction analysis. In order to quantify or process the microstructural features of these obtained images, they must be prepared or formatted in a specific and tailored way. The tools used in this study require that images are converted from 8 or 12 bit format to a binary format, which allows the tools to recognize and analyze particles. This is accomplished by thresholding the image so that any pixels above a desired saturation value are converted to white, and all pixels below the desired saturation value are converted to black. If the threshold level is appropriate, this approach highlights the desired tissue features as white on a black

background or black on a white background as is desired. When attempting to highlight and separate particles, a simple threshold may not best capture all the features. One issue with simply thresholding an image is the connection of particles which should not be considered connected for the purposes of image analysis; adjacent particles maybe detected as one, and thus will be analyzed incorrectly in further analysis. Another common issue occurs when the thresholding fails to convert all or some portion of a desired feature to a binary particle. This often happens at the edge of particles where the intensity values transitions into the voids. Similarly, features which are not desired may be converted into particles, such as red blood cells in vascular tissue. While blood cells do contribute to viscosity and other fluid mechanics aspects of blood, they are not a major part of the solid phase mechanics but are likely to be identified as solid in a simple thresholding. To address the artifacts created by applying a threshold to the entire image, we have decided to trace the key features so that only the relevant morphology is converted to particle data.

To accomplish this, the Gnome Image Manipulation Program (GIMP Project, Groton MA) was used. 12-bit RGB TIF files of the previously obtained light microscopy micrographs were imported to GIMP and converted to .XCF file format, the native image format for GIMP, and a new image layer with a transparent background was created above the original image layer. The desirable morphological features were traced in fully saturated black (0,0,0 in the RGB channels) using the circle brush tool. To aid in the accuracy and feasibility of this tracing, a Wacom Cintiq 22HD Pen Display tablet monitor was used. This tablet monitor greatly increases the accuracy and speed with

which a researcher can trace morphological features, when compared to a conventional mouse or trackball input device.

For the human placenta, the primary morphological features of interest are the blood vessels and connective tissues which comprise the solid portion of this biological material. The features we wished to exclude from selection were the red blood cells and unstained voids, which represent the liquid portion of the tissue. Blood vessels and connective tissue were traced as described above, so that individual blood vessel structures would be separate particles under image analysis, even if those particles were essentially adjacent despite being distinct features. Once all particles in a given micrograph had been traced, the traced layer was isolated and exported again as a TIF. The result of this process is a TIF image file with all the relevant morphology appearing as black objects on a white background. This process was repeated for all light micrographs previously discussed.

Morphological Measurements

The image files created during the preparation for analysis were imported ImageJ software (National Institute of Health, Bethesda MD) for particle measurement and analysis. As previously stated, the Analyze Particles function in ImageJ requires binary images, and the TIFs imported are in 8-bit RGB format. Imported images were converted to 8-bit gray scale, and then the Threshold tool was used to complete the process of conversion to binary. The exact value of thresholding is not relevant because, while the imported images are in an 8-bit format, the actual pixel values are either 255 or 0 as a result of the tracing settings; any threshold value between 1 and 254 will yield an identical binary image for analysis. After conversion the Set Measurements tool was used

to select the following measurement options: Area, Perimeter, Aspect Ratio, Solidity, Circularity, Roundness, and Corrected Angle. The Analyze Particles tool was used, and the results data were copied into Microsoft Excel for processing and data analysis.

Spacing Related Measurements

The CAVS ImageAnalyzer was used to analyze Number of Objects, Solid Area Fraction, and Nearest Neighbor Distance. All traced micrographs used in the morphological measurements were loaded into the CAVS Image analyzer. This software kit features a scale bar tool for calibrating actual size to particles. A non-edited image with an intact scale bar was used to calibrate our testing, and values of 200 μm per 504 pixels were used. The desired measurements were selected and the software kit processed and output the data to a Microsoft Excel compatible text file.

Data Processing and Analysis

The data from the ImageJ "Analyze Particles" tool was further analyzed in Excel to observe quantifiable trends in morphological parameters. Data was analyzed by averaging and taking the standard deviation of a desired parameter across the entire pool of particles. This process was completed for each desired shape descriptor. Because smaller particles may be features which are sectioned so they cannot be observed or possibly damaged an no longer bearing load, a simple filter for minimum particle size used. This filter process was repeated for each parameter in all images with levels of 0, 1000, 2000, 3000, and 4000 μm^2. This allowed us to isolate the larger and more dominant features in our images. Column charts were created to display data for shape parameters

across three strain levels, and compare across all five filter levels, and then repeated for each stress state.

The data from the CAVS ImageAnalyzer was also processed in Excel to better understand the quantifiable aspects of the microstructural spacing. Data for Number of Objects, Solid Area Fraction, and Nearest Neighbor Distance were organized so that each parameter could be compared across strain levels within a stress state. Column charts displaying this data were created.

Results

Light Microscopy

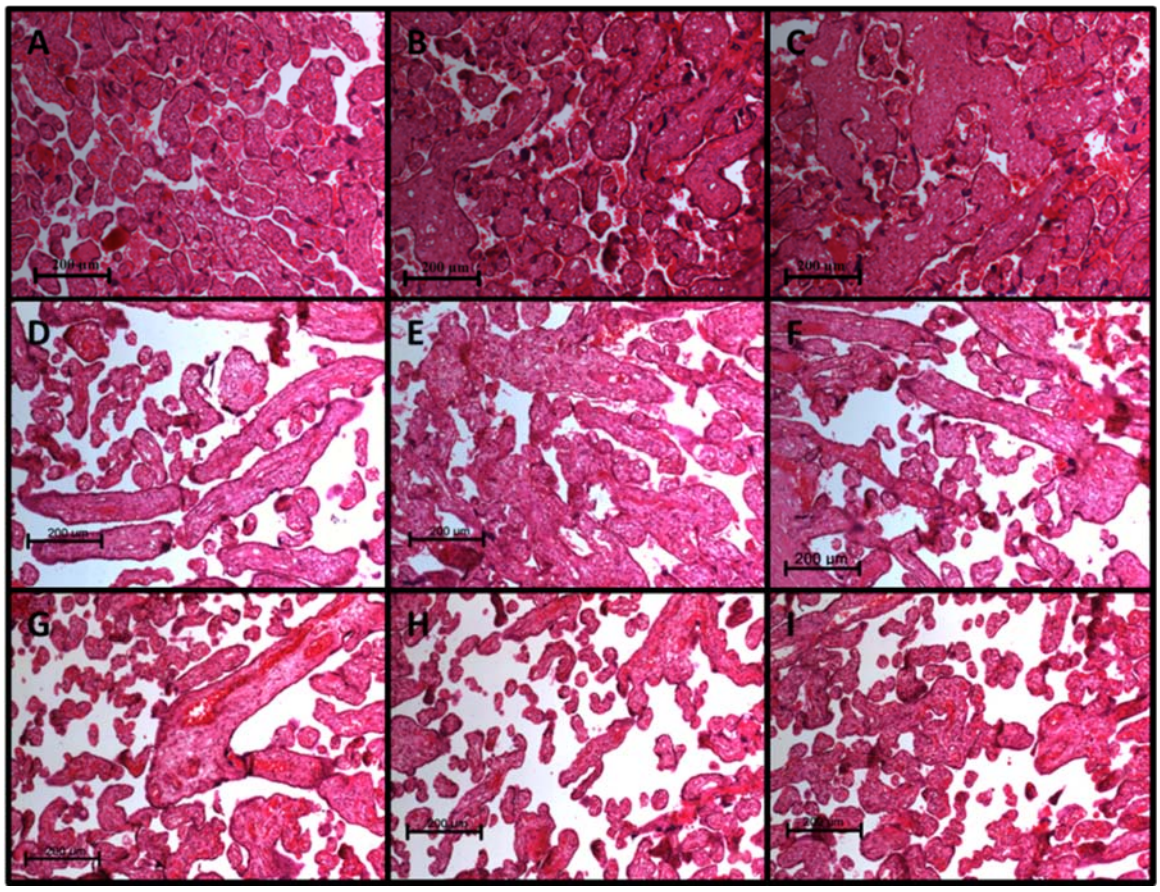

Figure 15 Light Micrographs of Interrupted Tensile Tests

Figure 15 shows light micrographs of interrupted tensile tests. Figure 15, panel A-C shows undeformed specimens. Figure 15, panel D-F are specimens which were interrupted at 25% engineering strain. Figure 15, panel G-I are specimens interrupted at 50% engineering strain. Figure 16 shows light micrographs of interrupted compressive tests. Figure 16, panel A-C shows undeformed specimens. Figure 16, panel D-F are specimens which were interrupted at 30% engineering strain. Figure 16, panel G-I are specimens interrupted at 60% engineering strain.

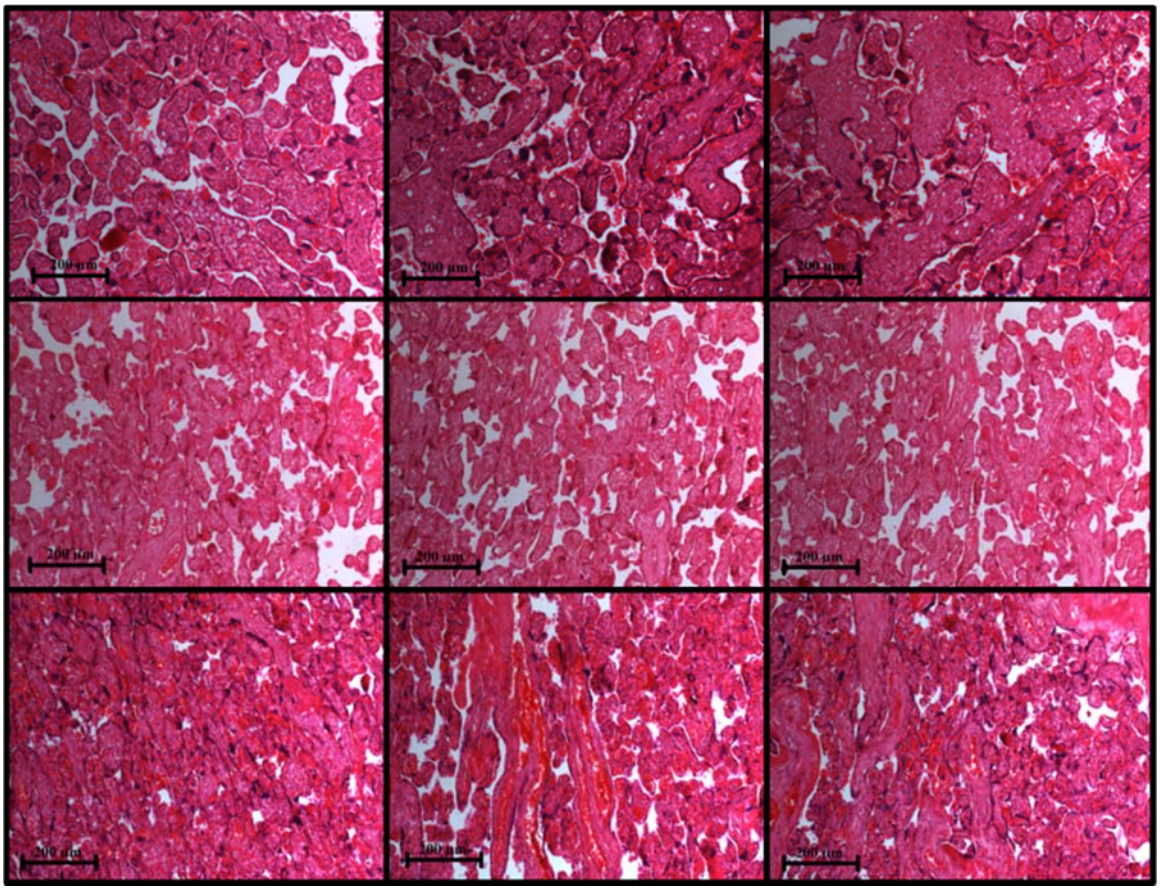

Figure 16 Light Micrographs of Interrupted Compression Tests

Figure 17 shows light micrographs of interrupted shear tests. Figure 17, panel A-C shows undeformed specimens. Figure 17, panel D-F are specimens which were interrupted at 50% shear strain. Figure 17, panel G-I are specimens interrupted at 100% shear strain.

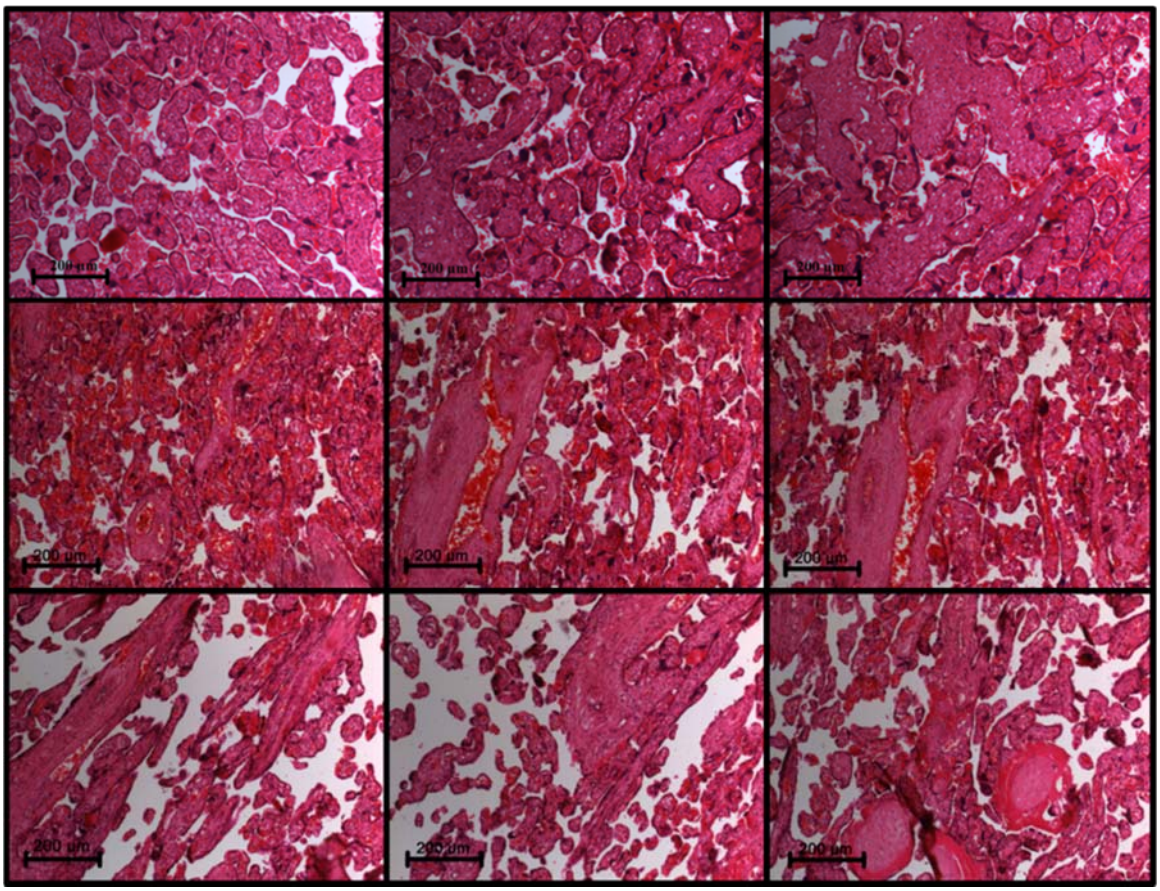

Figure 17 Light Micrographs of Interrupted Shear Tests

Qualitative Analysis

Our qualitative analysis yielded some morphological trends for each stress-state being evaluated. Micrographs of interrupted compression tests showed a strong tendency

for the blood vessels to compact and collapse. Vessels appear to align against the direction of compression, with a noticeable decrease in the space between vessels. At the lower level of compression there is a marked increase in vessel alignment against the loading axis, and some but not all spaces between vessels have collapsed or been reduced. At the higher level of compression, the alignment is even stronger and the space between the vessels has almost completely collapsed across all images. These trends are reasonable when considering how hollow structures can compact and flatten under compressive loading. As it relates to quantification, the elongation of vessels can be shown through parameters such as aspect ratio, roundness, and circularity. The alignment of the vessels perpendicular to the loading direction is likely to manifest in corrected angle of major axis and the recruitment of those vessels into the elongated morphology to show a reduced standard deviation of corrected angle of major axis. The general compaction may also be observed through an increase in the total area fraction of the particles.

Micrographs of interrupted tensile tests showed a somewhat reversed trend to the compressive samples. Tensile samples appear to show alignment of the vessel structures parallel to the direction of loading. They extend and elongate with the loading axis, and the spaces between vessels appear to increase. In the lower level of tension the large vessels appear to have aligned with the loading axis, and the overall space between vessels appeared larger. The smaller the vessels in this image series, the less aligned they appeared to be. This trend may be indicative of damage events where vessels break and can no longer remain aligned with the direction of tension. It may also simply be that those smaller vessels were out of plane with the microtome during histological sectioning

which could cause a vessel that is relatively well-aligned with the loading direction in three-dimensional space to appear as a smaller and less aligned particle when captured in a two-dimensional slice that is only five microns in thickness. In keeping with the trending relationship to compressive loading, the elongation with the direction of loading is likely to show as an increase in averaged aspect ratio and the aspect ratio driven parameters circularity and roundness. The progressive recruitment of vessels through tensile loading may be apparent through both the average and the standard deviation of the corrected angle.

Interrupted shear specimens show a somewhat hybridized combination of tensile and compressive trends. At lower levels of shear strain there appears to be some compaction and alignment towards the loading direction, somewhat similar to compressive loading conditions. As the loading increases to the higher level of shear strain, there is a marked elongation and diagonal alignment of the larger vessels towards the shearing direction, in a manner similar to higher levels of tension.

Quantitative Particle Analysis

Figure 18 shows tracings micrographs of interrupted tensile tests. Figure 18, panel A-C shows undeformed specimens. Figure 18, panel D-F are specimens which were interrupted at 25% engineering strain. Figure 18, panel G-I are specimens interrupted at 50% engineering strain.

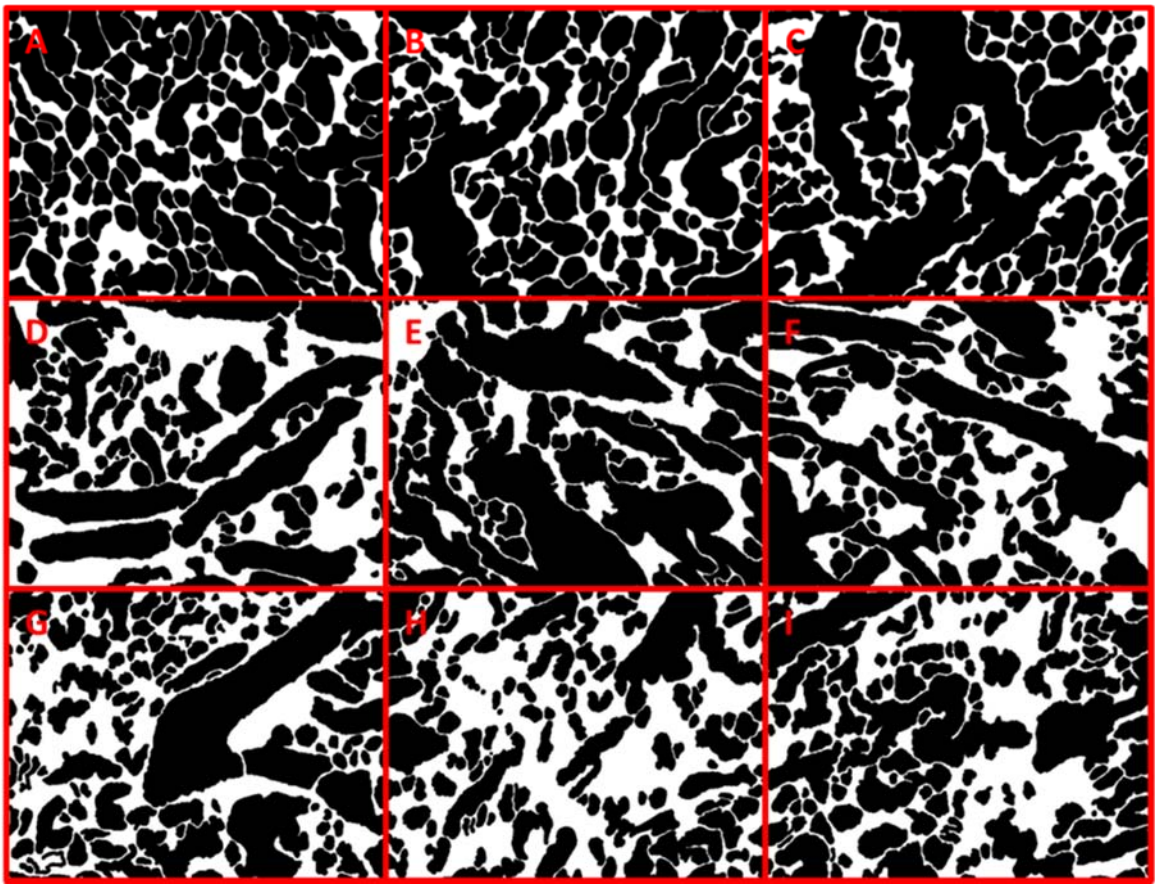

Figure 18 Tracings of Interrupted Tensile Test Micrographs

Figure 19 shows tracings of micrographs of interrupted compressive tests. Figure 19, panel A-C shows undeformed specimens. Figure 19, panel D-F are specimens which were interrupted at 30% engineering strain. Figure 19, panel G-I are specimens interrupted at 60% engineering strain.

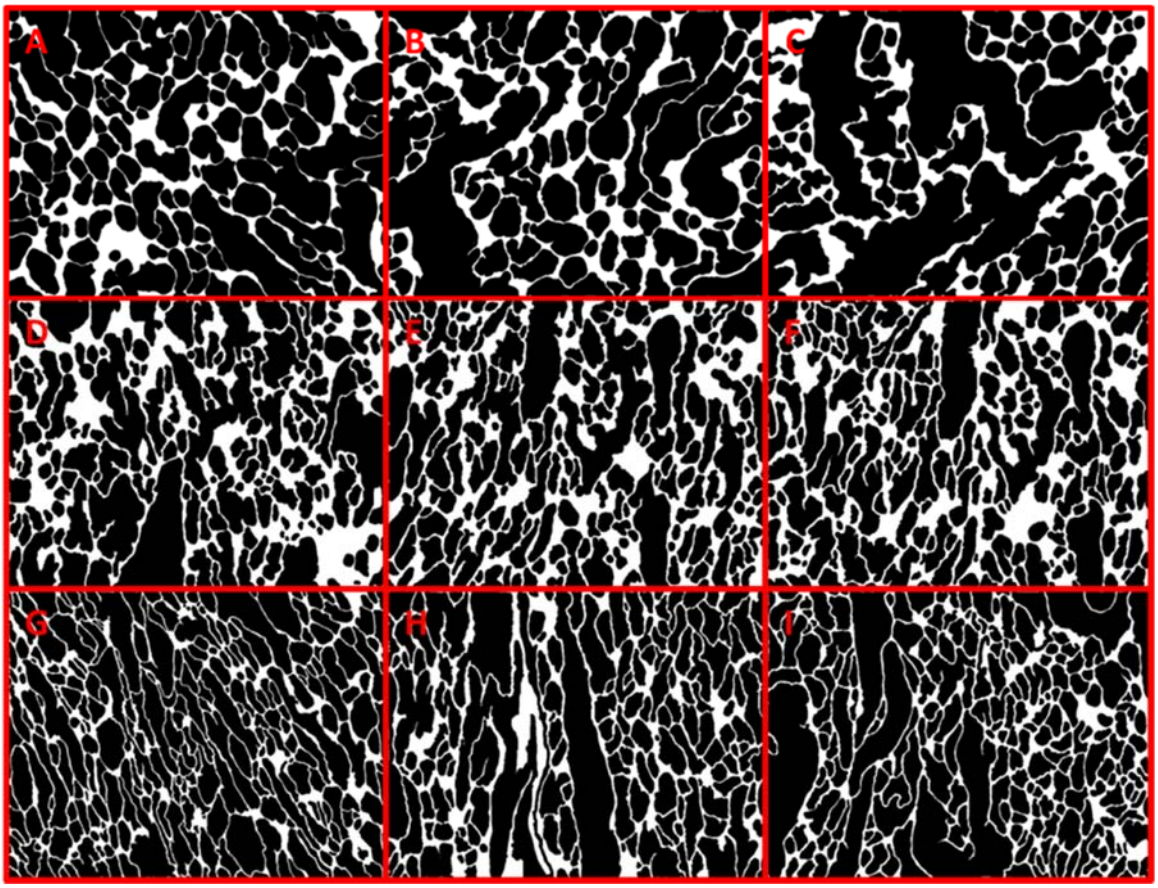

Figure 19 Tracings of Interrupted Compression Test Micrographs

Figure 20 shows tracings micrographs of interrupted shear tests. Figure 20, panel A-C shows undeformed specimens. Figure 20, panel D-F are specimens which were interrupted at 50% shear strain. Figure 20, panel G-I are specimens interrupted at 100% shear strain.

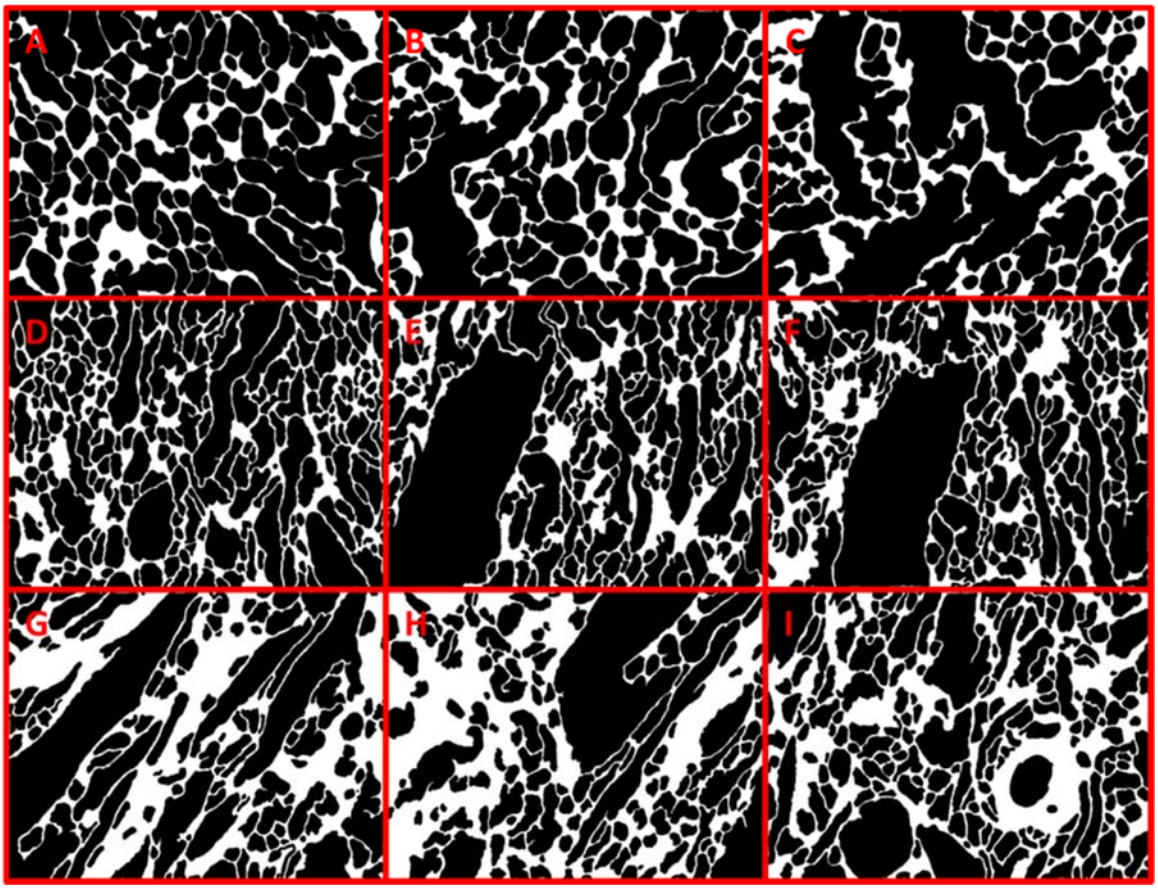

Figure 20 Tracings of Interrupted Shear Test Micrographs

These images represent the blood vessel portions of the placenta and are the final preparations for image analysis. Each image was hand-traced by the same researcher to ensure that, at least within this sample group, there is little to no variation in selection methods and, therefore, these are the best available images for obtaining quantitative particle analysis data. All twenty one images, undeformed images were the same for all three groups, are represented in the subsequent quantitative data.

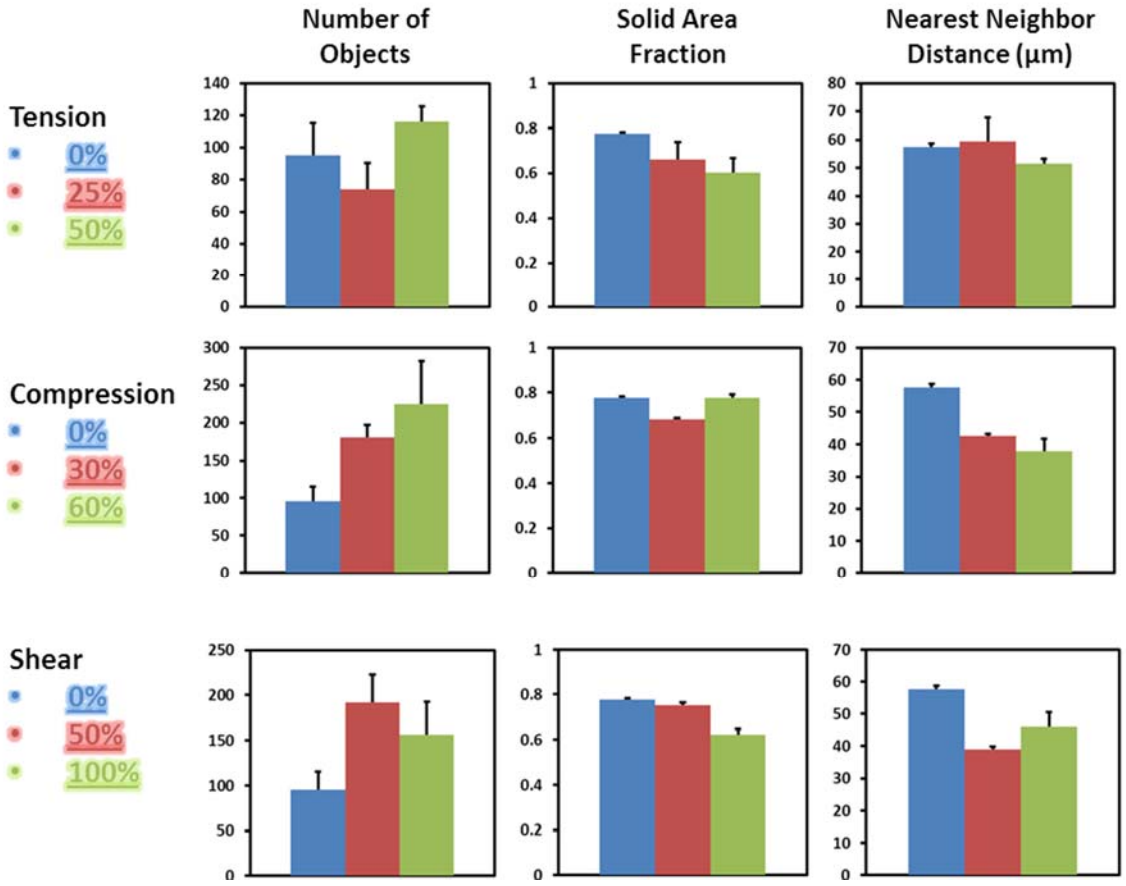

Figure 21 Particle analysis results for spacing parameters

Quantitative Results

Figure 21 shows spacing parameters for each stress state organized with the undeformed, strain level 1, and strain level 2 indicated by blue, red, and green; respectively. This data is extremely compelling, especially since the analytical processes used in spacing analysis are somewhat simpler than morphology and shape analysis, but the trends appear to be stronger than some of the morphological trends described later. Tension had interesting trends in all three shape descriptors, especially when each is considered in the context of the other 2. Solid Area Fraction appears to decrease as

tension increases, which is logical for tensile loading increases and the space between microstructure features increases. Number of Objects shows a decrease from undeformed to 25% engineering strain and an increase from 25% to 50% engineering strain. This is interesting as the number of objects increases while the total space covered by objects decreases. Figure 22 includes a particle size comparison for each tensile strain level, and we can see that the average particle size is highest at 25% tensile strain, and actually lowest at 50% strain. A larger number of smaller particles, as indicated by this data, may be the result of large load bearing structures coming into alignment at lower strains, and those same structures undergoing damage and fragmenting into smaller structures at higher strain. Nearest Neighbor Distance also follows this logic with an increase in neighbor distance caused by the relatively longer distance between larger particles at 25% tensile strain being a symptom of the fact that Nearest Neighbor Distance does not normalize for particle size. The large number of smaller scattered particles at 50% tensile strain would be on average closer to their nearest neighbor once damage had fully occurred. Overall, spacing descriptors across our tensile strain levels indicate a trend of increasing of total void space and a fragmentation of larger particles consistent with traditional understanding of accumulated tensile damage in material science research.

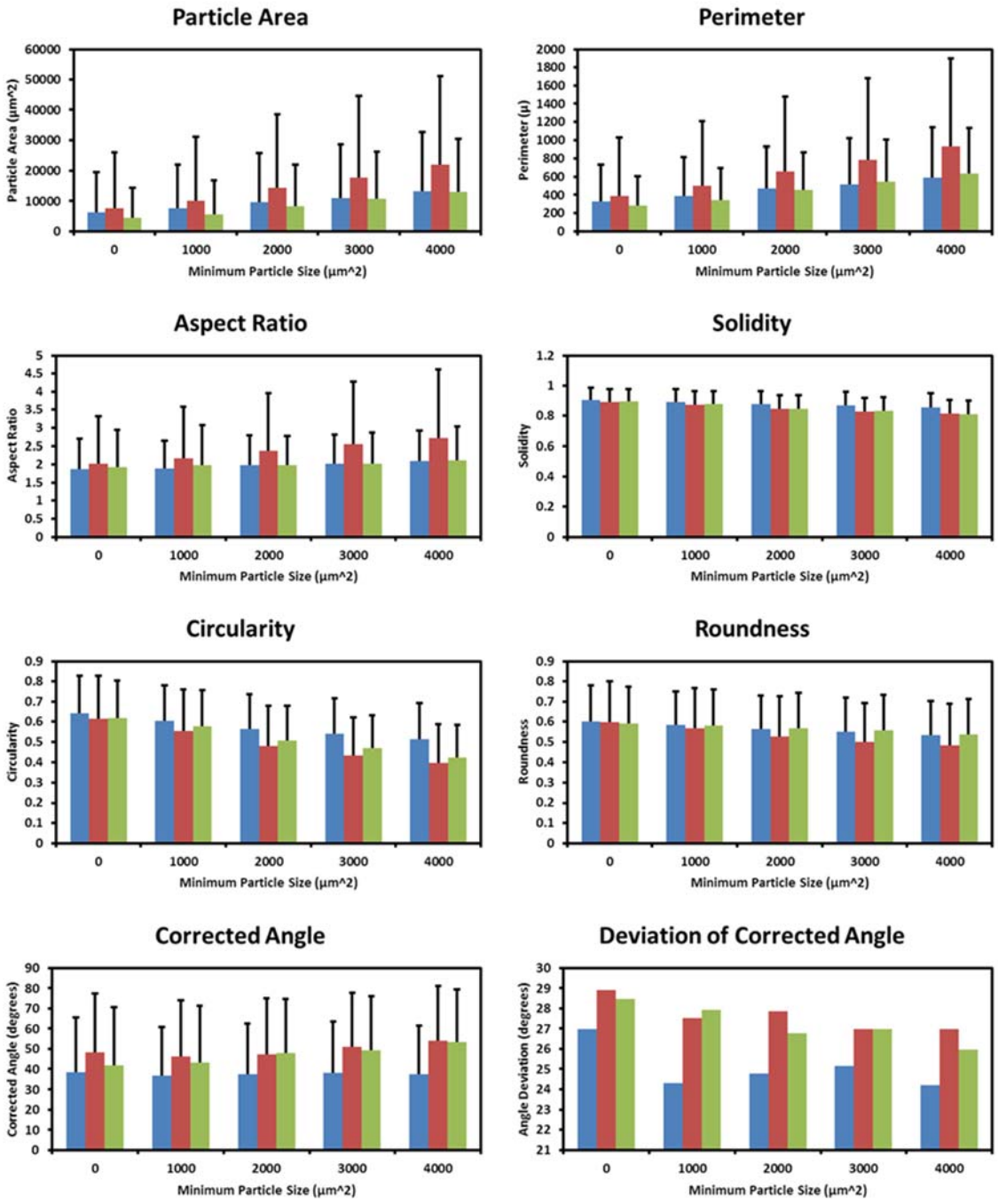

Figure 22 Morphological Particle Analysis Results for Tension

Spacing parameters for compression, shown in figure 21, are also compelling, with a steady increase in the Number of Objects being the most profound trend demonstrated. This fits extremely well with conventional understanding of compressive loading where structures collapse and decrease in size while compacting, which ultimately fits more structures in a given volume of material. Solid area fraction actually decreases at 30% compression before returning to nearly the equivalent of undeformed at 60% compression. At first this is somewhat puzzling because of compression would most likely show a steady increase in solid area fraction, but when taken in the context of particle size shown in figure 23, we see that particle size has decreased to essentially complete saturation by the point of 30% compressive loading. Nearest Neighbor Distance consistently decreases with increasing compressive loading, consistent with a larger number of smaller and closer objects at the highest levels of compaction and compression. This trend of fully collapsed particles at 30% compression continuing to compact on each other at 60% compression is reasonable and may account for the Solid Area Fraction's down and then back up behavior. Furthermore, there are some regions in our 30% compression micrographs where nearby particles appear to have an almost puzzle piece fit, but a gap which separates them. While difficult to confirm, this may be an artifact of our testing protocol wherein some elastic recovery occurred between structures, but was not recovered within the structural features themselves. Such behavior would be consistent with drop in Solid Area Fraction and a simultaneous drop in Particle Size. The steady drop in Nearest Neighbor Distance even with the counterintuitive drop in Solid Area Fraction could be explained by the large number of smaller particles being more evenly and therefore closely distributed. The combination of the spacing and the

shape descriptor results indicates that compressive loading causes placental microstructures to collapse and compact onto each other, as is seen in compressive loading of other materials such as brain.

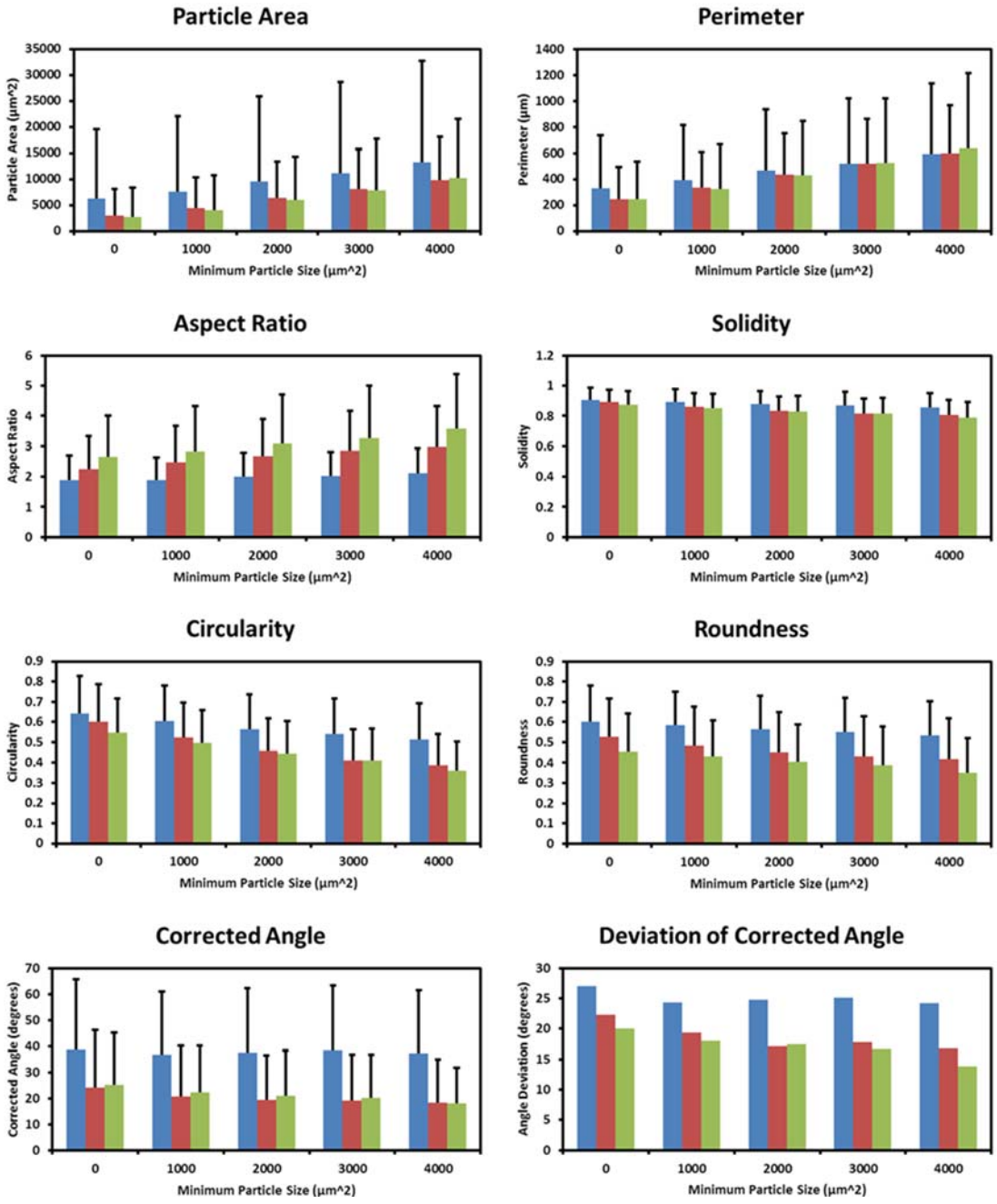

Figure 23 Morphological Particle Analysis Results for Compression

Shear loading trends for spacing parameters, shown in figure 21, indicate some very interesting trends, especially when considered in the context of our compression and tension analysis. As shear loading increases from undeformed to 50% shear, there is a large increase in number of objects, a decrease in average particle size is seen in figure 3.24, a small decrease in Solid Area Fraction, and a larger decrease in nearest neighbor distance. These trends are extremely similar to those shown for spacing descriptors in compressive loading as compression increased from undeformed to 30% compression. It is possible that a similar trend of vessel collapse at lower strain levels exists between shear and compression. As shear loading increases from 50% to 100% strain there is a decrease in the number of objects, a continued holding of the smaller particle size, a relatively large decrease in Solid Area Fraction, and a slight increase in nearest neighbor distance. The thing that is most interesting about this transition is that the values for shear appear to be moving towards those seen in tension, where a shift from early microstructural response transitions into the extension and ultimate failure of microstructure features under larger strain levels. Overall this indicates that shear moves through a compression like state where lower shearing mimics compressive microstructure changes of vessel collapse, but as shear increases the loading begins to mimic that of tensile loading response characterize by increase in voids and likely accumulation damage.

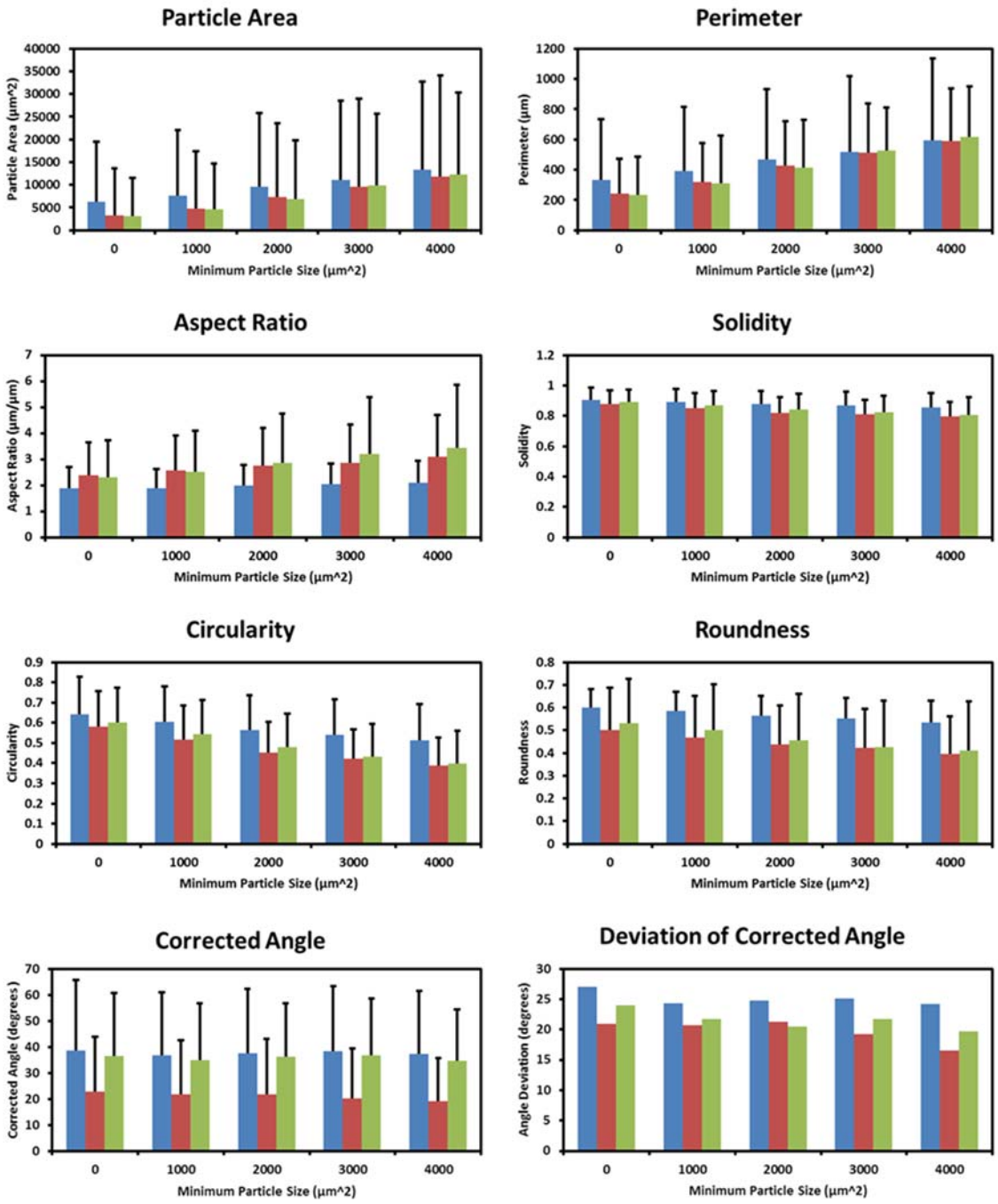

Figure 24 Morphological Particle Analysis Results for Shear

For the morphological parameters displayed in column charts are aspect ratio, solidity, circularity, roundness, corrected angle, and standard deviation of the corrected angle. Aspect Ratio, Circularity, and Roundness all pertain to a particles elongation. Corrected angle and the standard deviation of the corrected angle are closely related to alignment of the particles. Solidity can be an indicator of compaction and elongation, as either of these can affect the amount of convex space in a particle. The data are arranged so that levels undeformed (blue columns), strain level 1 (red columns), and strain level 2 clustered (green columns). As the clusters increase from left to right, the minimum particle size increases by 1000 square microns. This filtering process helps to show the behavior of the largest particles which bear the most load.

Compression results in Figure 23 show apparent trends in the elongation parameters particle area, aspect ratio, circularity, and roundness, as well as a less defined but potential trend with alignment parameters corrected angle and standard deviation of corrected angle. Particle area drops greatly from undeformed to 30% compression and then remains relatively similar as compression increases. In terms of aspect ratio, there is a trend of increasing aspect ratio as strain increases. This is consistent with the observation of the elongation of the particles as they compact at higher compression. Likewise circularity and roundness both decrease as strain increases, indicating particles are less round and more elongated. Corrected angle measurements become lower and more aligned as compression increases, but appear to be nearly saturated by 30% engineering compression. The standard deviation of the corrected angle, in particular at the higher filter levels, appear to have a strong decreasing trend, indicating that these particles are more highly aligned, or recruited, against the loading direction. Solidity and

perimeter did not appear to show strong changes across the different strain levels. Over all these results are extremely promising, as they quantitatively reinforce our qualitative assessment of the morphological microstructure evolution of placenta in compression. The most likely candidates for structure properties to drive the compressive stress-state portion of constitutive relationships will be aspect ratio, and roundness. Deviation of corrected angle may also be a good candidate. All of these relate directly to the alignment and elongation as placental vessels collapse and compact under compressive load.

Figure 24 shows shear quantitative results. Particle Area appears to drop slightly at lower strain levels, and then hold steady through higher levels. Not unexpectedly, a similar trend is observed in perimeter. Aspect Ratio has the strongest trend, increasing with increasing shear, and is the best candidate for use in constitutive modeling. Circularity and Roundness do not share this trend as strongly, decrease at 50% shear, but little to no change as shear increases to 100%. Alignment parameters for the corrected angle and deviation showed a reverse trend, perhaps indicating some shift from a compression like state at low shear, to a tension like state at high shear.

Particle analysis results for tension are shown in Figure 22. For Particle Area, Perimeter, and Aspect ratio there is a common trend of increase and then decrease, especially when filtered for only the largest particles. This may indicate elongation at low tension, with larger vessels being recruited under loading, and then a reverse of these numerical trends at high tension may be related to damage as discussed earlier for tension. Solidity did not offer a compelling trend. Circularity, especially for larger particles, decreases with tension, but appears to reverse a bit towards the higher levels of strain. This may mirror the damage like trends shown in aspect ratio, where particles

become more elongated with load then break and return to a less stretched shape. A similar but less profound trend is seen in roundness where there is a dip in the value at 25% tension and a return to nearly undeformed levels at 50% tension. Corrected angle and the standard deviation thereof are interesting, as, there is an increase in angle with tension, but an apparent saturation between 25% and 50% tension.

Discussion

Relationship to Mechanical Data

The mechanical testing results from our previous studies have been restated here in terms of true strain (Figure 25); for convenience of discussion the conversions from the engineering stress-strain levels discussed throughout this chapter, and the true/effective stress-strain curves displayed are included in Chart 3.2.

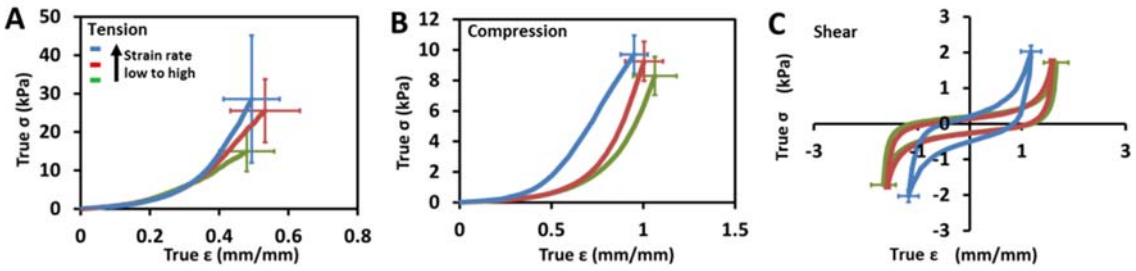

Figure 25 Strain Rate Comparison

It can be seen the each strain level was selected to correspond to approximately the end of the toe-in region where uncrimping and recruitment have become somewhat saturated, or the center of the linear region where load is very much resisted and damage begins to accumulate. For Tension in particular, our level of strain was targeted at being

relatively close to failure. This is why it was not surprising to see smaller particles and reduced Solid Area Fraction at higher tensile strain. It is worth noting that while there was not an extremely high level of resistance to loading near the end of the tensile toe-in region, there was a much larger mechanical response in tension than the other 2 stress states where the transition to linear region abruptly leads a profound mechanical response. Compressive loading is interesting because the initial level of compressive strain offers almost no mechanical resistance, but a very abrupt transition out of the toe-in and an extremely steep linear region both mean that the higher level of compressive strain is under and extremely high stress. This is consistent with our particle analysis which showed that early compressive loading is dominated by particles collapsing which is not likely to elicit a significant mechanical response in our case; blood vessels tend to have very little resistance to collapse without internal pressure. The higher levels of compression were shown to be dominated by compaction of the fully collapsed blood vessels which is likely to produce a more profound response to compressive as the spongy network has become a stack of collagenous connective tissue and vessel walls. Shear loading has similar trend to compression with very little mechanical response despite a relatively large amount of shear strain at the 50% shear strain level, but a much more significant mechanical response near 100% shear strain.

Applications in Modeling

This data offers a strong foundation for the future development of constitutive relationships based on structure property derived internal state variables. We have shown morphological trends with quantitative results for each stress state. These trends are most promising because they occur in the hypothesized parameters, indicating that the link

between the conceptual understanding of the particles and their morphology is quantifiable. Compression is arguably the most successful stress state in this study because more of parameters show a steady increase or decrease with strain. Qualitative analysis showed compression images to show particle compaction and alignment against the loading direction as blood vessels collapse and pack in at high levels of compression. All of the elongation and alignment parameters show enough trending, especially when filtered for smaller particles, to be candidates for driving variables in constitutive models. Tension and shear each had some interesting reversals for these parameters, which may indicate a transition of trends which was not captured by our three data points. It is worth noting that our strain levels are extremely large in a traditional mechanical engineering context. It would be valuable to have not only a larger number of samples at our current strain levels, but to have additional intermediate strain levels. I believe that for tension in particular, there is going to be a period of extension, elongation, alignment and recruitment with the loading direction, but once the toe-in region has been completed and the majority of fibers has become uncrimped and recruited there will be a downturn in these parameters as microstructural damage begins to accumulate. In compression I believe there will be an initial collapse and then a compaction transition as the toe-in region leads into the linear region. This study actually selected for the end of toe-in region and the end of the linear region as its points of interest so the data points shown in this document likely represented the near-saturation point for each region of the stress-strain curve. The intermediate points would allow for more robust models when this data becomes incorporated as such.

Limitations in methods

Our methods have some inherent limitations. Among these are the fact that hand tracing is a subjective process and will likely vary to some degree amongst different investigators. While our study did use a single investigator for all hand tracing to control within our own experiment, reproducibility will always be subject the human factor of variability. An extension of this is the decision of what to include and exclude while tracing. Our investigator sought to include vessels and supporting connective tissue but exclude debris such as clots and red blood cells, but with those guidelines different investigators may still select or exclude different particles.

The relatively small size of our data set may introduce some variability. While this much data analysis for 21 images was certainly not a short process, more than 3 images per strain level may have offered more complete results. Additionally, strain levels in all 3 stress states were selected to correspond to certain points along the stress strain curve, but microstructure analysis at more points along the curve would be extremely helpful for understanding the processes involved in the microstructural evolution.

There is an issue concerning the formulation based simply on micrographs of equivalent size, particularly when considering the spacing related parameters Number of Objects and Solid Area Fraction. These parameters have direct relations to the amount of area involved in the particle analysis, and by proxy the volume and mass of material or tissue represented by that two dimensional image. When a tissue sample is deformed, the representative volume is deformed as well. To wit, a compressive stress state in placenta will add more vessels to the same microscope field than an undeformed specimen, and a

tensile stress state will remove vessels from the microscope field. In addition to the primary loading direction, Poisson's ratio effects will also add or remove blood vessels in an opposite manner. This means that future formulations based on the reported data may need consider how the strain state of the tissue affected the represented particles, and adjust or normalize accordingly. Corrections could be driven by adjusting the analyzed region to a strain-matched size. When considering the effects of the reference frame on the morphological particle data, the biggest issue lies in the fact that the data is based on individual particles. This means that compressive stress states have much larger data sets than tensile and shear. A larger number of tensile and shear strain micrographs would need to be analyzed to reach a sample size of total particles that was equivalent to our compressive values.

The previous state-of-the-art in this field involved phenomenological polynomial models which could capture hyper elasticity, but did not capture more complex phenomena [53, 170]. The availability of structure property data for use in ISV models is a significant extension of the available experimental body to supplement future modeling efforts.

Future Research

Future work for this research will include the translation of our current structure property data into a constitutive relationship for use in finite element modeling. This constitutive modeling will be able to include numerous structure property relationships, as well as the stress state and strain rate dependency demonstrated in the mechanical testing portion of our studies. As was discussed previously, there may be a need for additional data for existing strain levels, as well as the addition of intermediate strain

levels to further understand this microstructural evolution. It is worth noting that while this study may not ultimately require such measures, future research with other biological materials would benefit greatly from 5 or more points of microstructure analysis along the stress strain curve. Despite this possible limitation, the data presented here is an excellent basis for future modeling. Such a model will provide a powerful tool for studying placental abruption and other placental pathologies via finite element method. Ultimately, such simulations could contribute to the development and validation of injury prediction or pregnancy specific safety gear for automotive use.

Moreover, this process can be applied to other tissues as there is much need for mechanical testing in current biomedical research. The methods described in this section are very nascent, but offer a promising area of research for biomechanical engineers. Materials science has been extremely successful in improving our understanding and real world implementation of complex materials such as metal alloys, polymers and composites. With continued efforts towards extending such research into biological and biomedical materials, there is hope to see similar advancement in these fields.

CHAPTER IV

GENERATION OF ANATOMICALLY DERIVED MESH OF LATER TERM PREGANCY FOR USE IN FINITE ELEMENT SIMULATIONS

Maternal trauma is exceedingly difficult to study through direct experimentation because of logistical and ethical issues. While accurate understanding is important, there is no appropriate *in vitro* surrogate which can address all of the important research questions. Human cadavers are difficult to obtain and will have significantly altered material properties due to post mortem effects. The use of animal surrogates is unlikely to be feasible. The anatomy of placentation differs greatly among species, perhaps more than any other organ[76]. Humans have a discoid hematochorial placenta which found primarily in primates. Since primate research is arguably more difficult and costly than human research, this is unreasonable pursue. Rodents have a form of discoid placentation but it is histologically distinct and is also subject to altered morphology and mechanical loading requirements due to litter versus single fetus pregnancy. Because of these difficulties, the prospects of computational simulation of trauma are especially promising for maternal trauma research. With relatively few physical specimens required, a plethora of questions regarding maternal and fetal injuries and susceptibility ies can be addressed. Previous groups have studied maternal trauma using finite element simulations. Moorcroft showed that pregnant passengers are safer and less likely to experience placental abruption while wearing a safety belt, as compared to not wearing a safety

belt[49]. This study used a simplified geometry and linear elastic material properties. They also did not include a fetus, assuming the hydrodynamic forces of the amniotic fluid dominated placental loading during trauma. While the study does make considerable simplifications, it effectively validates the safety belt for pregnant occupants. Our goal was to continue this research approach using anatomically correct meshes based on more realistic material models. The first step in creating our finite element mesh based on realistic human anatomy was to obtain appropriate medical imaging scans of appropriate pregnant individuals. Because the risk of injury to both mother and child increases in the third trimester, and likely is most risky the later the pregnancy, scans from full or near term pregnancies were indicated as a preference. Additionally, an absence of pathologies which may change our modeling results was indicated as a preference for this study. Our collaborators at University of Cape Town (Cape Town, South Africa) in both the Cardiovascular Research Unit and the Obstetrics and Gynaecology Department assisted in obtaining these images. Because the medical school's radiology department maintains a relatively large library of images from previous patients, a retrospective release of images was proposed as an alternative creating a new scan and involving the risks, albeit relatively low, of a currently pregnant patient. In the case of pregnant imaging, MRI is almost always considered to be preferable to CT scanning, because the magnetic resonance is believed to pose a less significant risk to the developing fetus than the radiation associated with CT scans. CT scans are occasionally used in emergency cases, such as trauma, when the additional time required to complete an MRI scan are unacceptable. For these reasons, there were a larger number of potentially usable MRI scans than CT and MRI was selected as the preferred image modality. A retrospective

release of five sets of existing images was approved by the Human Ethics and Research Committee at University of Cape Town, and was subsequently approved by the Institutional Review Board at Mississippi State University. MRI scans from late term pregnancies were reviewed and a set of scans were selected by the medical faculty of the Radiology and Obstetrics and Gynaecology Departments as the initial candidate, because of a lack of major maternal or fetal pathologies. Images were sanitized of any potentially identifying information such as patient name or the date of collection for the scan. The images were transferred University of Cape Town to the Mississippi State Biological Engineering Department laboratories through a secure file transfer terminal, and no web or cloud based versions of these images remain in existence.

Review of Images for Planning of Mesh Generation

Images were received in DICOM format, which is common for medical images and includes certain data relevant to stacking of images, and were evaluated using the MicroDicom Viewer (MicroDicom, Sofia Bulgaria) software package to confirm suitability of the scans. A selection of images from each the scan is shown in Figures 26, 27, and 28.

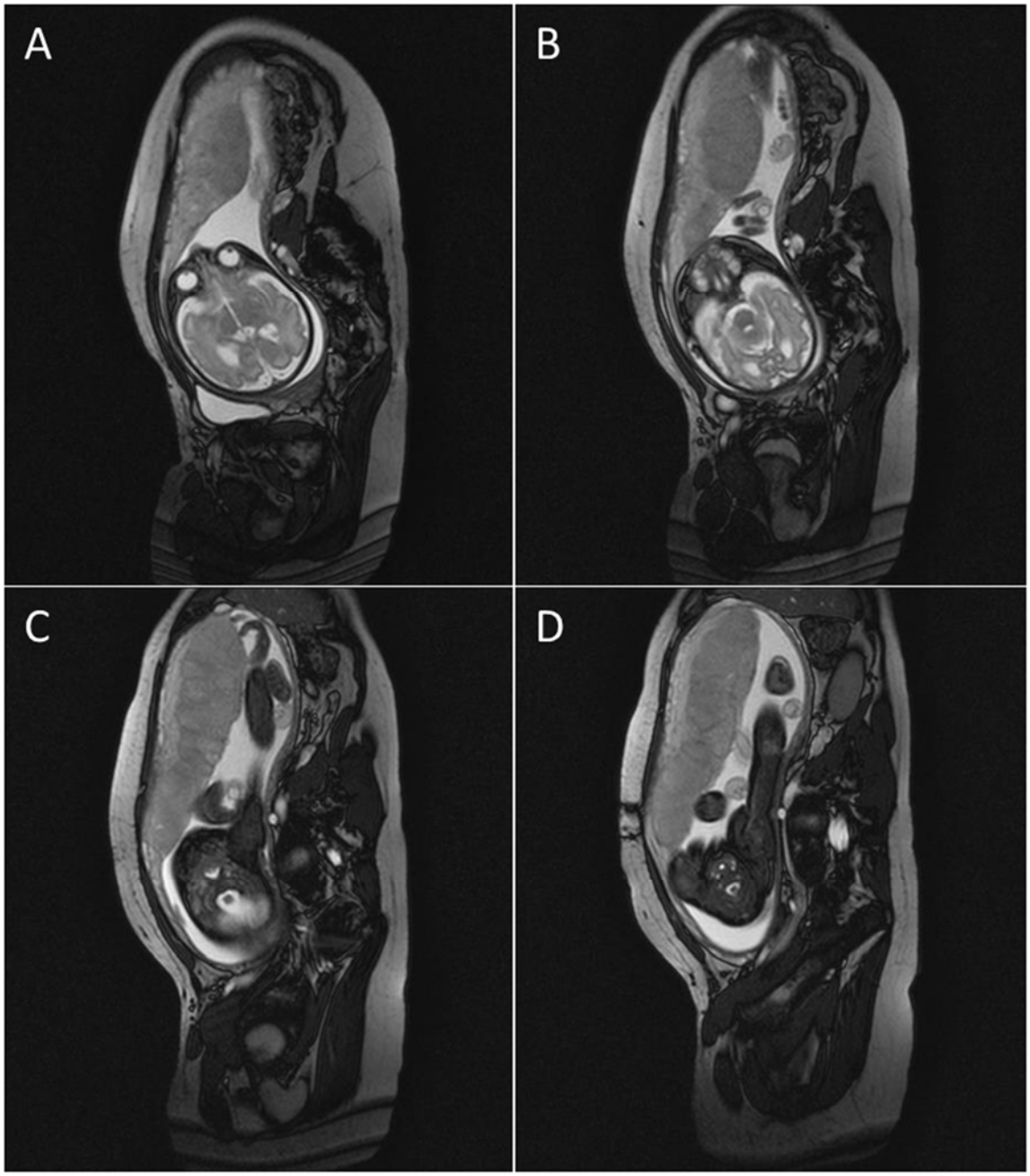

Figure 26 Transverse Plane MRI Scans of Human Pregnancy

The scan shown in Figure 26 is in the transverse plane, and includes an excellent view of the placenta, uterus and fetus, but does not include a large portion of the abdomen and has some symmetry issues due to patient positioning. Furthermore, Figure

26 can be seen to have some artifacting near the edge of the image where there is still relevant anatomy.

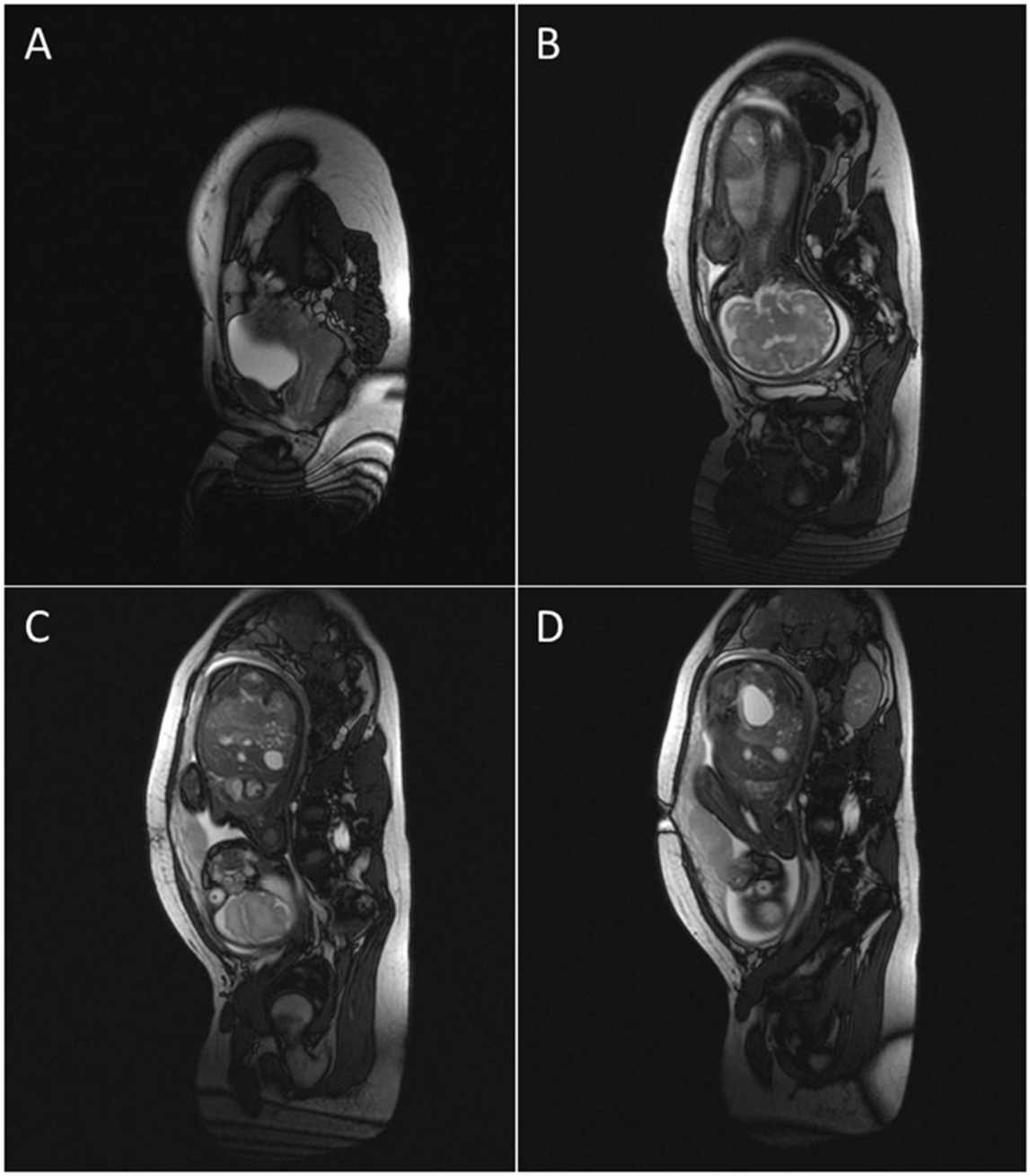

Figure 27 Sagittal Plane MRI Scans of Human Pregnancy

The scan shown in figure 27 is in the sagittal plane and, like the transverse scan, also offers a good indication of the major organs of pregnancy, but does not include a large portion of the abdomen on the lateral ends of the sagittal plane. Notable features in Figure 2 include a large amount of artifcating shown in Figure 27A, which was the first image obtained in the scan and closes to the patient's side. Another interesting feature is seen in Figure 27D where the uterus protrudes into the space behind the navel, as though the intrauterine pressure has pressed against this stress concentration and caused the uterus to fill the void. The scan shown in Figure 28 was chosen for use in our mesh construction, as it included the entirety of the pregnancy, and almost the entire abdomen.

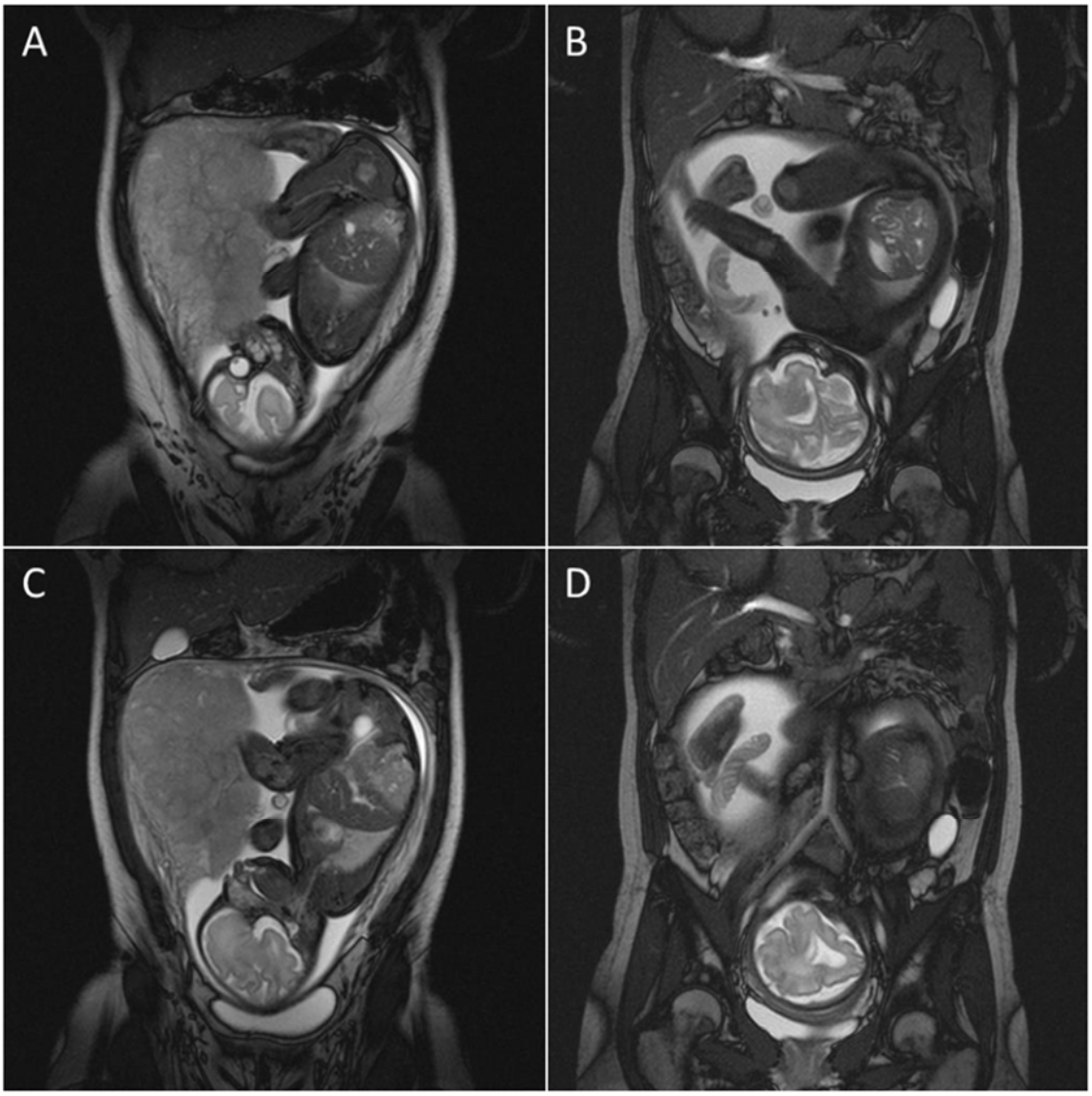

Figure 28 Frontal Plane MRI Scans of Human Pregnancy

Figure 28 is in the Frontal Plane and can be seen to include the entire abdomen, uterus, and fetus. The selected scan is a 36 week pregnancy and is in normal presentation with the fetal head locked into the pelvis. The image set is composed of thirty eight slices at four millimeter spacing, and includes the entire abdominal region, plus the lower part of the thoracic cavity and majority of the pelvic anatomy. A full body scan may

eventually be needed for more advanced simulation efforts, but for our current needs, the abdominal portion is more than sufficient. Images were further reviewed and compared with anatomy texts to improve the quality of selection of anatomy during premask tracing.

ScanIP

Images were imported to the ScanIP Software Package (SimpleWare, UK) for use in mesh creation. This software package creates three-dimensional masks from two-dimensional images in a Z-stack configuration, and then uses meshing tools to export this mesh for CAD or Finite Element use. Our goal was to create masks for as much relevant anatomy as possible, allowing us to create meshes with different levels of anatomical sophistication and complexity. This process allows experiments to be scaled up for increased accuracy, but allows for the availability of early results and progressive improvement and refinement. The organs selected for mask processing were skin, pelvis, spine including discs and vertebrae, uterus, placenta, and fetus. The space not occupied by the listed anatomical components, essentially the background within the skin, was assigned as muscle, but may include some sub-cutaneous fat or connective tissues such as fascia. These organ and tissues represent the major structures involved in a maternal trauma event, and should allow for a significant amount of useful simulation data to be created. Notably missing structures include amniotic fluid, the bladder and gastro-intestinal tract, and the detailed fetal anatomy. Fetal anatomy, especially fetal skull and brain, could be a focus of future research efforts because of the frequency of reports of fetal head trauma. Despite these specific anatomical features, our included anatomy is a

significant improvement over the existing models that have been published, where the current state of the art is CAD approximations of natural anatomy [49].

The desired anatomical were assigned their own respective masks and defined with the appropriate priority relative to the other organs, so as to match features on overlapped tracings. Each feature/organ was then traced within its own mask, using the Wacom Cintiq 22HD tablet monitor described previously, for each of the image slices. This process is extremely time consuming, but provides significantly better results than some of the thresholding and flood filling tools built in to ScanIP, since the relative intensities for MRI features are more subtle than these tools can capture. The completed process included a series of progressively more sophisticated masks, which can be continually improved and used in future research as needed, but can be scaled back to meet the needs of earlier simulations with less sophistication. The geometry used in the simulations described included the skin, bones, muscles, uterus, fetus, and placenta. The most sophisticated masks completed for this project included a decomposition of the bones into the pelvis and the spine, which was further masked to include each separate vertebrae and intervertebral disc.

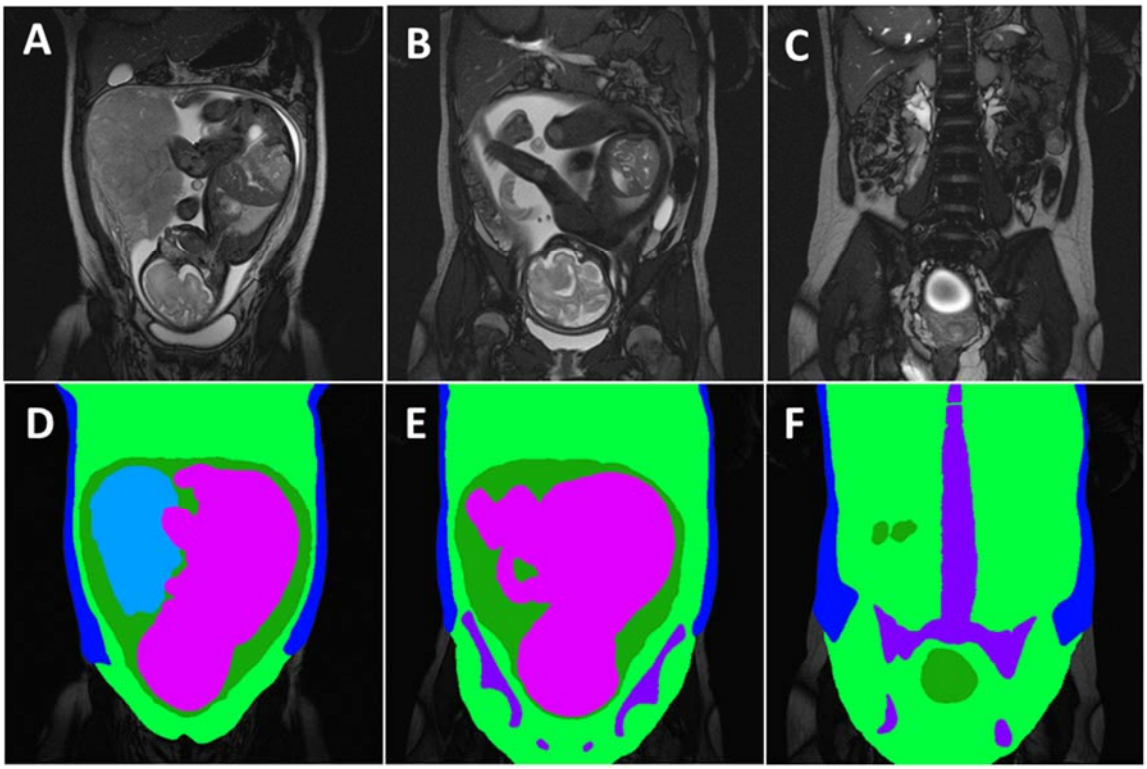

Figure 29 Tracing of MRI Scans for ScanIP

Figure 29 shows two-dimensional traces of the key anatomical features; this process of selecting for correct anatomy to incorporate in simulated geometry is repeated for each image in the Z-stack. ScanIP then processes these two dimensional tracings and uses a meshing algorithm to render three-dimensional geometry for subsequent use in other software packages.

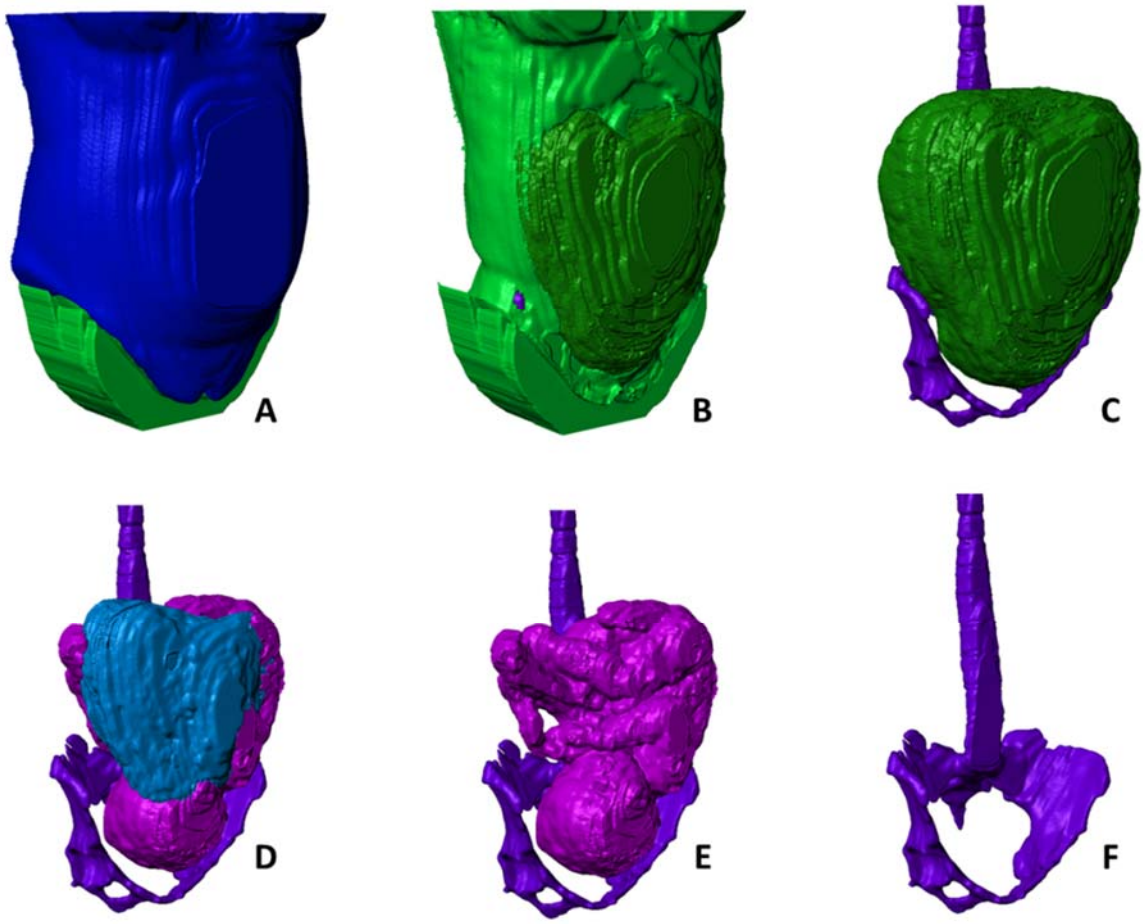

Figure 30 Three-Dimensional Previews of ScanIP Geometry

Figure 30 shows the three-dimensional reconstruction of these two-dimensional tracings as three dimensional organ masks. These organ masks were created using the Preview function under the Mask module in ScanIP, and have not yet been meshed into finite element geometry. They have many smoothed features, but retain some artifacts and lumpiness because the Preview tool is for visualization during the masking process and only approximates the final product of mesh creation.

Creation of Seat Belt

Our method of simulation required the incorporation of a seatbelt shaped region on the front of the abdomen, which could be used to apply appropriate boundary conditions within the simulation. Rather than create a seatbelt that would require mechanical properties of its own, we opted to create a surface set that could function within the boundary condition toolkit provided by our finite element simulation software package. To produce this result, a set of large rectangular masks, shown in Figure 31A were created across the approximate regions where lap and shoulder belts would be located. These masks were assigned the properties of a Non-Exportable Part which allowed them to continue to create surface-to-surface matched meshes with adjacent geometry, but not be exported as geometry themselves. As can be seen in Figure 31B, The beige horizontal region across the waist and the white diagonal region across the upper portion of the abdomen represent the lap belt and the shoulder belt, respectively. As a point of emphasis, these horizontal bars are only in place to select an area on the surface of the skin, and are not included or exported during the meshing process.

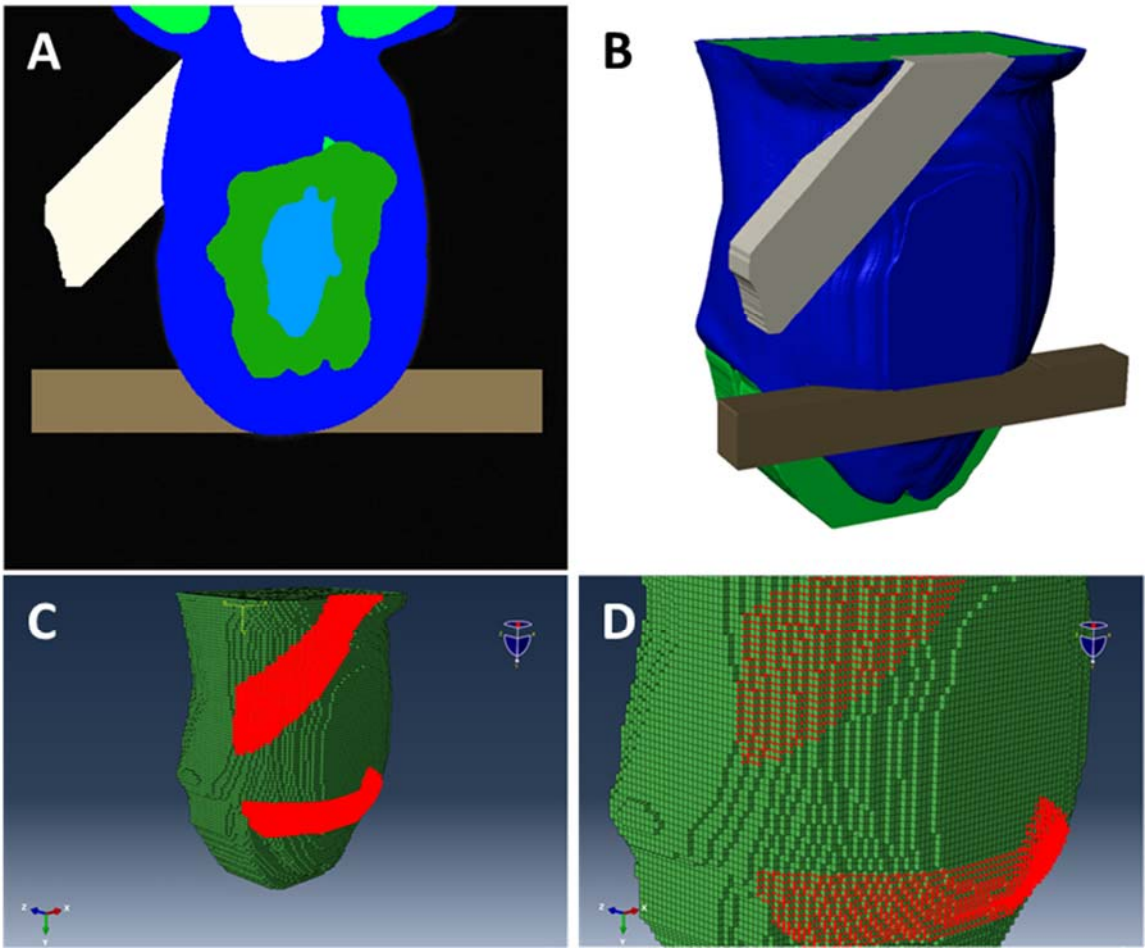

Figure 31 Creation of a Seatbelt for Simulation

Export to Abaqus at Different Refinement Levels

Completion of the masking process allows for ScanIP to export to a large number of file formats for subsequent use in other software packages. Our target software is the Abaqus CAE 6.10-2 (Dassault Systemes, Vélizy-Villacoublay, France) for finite element simulation. ScanIP accommodates the use of their geometry in Abaqus through the use of an input file type (.INP) which imports as a model with many relevant selections and settings arranged. The most important of these is the selection of matched geometric

surfaces for the interfaces between organs and tissues. These surfaces allow for the connection and eventual optimization of all interfacing surfaces, including features such as unfailing tied connections, friction, and failure. ScanIP was configured to export surfaces between all adjacent anatomical features to allow for a complete and continuous connection of all geometry. It is important to note that the meshes created at this stage of our maternal trauma simulation are created as voxel meshes, as opposed to meshes with smoothed surfaces. This is because the tetrahedral elements employed in smoothing of surfaces between Z-stack slices are often elongated or have a high-aspect ratio in at least one plane, and these type of elements often suffer from simulation instability, and typically require increased computing times even when functioning correctly. The instability of tetrahedral meshes is related to their tendency to rapidly increase in aspect ratio under large deformation. As their aspect ratio changes they begin to distribute stresses very poorly due to integration over an increasingly miniscule *dx*. This ultimately leads to incorrectly formulated stress concentrations which can be many orders of magnitude above nearby elements [171, 172]. The voxel meshes uses a mix of tetrahedral and hexahedral elements, but endeavor to create mesh with essentially cubic geometry. Tetrahedral elements assist with certain transitions between element sizes or surfaces, but are not required to smooth or round corners, and are therefore allowed to remain within acceptable geometric limits. These voxel meshes, while arguably simplified, allow for a great deal of detail and accuracy to be obtained while overcoming some of the logistical limitations in our current finite element simulation capabilities.

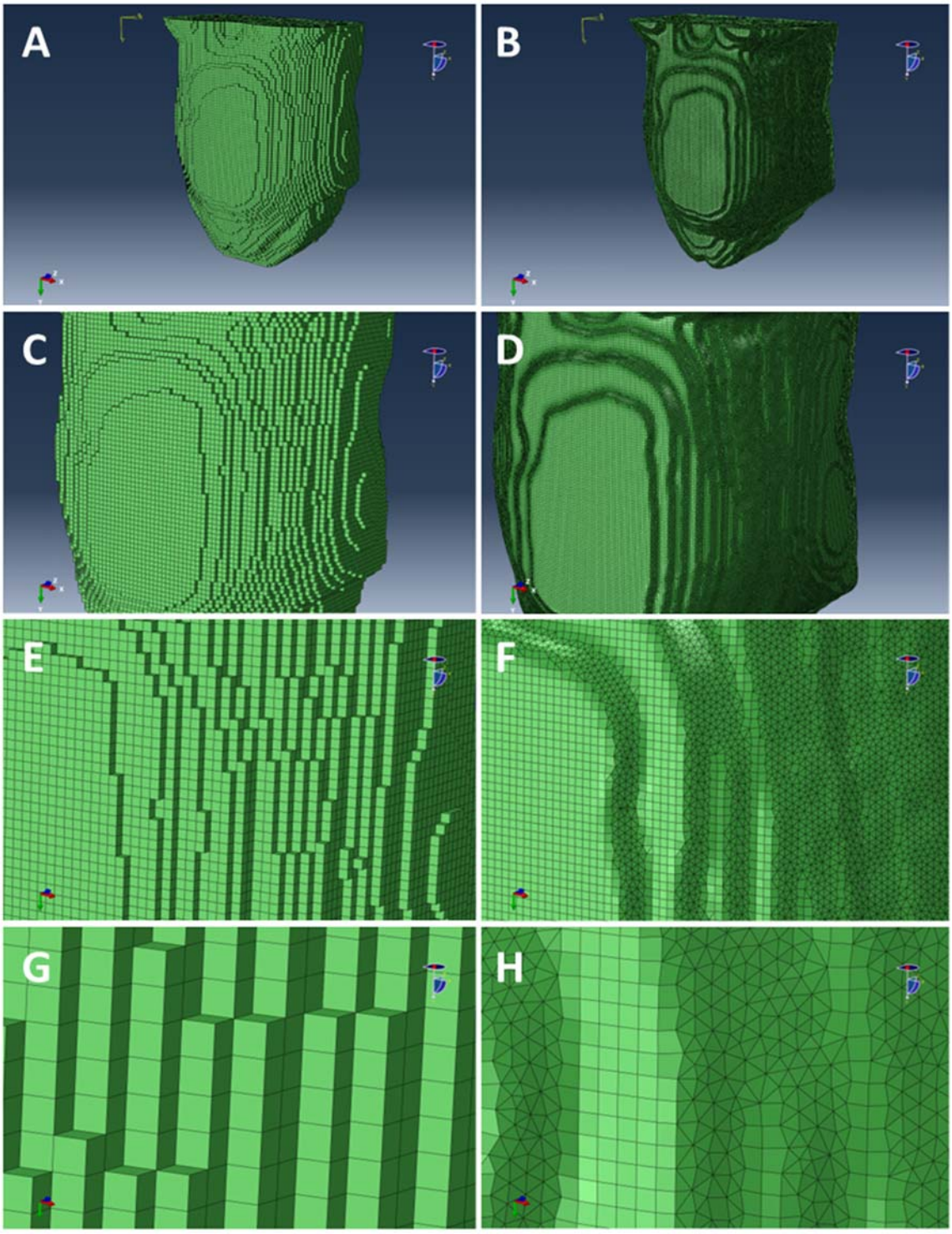

Figure 32 Comparison Between Voxel and Smoothed Meshes

A comparison between voxel and smoothed meshes is shown in Figure 32, where the same base set of masks was used to create a matched set voxel, the left hand column, and smoothed, the right hand column, meshes. Panels E, F, G, and H in Figure 32 do a good job of demonstrating the different approaches to rounding of geometry between the voxel and smoothed meshing processes. Recent research involving traumatic brain injury showed a convergence of solutions between voxel and smoothed meshes created by ScanIP and benchmarked through Abaqus . The voxel mesh returned substantially similar data to the smoothed meshes with a significantly lower computing time, ultimately creating a more useful and efficient tool for simulation. Future research may require the incorporation of smooth surfaces when frictional forces, or other behaviors at the interface between different parts, become a more important portion of this research, but our current simulation approach will use tied surfaces which are well supported by voxel meshes.

As part of the mesh development process, a mesh refinement study is often desired. This process allows the analysts to determine the coarsest possible mesh that can still give accurate results in simulation, to improve simulation efficiencies and computing times. Three levels of mesh refinement were created for our initial review of the geometry. The resampling process is important in voxel meshes because the resampling must take an essentially smooth curve created during mask tracing, and then convert that curve to a lower resolution digitization that will meet the target voxel size in the mesh. The resampled masks must be manually reviewed for consistency and accuracy, as the resampling process may alter certain anatomical geometries or create voids, projections, or other unacceptable features. Once a resampled set of image slices process uses

processes and algorithms which are internal to the software, and creates a mesh in the .INP format, which is easily imported to Abaqus. Selected settings for interpolation methods in our model were kept as Linear and Nearest Neighbor, respectively. The Maximum Target Grid Size for internal features was selected at 32x32x32, the highest setting available in the software. This setting helps mitigate the exponential growth in the total number of elements within a mesh as the size of individual elements decreases by meshing interior elements in large parts with larger elements while continuing to use refined elements near contours, surfaces, and interfaces. The original set of tracings was saved and defined as the master for the resampling process. Cubic resampling was used at two millimeters, the resultantly pixelated masks were meshed to create the mesh with the finest element size, and the .SIP file was archived at this resampling. This process was repeated for cubic resampling values of three millimeters, and four millimeters, which created the medium and coarse meshes, respectively. Figure 33 demonstrates the changes to the tracing masks caused by resampling, specifically the pixilation of smoothed features as a preparation for voxel meshing; the first row is not resampled and the subsequent three rows indicate the three meshes exported at each level of resampling.

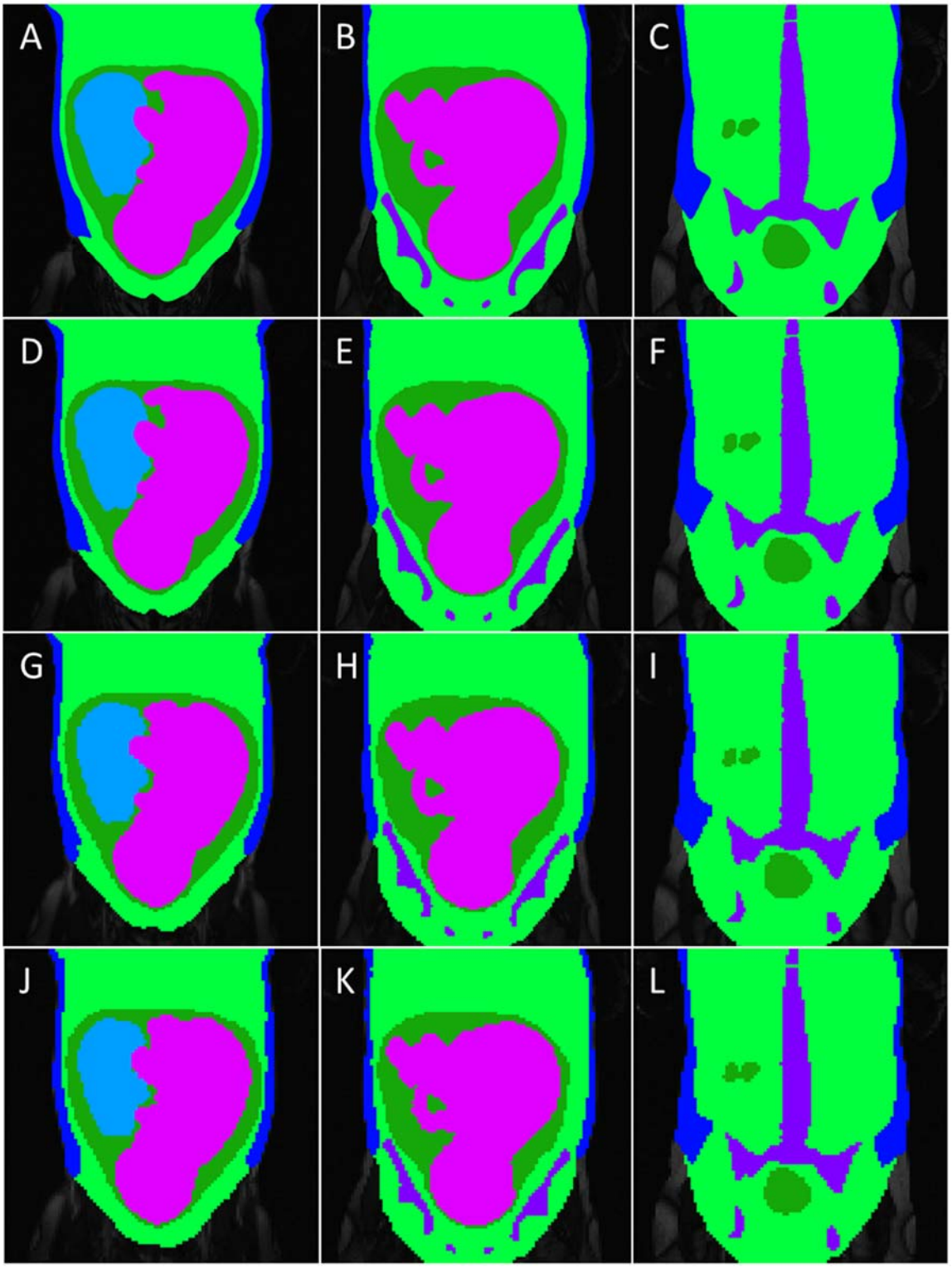

Figure 33 Resampling of Mask Tracings in ScanIP

Table 3 shows the important information regarding the meshes of different refinement levels.

Table 3 Mesh Details Concerning the Mesh Refinement Study

A	Fine Mesh	2x2x2 mm resample		
	Total Nodes	Total Elements	Hexahedrals	Tetrahedrals
Full Model	1,459,813	1,786,354	1,062,724	723,630
Skin	399,390	380,513	306,157	74,356
Muscle	495,491	727,558	352,872	374,686
Uterus	267,087	261,999	197,503	64,496
Placenta	67,191	96,153	46,585	49,568
Fetus	154,815	251,732	104,560	147,172
Bones	75,839	68,399	55,047	13,352
B	Medium Mesh	3x3x3 mm resample		
	Total Nodes	Total Elements	Hexahedrals	Tetrahedrals
Full Model	499,691	535,177	356,293	178,884
Skin	129,398	101,802	94,314	7,488
Muscle	177,057	231,846	127,130	104,716
Uterus	85,895	66,167	60,835	5,332
Placenta	23,182	29,097	16,413	12,684
Fetus	59,242	88,754	40,630	48,124
Bones	24,917	17,511	16,971	540
C	Coarse Mesh	4x4x4 mm resample		
	Total Nodes	Total Elements	Hexahedrals	Tetrahedrals
Full Model	244,527	237,866	170,182	67,684
Skin	63,320	45,304	44,004	1,300
Muscle	87,387	103,873	62,797	41,076
Uterus	40,526	27,047	27,047	0
Placenta	11,596	12,617	8,281	4,336
Fetus	30,462	42,082	21,110	20,972
Bones	11,236	6,943	6,943	0

Figure 34 illustrates the differences in the relative refinements; indicating the increased detail captured by finer elements in Figure 34A-C, as compared with the least refined mesh shown in Figure 34G-I.

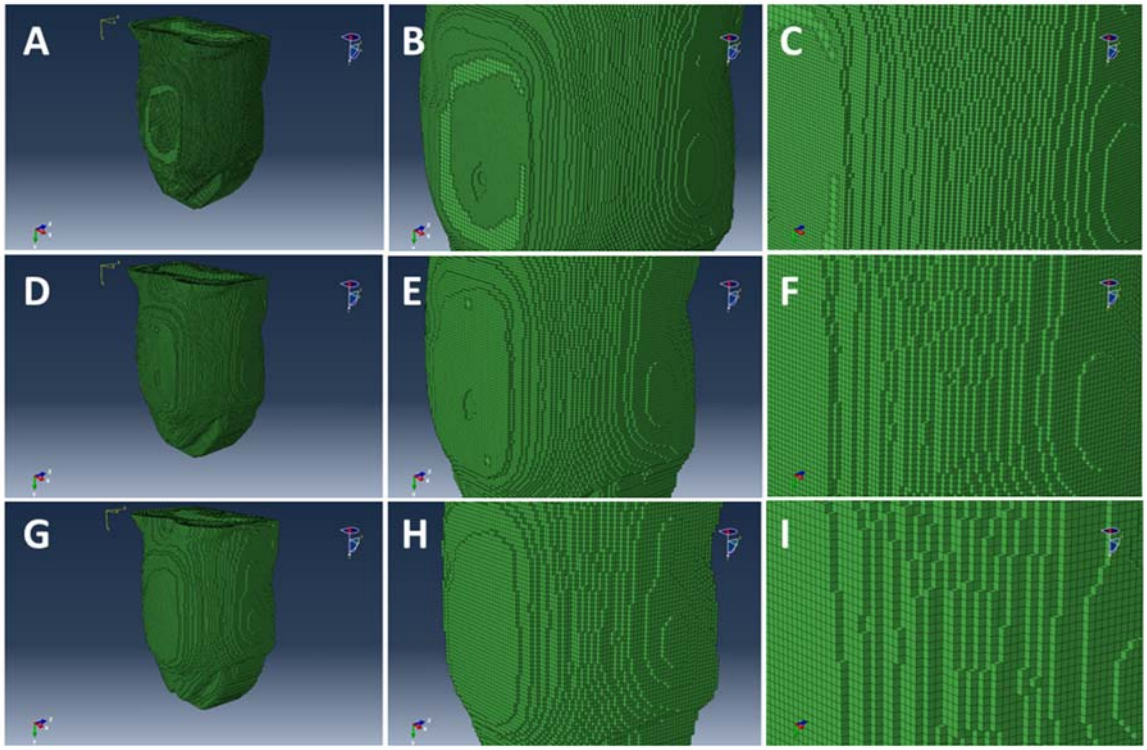

Figure 34 Abaqus Screenshots for Different Levels of Mesh Refinement

These meshes were exported in .INP format to the servers at the Mississippi State University Center for Advanced Vehicular Systems, where they were imported to Abaqus 6.10-2 for use in simulations of automotive maternal trauma. This level of anatomic detail is beyond previously the strongest previously published simulation, which simply used CAD derived geometries.

CHAPTER V

IMPLEMENTATION OF ANATOMICALLY DERIVED GEOMETRY INTO FINITE ELEMENT SIMULATIONS OF AUTOMOTIVE COLLISION

Background

Motor vehicle related mortality in pregnant women is highest in USA and account annually for about 93,000 cases [1]. Additionally, the number of fetal deaths since four decades has increased as much as seven time the mortality of infant deaths [2]. Pregnant drivers involved in vehicular collision can suffer from abruptio placentae [14-19], placental separation [20], uterine contraction[21], uterine rupture [16, 22, 23], abdominal pain or injuries [18, 24, 25], preterm labor [15, 18, 26], pelvic fracture [27], fetomaternal hemorrhage [16, 28, 29], vaginal bleeding, maternal tachycardia [18], "seat belt" injury [29], chest injury, head injury [18], extremity injury, etc. [7, 173, 174]. Other complications include preterm delivery [14, 18], increased risk of fetal hypoxia [30], fetal skull fracture [31], fetal prematurity [15, 30], abnormal fetal heart beat or rate [18, 21], lower fetal weight [7, 30], fetal growth restriction [15] etc. Risk factors such as improper restraints or no seat belt use [7, 14, 32-38], vehicular speed of more than 30 mph [14, 21] and absence of airbags [1, 35, 39, 40], are few of the several reasons for the cause the pathologies mentioned above. Although many animal studies have been conducted to mimic placental injuries during car crash, the anatomy and morphology of the discoid type placenta in mammals is highly unique in its material characteristics [175-

179]. Ethical limitations exist in both human and animal cases due to the very nature or type of the experiment required to simulate the real life condition of a vehicular crash. For these reasons, finite element simulations provide us with a better alternative for analyzing automotive collisions involving pregnant passengers.

Finite element model

One of the first pregnant female models were developed by Moorcraft and is perhaps, the most complete version of pregnant female passenger crash simulation with focus on the placetal abruptions and damage in view [180, 181]. The model includes an entire body, amniotic fluid, uterus, placenta and ligaments, and also includes seat belts, steering wheel, knee bolster, back rest and head rest. This is relevant because most of the fetal or maternal injuries involve steering wheel, air bags or similar external objects[182, 183]. The ROBINA model which was developed by Jansova et al., compared two different types of materials for uterine tissue, elastic-plastic and viscoelastic, and found the viscoelastic model to be a better predictor of maternal injury in a car crash scenario [168]. Neither of the above mention studies had included a fetus in their respective models. Acar et al. (2011) used a similar full body pregnant passenger crash model with uterus and placenta, but their focus was primarily on head and thoracic injuries caused during frontal crashes, with or without seat belts/restraints and airbags [33]. Delotte used a modified Radioss-Humos model in which the abdominal region and fetus were added using MRI scans of a full term pregnant woman, to simulate frontal impact at a speed of 20 km/h [184, 185]. Even at such low speed, strains up to 20% were observed and utero-placental interface was evident. Most of the FEA studies on placenta tissue material is extensively simulated around the experimental setup [186, 187] to replicate the exact

material property of placenta tissue *in silico*. The computation model used in our study was reconstructed from MRI scans of a pregnant women at about 36 weeks in her pregnancy. The average range of pregnancy stage for drivers invloved in vehicular injury ranges from 25-38 weeks [6, 14, 21, 24]. At this stage, the abdominal size is almost at the maximum level, and therefore closer to the steering wheel and at higher risk to the fetus [188]. Additionally, due to the increased size of the abdomen, the seat belt does not fit or harness the pregnant driver as correctly as it should and making female drivers in their last stage of pregnancy even more suceptible to the normal set of possible vehicular injuries.

Over the past forty-five year, the number of fetal deaths due to motor vehicle accident has increased sevenfold compared to the mortality of infants in a crash [2, 40]. Pregnant passengers involed in car crash or accident have shown to have greater incidence of fetal head damage either during child birth or secondary post-natal defects. Fetal accelerations were shown to triple during car crash simulations as compared to the mother, making the inclusion of the fetus in our model even more important. Case studies have reported fetal skull fracture even though the mother has no visible injuries from the crash [31, 36]. In mathematical terms, it is believed that a speed of more than 35 mph and/or uterine tissue strain of $\geq 60\%$ near the placenta is sufficent to cause placental abruption or tear in utero-placental junction and ultimately fetal loss [40, 181, 189] Delotte reported that strain of about 20% at the uterno-placental interface is sufficent to cause placental abruption [184].

Materials and Methods

The boundary conditions used to create a crash simulation were derived from an experimental study which used post-mortem subjects in a sled crash to collect acceleration information for a frontal impact. In this study, the pregnant uterus was removed from the cadaver, and was used to create a ballistic phantom. This uterus phantom was loaded with a set of accelerometers which allowed the collection of crash data. The accelerometers were placed near the locations of the fetal head and the fetal buttocks in the ballistic gel phantom as well as at the wing of the maternal iliac, a portion of the pelvis. The phantom was placed inside the cadaver as though it were the native uterus, allowing for acceleration of the specific areas of interest to be recorded during crash testing. It is worth noting the relative locations of each of these accelerometers in testing configuration. In a normal late term pregnancy the fetus is positioned with the head near or locked into the pelvis near the pelvic inlet, and the buttocks is pointed upwards and near the middle or top of the abdomen. The accelerometer for the fetal buttocks would therefore provide data relevant to the top of the abdomen, and the other two accelerometers would record the accelerations near the groin. The profiles are shown in figure 35.

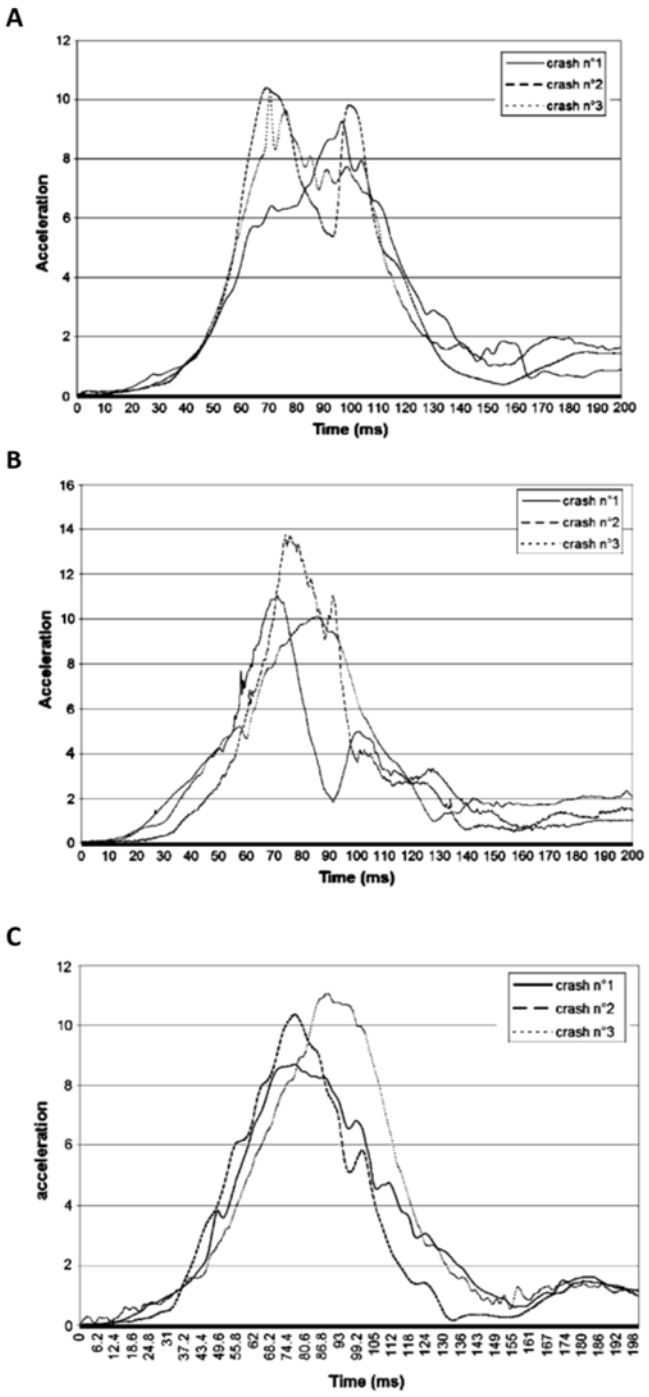

Figure 35 Acceleration Profiles from Post-Mortem Study

The cadavers with accompanying data acquisition capabilities were loaded into a crash sled, which recreates car crashes in an experimental context, and were crashed at 20 kilometers per hour. Data from three post mortem subjects was obtained, and the acceleration profiles of the crash were published as acceleration, in accelerations of gravity, versus time. To incorporate these profiles into our model, we had to create tabular versions of the profile graphics available in the publication. This was accomplished using the DigiData (Thunderhead Engineering, Manhattan KS) software packages, which allows a user to capture an image of a graph or chart from publication, and then trace points onto the image. These points are used to create a file that can export as a text or spreadsheet for further uses. The tracing process was repeated for all three curves amongst each of the three regions, fetal head, fetal buttocks, and maternal iliac, to recreate the nine recorded acceleration profiles. Once the tabularized data was transferred to Excel, a custom averaging and interpolating software tool created by collaborators at the Center for Advanced Vehicular Systems was used to convert the hand selected points along the graph to 300 evenly spaced points. This is convenient for subsequent use in simulation, so that timing of changes occurs at regular intervals, instead of what are potentially inconsistent intervals when selected by hand. The profiles were averaged within regions to create three characteristic acceleration profiles for each of the three regions during a twenty kilometer per hour crash. These acceleration profiles were then integrated within the tabular format to create a set of corresponding velocity profiles, which will be used in this study to create our crash simulation. Integration was performed by simple kinematics:

$$V_n = V_{n-1} + \left(\left(\frac{(A_n + A_{n-1})}{2}\right) \times (t_n - t_{n-1})\right) \quad (5)$$

Where V_n is the velocity of the current time point, V_{n-1} is the velocity of the previous time point, initialized at twenty kilometers per hour for velocity at time zero. A_n is the averaged recorded acceleration for the current time point, and A_{n-1} is the averaged recorded acceleration from the previous time point, initialized at zero for time zero. Finally, t_n and t_{n-1} are the current and previous time points, respectively. Essentially this formula averages the instantaneous accelerations of two adjacent time points, multiplies that acceleration by the elapsed time to obtain a change in velocity for that time, and adds that change in velocity to whatever the existing velocity had been at the beginning of the time period of interest. This formula was implemented in Excel so that a simple copy/paste converts the entire tabular acceleration profile into the corresponding tabular velocity profile. The velocity profiles were then normalized so the starting velocity, which is twenty kilometers per hour in our initial testing but should be easily adjustable, would be a unitless one. This allows for the coefficient term in the Abaqus software package to be used to assign or change the initial velocity and corresponding profile, rather than adjusting the entire profile in future studies. It can be seen in figure 36 that the acceleration profile for the maternal iliac and the fetal head begin to drop approximately twenty milliseconds before the fetal buttocks' acceleration profile. This makes sense if one imagines the forward rotation of the head and torso during a motor vehicle collision. An additional profile was created for use in simulation without this rotational behavior, by simply averaging the curve for the fetal buttocks and curve for the fetal head. The normalized profile was then exported to a tab-delimited text file, which is easily pasted into a Tabular Amplitude in Abaqus CAE.

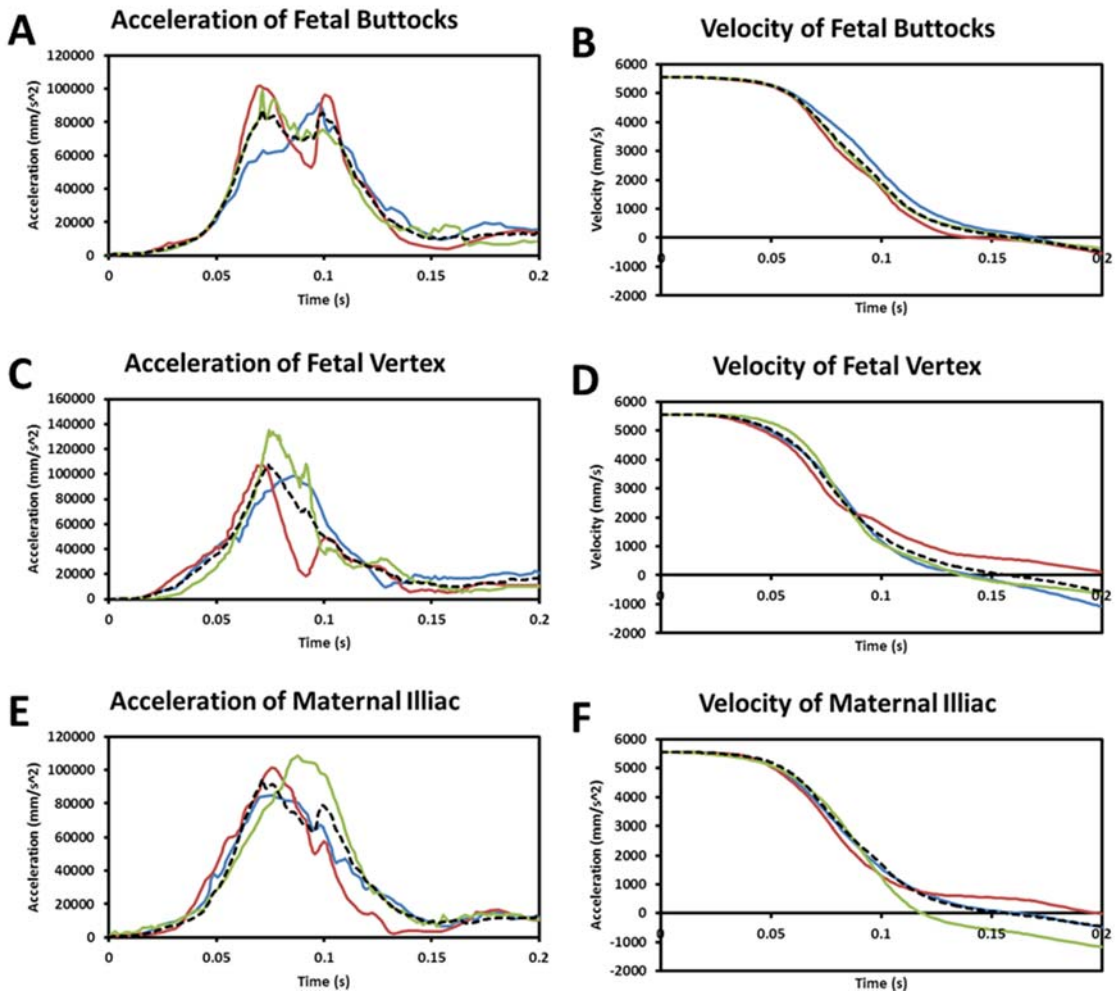

Figure 36 Digitized Acceleration Profiles

To begin the implementation of our simulations, the input files previously described, .INP file type exported from ScanIP, were imported to Abaqus using the File>Import>Model menu option. This processes and opens the ScanIP geometry as an orphan mesh with all of the features assigned for export. This includes a large number of node sets which can be used to define the interactions between surfaces and assign other capabilities based on node sets such as kinematic constraint of boundary conditions. The default import process created an initial step type of Static General, which is not

appropriate for our planned implementation and was changed to Dynamic Explicit. The step length was set to 0.14 seconds, the length of the acceleration profiles, and the number of intervallic field output was set to forty, providing forty data points across the simulation instead of the default of twenty. This required the deletion of the default interaction properties between surfaces, which import as Interaction Properties and Contact Pairs were converted to Constraint - Ties. This Tie occurs between two sets of corresponding nodes on the surfaces of adjacent parts. The two node sets occupy the same three-dimensional space, and assignment of a Tie between them essentially prevents the two features from becoming separated throughout the simulation. This is obviously a simplification for certain tissue interfaces, as there may be an almost limitless number of possible mechanical behaviors occurring between anatomical features within a human body, most notably being friction between unattached surfaces or failure of a tissue structure connecting two surfaces. Such Ties were created for each interfacing set of nodes, with a Master to Slave definition set with the following priority order for assignment of the Master Surface relative to Slave Surface: Skin, Muscle, Bone, Uterus, Fetus, Placenta, such that where two organs interface, the earlier organ in the list is assigned as the Master Surface and the later organ is assigned as the Slave Surface.

Material Properties for each tissue were assigned as Linear Elastic materials, plus the required Density parameter. The Table 4 displays the material properties used for each material. The values used for placenta were based on our previous study of the biomechanical properties of placenta. The tangent modulus of the linear region of the true stress vs. true strain plot from our 0.1 strains per second, the highest strain rate tested, was used as the Young's Modulus value for placenta. The mechanical properties of uterus

were obtained from a previous study performed by researchers at the Virginia Technical Institute where samples of uterus from term human pregnancies were mechanically tested. The DigiData software package was used to tabularize the uterus stress strain curve and the slope of the linear region was calculated and implemented as the Young's Modulus for Uterus. The values used for Skin, Bone, and Muscle were obtained from available literature. Poisson's ratio and density for placenta and uterus were not previously reported, and so the values for muscles were used as an approximation (See Table 4).

Table 4 Material Properties Used in Simulations

	Young's Modulus (MPa)	Poisson's Ratio	Density (Mg/mm^3)
Skin	16.7	0.42	1.04E-09
Muscle	110	0.45	1.10E-09
Bone	15000	0.23	2.00E-09
Placenta	0.122	0.45	1.10E-09
Uterus	5.881	0.45	1.10E-09
Fetus	110	0.45	1.10E-09

To apply the boundary conditions within our simulation, a predefined field of twenty kilometers per hour was set for the entire model to recreate the test conditions from the post mortem study. The first step of the simulation, which was set to last 0.14 seconds or the length of the recorded acceleration profiles, was implemented with a pair of Velocity Boundary Conditions assigned to the seatbelt regions. These Velocity Boundary Conditions were assigned to the node sets which corresponded to the portion of the skin which contacted the shoulder belt and lap belt, respectively. Each boundary

condition was assigned a value of -5555.56 millimeters per second in the Z-direction, which is equivalent to a forward velocity of twenty kilometers per hour in the context of our model's coordinate system and the default unit system currently in use. The previously created tabular velocity profiles from the fetal buttocks and the fetal head were used to create Tabular Amplitudes for the shoulder belt and lap belt velocities, respectively. This method of assigning boundary conditions multiplies the tabular value by the initialize value for each recorded time step, and with profiles decreasing from 1.0 to slightly below zero, this method recreated the drop from traveling speed through the impact and includes a portion of the recoil.

For each subsequent iteration of or simulation throughout the time of this study, the simulation was prepared in the Abaqus CAE environment, including a Job module with the appropriate name and simulation number., and saved as a .CAE file type as an archive for future reference and reuse if desired. Once archived, the Job module was used to create an input file, .INP file type, for use with the cluster computing resources necessary for these simulations.

Because of the large size of our models, the simulations required the use of the cluster computing capabilities available through the Missisippi State High Performance Computing Collaboratory. These cluster computers allow for large finite element scripts to be distributed across a large number of processing nodes, each of which is equipped with an array of cluster processors. This parallelization process greatly reduces the real world time required to complete extremely long computational simulations by dividing the work amongst many separate processors, while endeavoring to keep the total computational time required for and managing the cluster low enough to make this

division of labor advantageous. The parallelization process is handled by using a Perl script created by the Center for Advanced Vehicular Systems entitled Abaqus Parallel, and works within the Portable Batch System (PBS) scripting process to allow users to easily scale the number of nodes and processors assigned to their script. The cluster computers available for use in this study were the Raptor cluster, which allows for use of up to 64 processors across 16 nodes, and the Talon cluster, which allows for up to 192 processors distributed across 16 nodes. Because these cluster computers are extremely large and service a large number of researchers, and are subject to issues of availability and maintenance, both clusters were employed throughout the course of this study. Additionally, because of the constraints for available licenses for Abaqus, and the consideration of other researchers, the maximum number of processors was only employed if there was a belief that the completion of a simulation was limited by computational capacity. Otherwise, a lower number of processors were used whenever possible.

To load a finite element simulation into the queue for one of the cluster computers, a folder must be created containing: the .INP file which includes the overwhelming majority of the relevant data, the PBS script which interfaces with the cluster's management and organizational systems, and the abaqus-parallel script which manages the distribution of the simulation data amongst the separate computational domains. These folders were created within the CAVS file systems, and organized to allow the easy access of earlier simulation as simulation development progressed. Once the folder was prepared, the script was run through a secure-shell interface by logging in to the cluster computer's login node, defining the current working directory as the folder

containing all of the simulation tools. The .PBS file is submitted to the cluster's job queue, which runs the simulation once a sufficient number of nodes and software licenses become available. It is this queue step that requires restraint when increasing computational time, as the institutional costs and impacts on other researchers using these cluster resources can be problematic when excessively long, large, or a large number of concurrent scripts saturate the nodes or licenses available to a specific cluster. As the simulation progresses, individual output frames are created at the defined time intervals. These output frames are the time points at which the simulation data such as displacement, velocity, acceleration, stress, and strain are recorded. Once a simulation has completed its run on the clusters, all the important results and performance data for the simulation are stored within the defined folder for review and analysis.

Upon completion, the Output Database, .ODB file type, for each simulation was reviewed in Abaqus CAE by opening the database in the Results window. The Results toolkit in Abaqus CAE can be used to visualize loading or deformation throughout the simulation by applying color contours which correspond to mechanical parameters, and by animating the movements of the geometry during the simulation. These results essentially create a video of the simulated crash, with a rainbow of color coding that corresponds to the stress, or strains experienced by the colored region. Data from each simulation were viewed in this results format for the initial qualitative assessment of the simulation results.

Python Script to export parameters for Excel Analysis

Quantitative analysis of simulation data is the most important aspect of the simulation process as it provides the most detailed information about the loading and

deformation throughout the simulation. The data is contained within the Output Database file once a given simulation has completed. These databases are extremely large and contain detailed load and deformation data for each node and element at each selected time point, which in the case of our models can be tens of millions of data points. For this reason, the export of important mechanical data was achieved through a Python script designed to average a selection of mechanical simulation results from a selected region of nodes and/or elements, and export that data in a tab-delimited text format that can be easily analyzed in Excel. The mechanical results selected for export in these simulations were: stress (S11, S22, S33, S12, S23, S13), strain (LE11, LE22, LE33, LE12, LE23, LE13), acceleration (A11, A22, A33), and velocity (V11, V22, V33). The regions of interest were the f etal head, the fetal buttocks, and the placenta, since the fetal head and fetal buttocks are the regions which should ultimately be compared with the original experimental data, and because the placenta and fetal head are the primary regions of injury in maternal trauma. The data for a given simulation was mined by the Python Script and exported to Excel for detailed analysis.

Results

The results from the comparison of our tilting and non-tilting simulation are shown in figures 37, 38, 39, and 40. Figures 37 and 38 show the stress and strain profiles across the 200 millisecond simulation for the fetal head and the placenta, respectively.

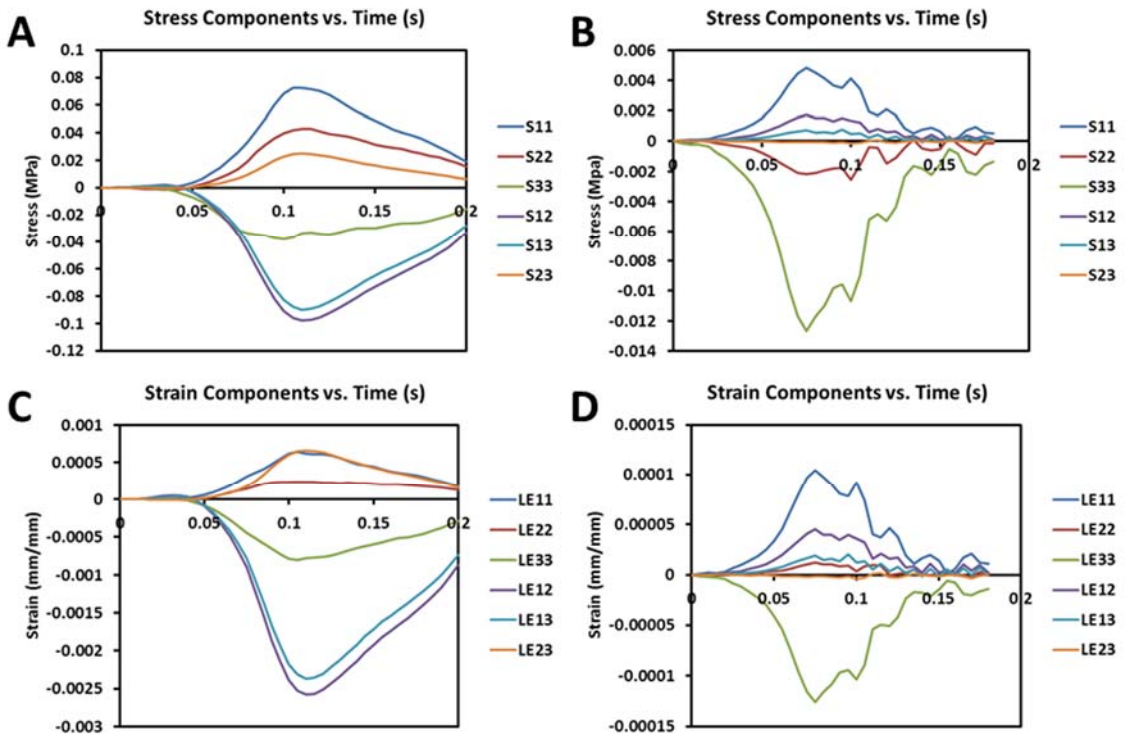

Figure 37 Stress and Strain Components in the Fetal Head

These profiles show that the tilting simulation has a much smoother and more stable loading profile, while the non-tilting simulation shows a large amount of unstable behavior, which is most likely the result of insufficient viscosity and internal friction to dissipate such effects. The peak stresses and strains in both simulations occur near 110 milliseconds, but the values are much higher in the tilting simulation as compared with the non-tilting, indicating that the non-tilting is shielding some of the stress effects. This may be the result the different orientations caused by tilting, or it may simply be an artifact of erroneous wave and momentum propagation from incorrect viscous damping effects.

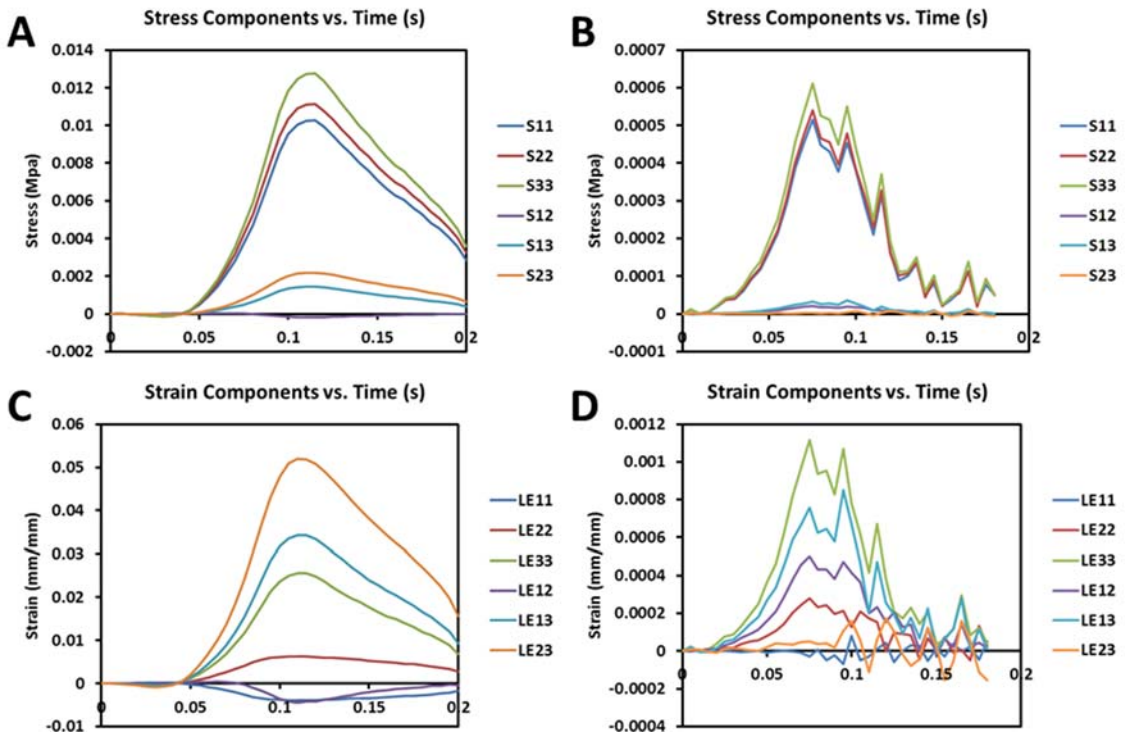

Figure 38 Stress and Strain Components in the Placenta

Figures 39 and 40 show pressure stress contours for pressure stress. Figure 39 shows the stress in the fetus, and the placenta, the two primary regions of damage, and show that both structures experienced complex multi-axial loading in the tilting simulation, but that there was a much lower level of load experienced by the fetus or placenta in the non-tilting simulation.

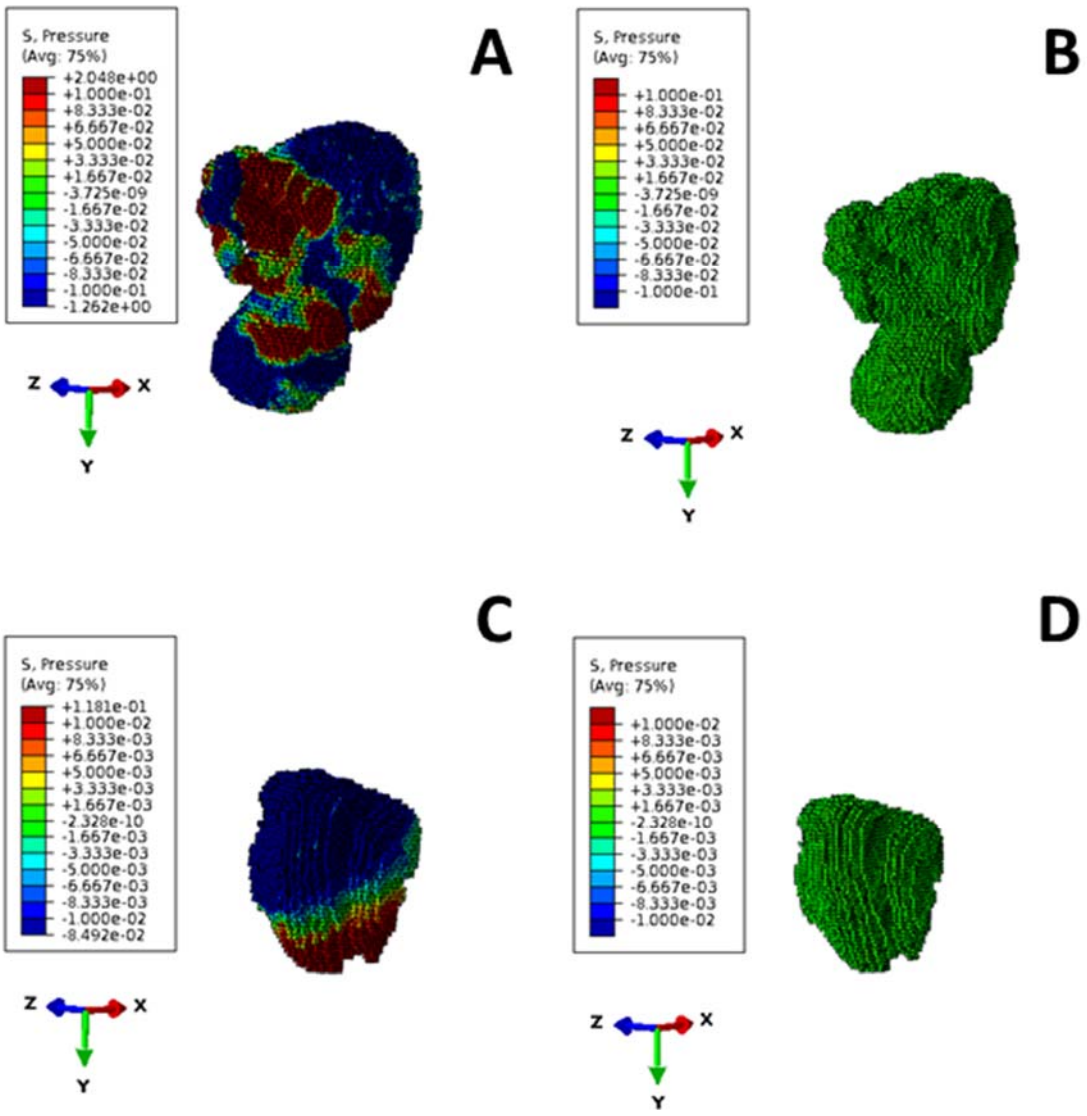

Figure 39 Peak Stress in Fetus and Placenta

Figure 40 shows a similar trend for the entire model, shown in its complete form, and with a cross-section to expose interior anatomy. Figure 40 shows a large reaction due to the seat belt boundary conditions in the tilting simulation, and a relatively small reaction in the non-tilting simulation

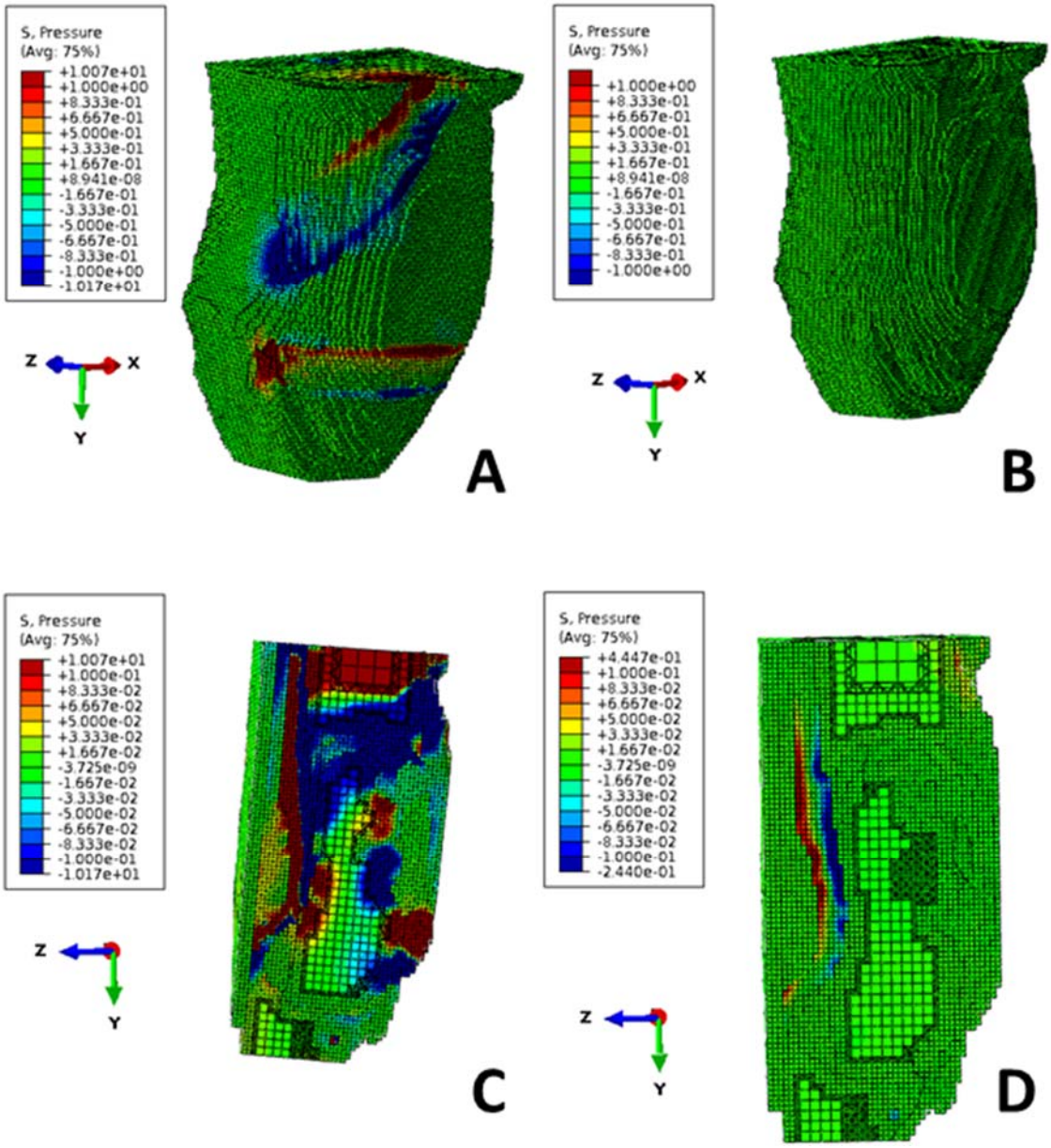

Figure 40 Peak Stress in Full Model and Cross-Section

Figure 41 and 42 show kinematic behaviors for the fetal buttocks and the fetal vertex, respectively. The profiles in figure 41 show that there is a strong correlation between our simulation results and the previously published experimental acceleration data, which was used to drive the model. This correlation is very strong early in the

model, but once the peak acceleration has been reached the propagated waves appear to be causing local acceleration instabilities. Fortunately, the net acceleration effects of this appear to be negligible, as the acceleration integrated from the recorded velocity does not have such uncertainties, indicating that the velocity remains stable despite the micro-accelerations.

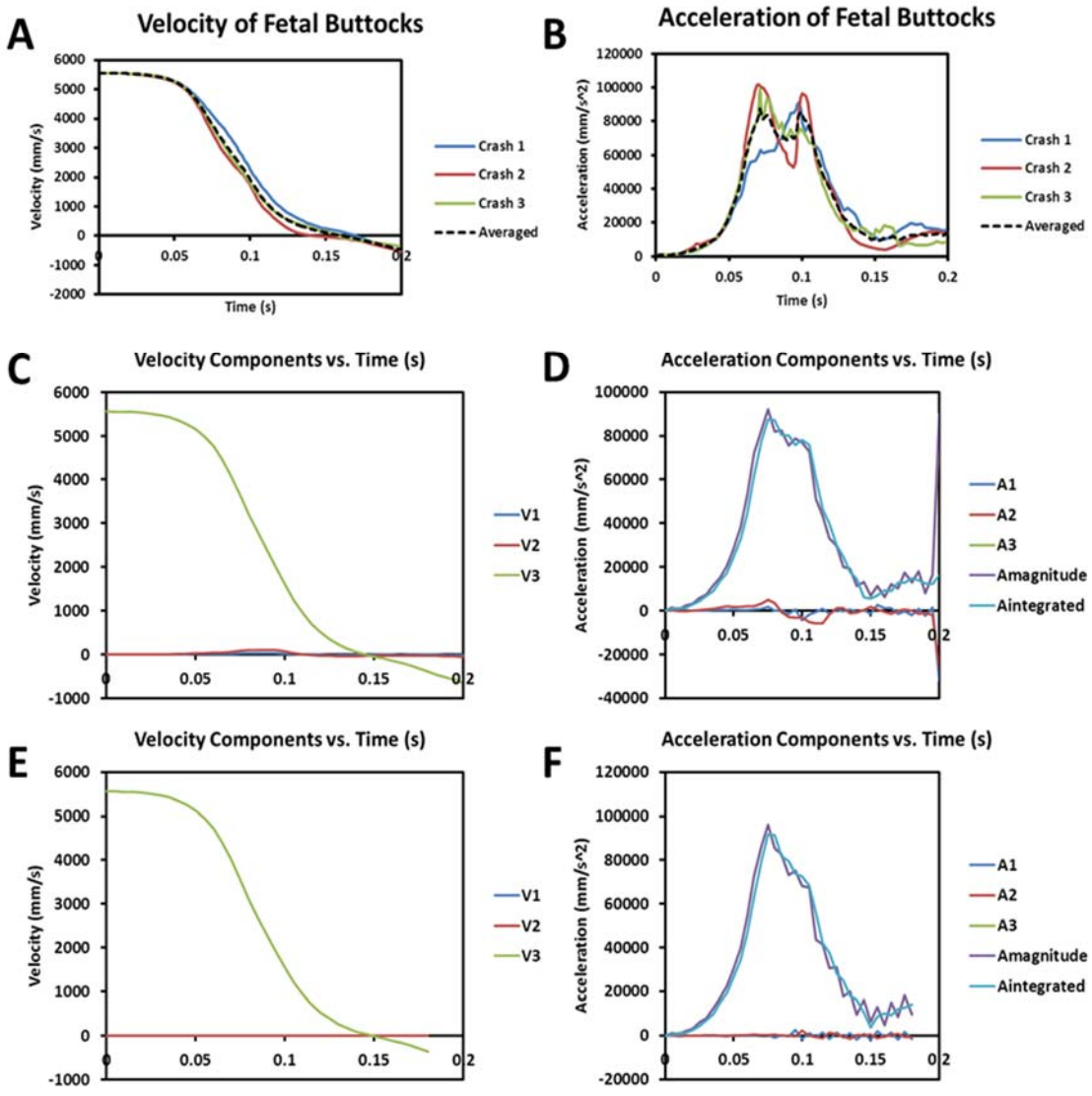

Figure 41 Kinematics of the Fetal Buttocks- Comparison of Tilting and Non-Tilting Simulations

A similar trend is seen in figure 42 where the accelerations for the fetal vertex show many peaks, but the integrated acceleration is stable and smooth, corresponding more closely to those previously reported acceleration profiles.

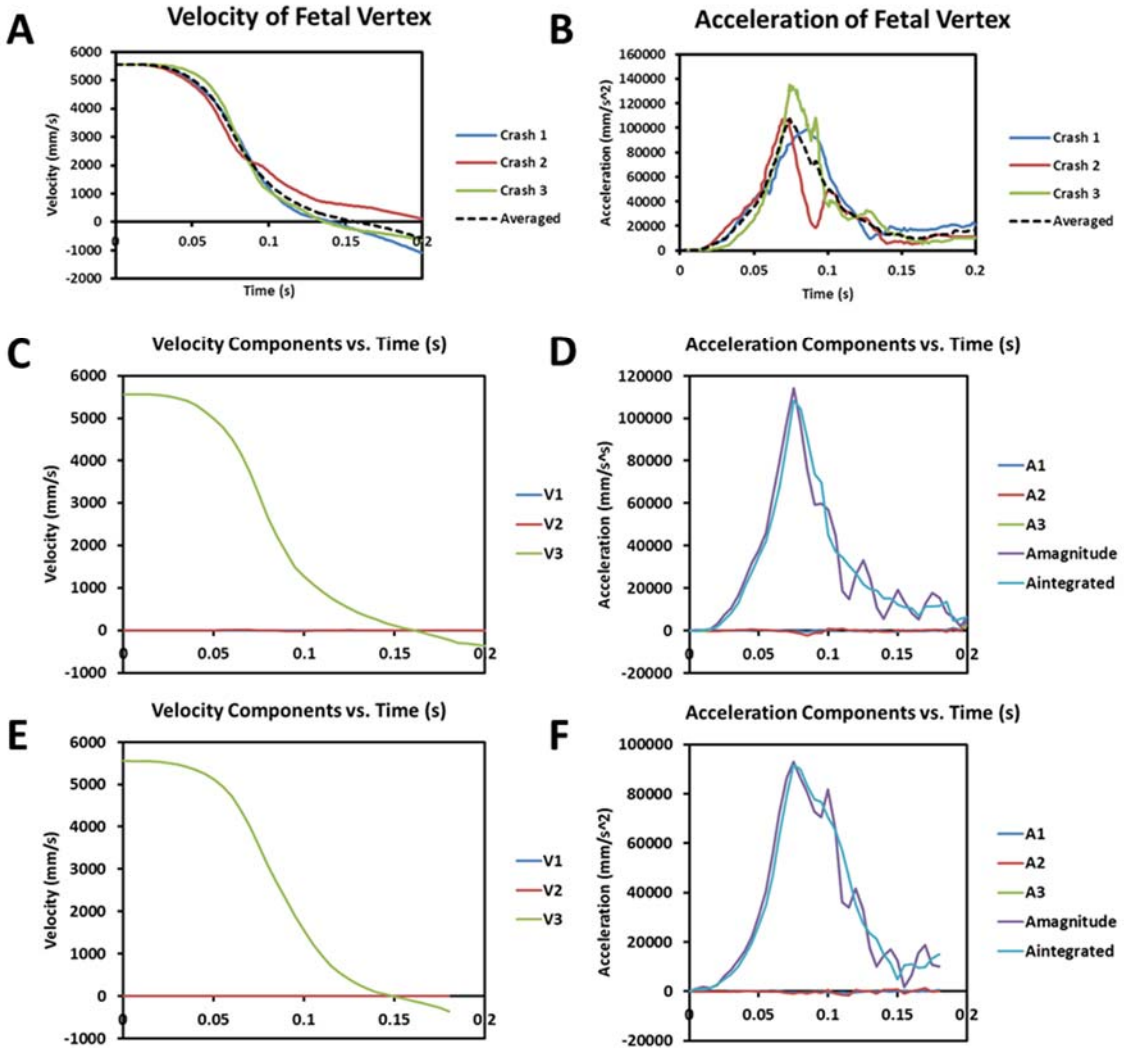

Figure 42 Kinematics of the Fetal Vertex

Figure 43 shows the results of stress in the direction of loading (S33) versus time, compared across three increasingly detailed meshes. The data indicates that each loading profile is within the same order of magnitude, and very similar in trend. Small differences in amplitude are observed.

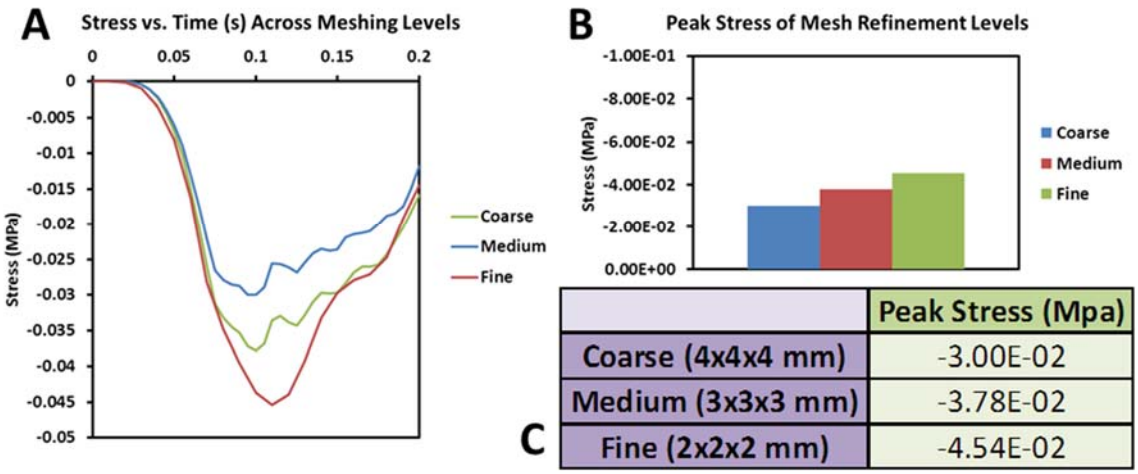

Figure 43 Stress and Strain Components of the Fetal Head

Figures 44 and 45 display the pressure stress contour plots for the fetus, placenta, full model, and cross-section of the full model. The consistency of the general trend is excellent, and the meshes appear to generally agree.

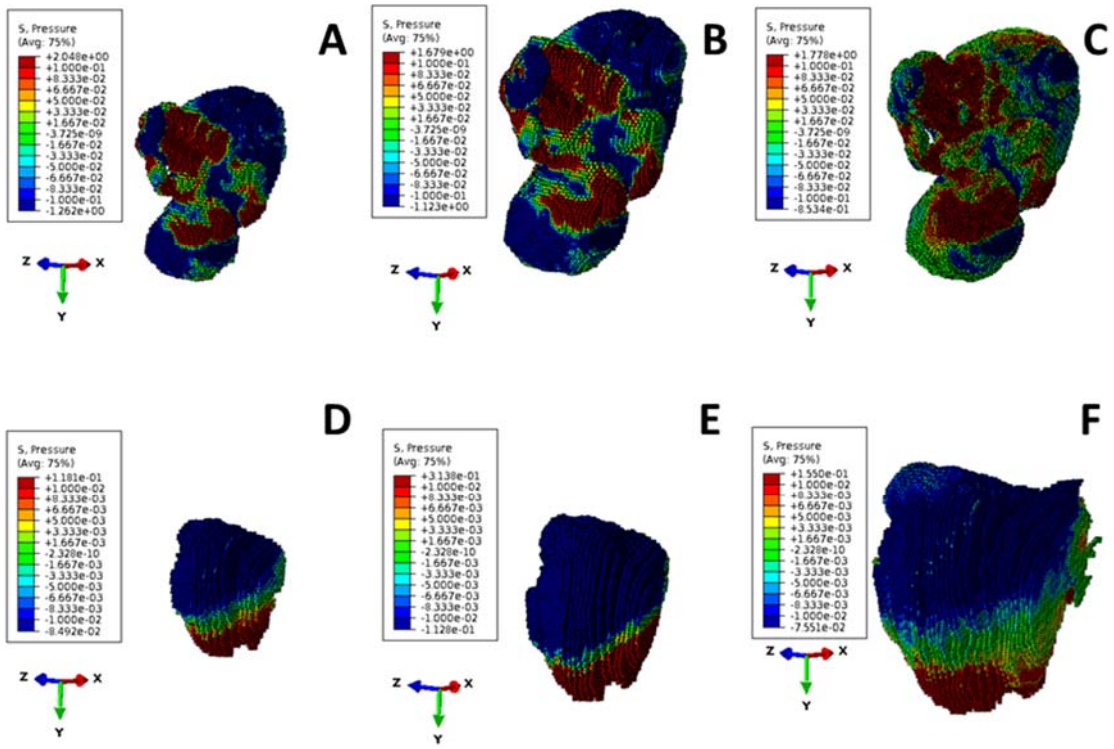

Figure 44 Peak Stress in the Fetus and Placenta

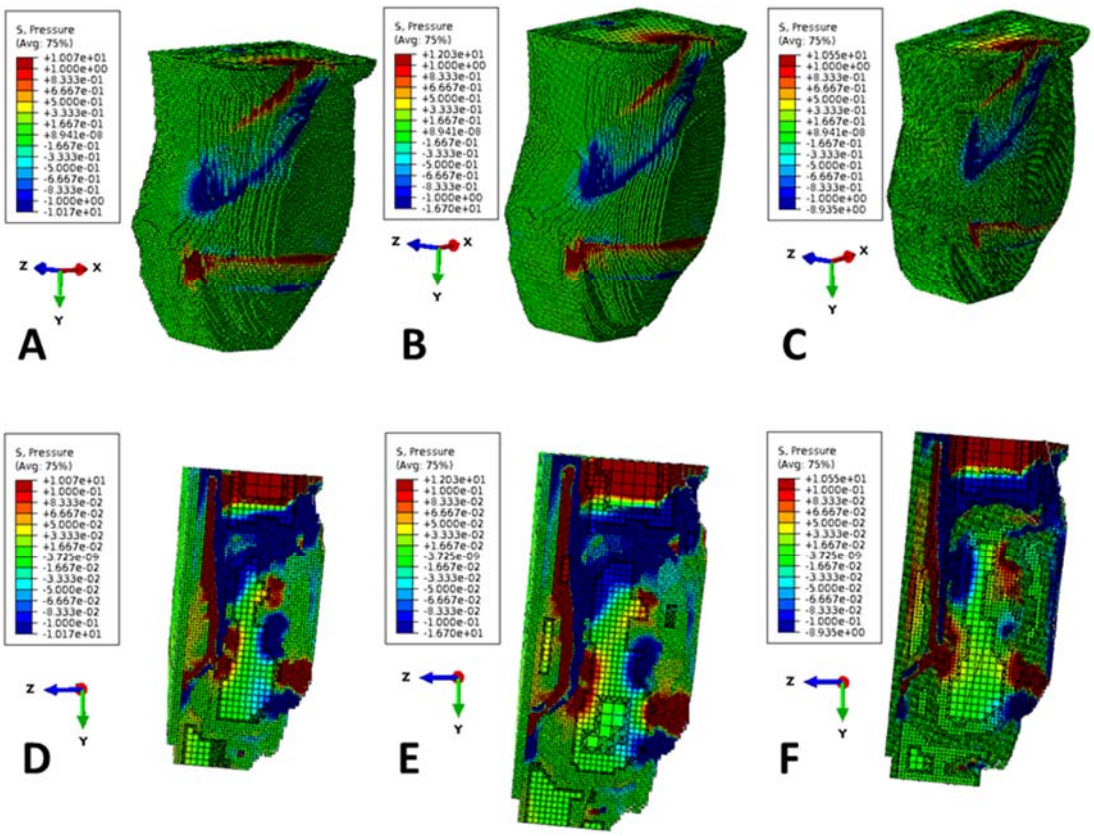

Figure 45 Peak Stress in the Full Model and Cross Section

Discussion

The process of extracting the post-mortem crash test data and incorporating that data into our simulation was extremely successful. The data sets chosen to drive the simulation were the fetal vertex and the fetal buttocks because the accelerometers measuring these regions were closest to the seatbelt regions, which apply the boundary conditions. The averages of these two regions have distinctive acceleration profiles, with the fetal buttocks showing a double acceleration peak as compared with fetal vertex profile which was a smoother peak with a few small bumps. It is important to consider that these acceleration profiles have many complex inflection points, but because the

value is positive they correspond to a steady drop in velocity. This means the general movement can still be considered to be something very similar to a logistics curve, which then transitions into a linear region of velocity decrease as the body comes to zero velocity and reverses direction. The velocity profiles derived from these accelerations are also interesting, because the fetal vertex begins to drop in velocity approximately twenty milliseconds earlier than the fetal buttocks indicating that there is some forward tilting related to this crash, as the resistance of the lap belt, and possibly the friction due to the seat. This aspect of the profiles that the regional specificity of the forces applied to the pregnant women in an automotive collision plays an important role. Because there are only three data sets of this type available the averaging process has captured some interesting trends, but has not yet reached the point of a fully smoothed curve. If more post-mortem data sets such as these were available for inclusion in the averaging process, a more correct characteristic curve could be understood. More data of this type would also provide more knowledge about the frequency and types of peaks in the acceleration, which may cause more damage than a smoother application of load due to short term spikes in local stresses and strains. The use of a series single-crash acceleration data in simulations could be used as an alternative to evaluate the effects of these very complex profile behaviors.

The use of the seatbelt as the driving region was based on assumptions of the free-body diagram which describes the pregnant women involved in an automotive collision. Essentially, the major forces applied to a crash occupant were assumed to be the seatbelt forces, separated into the lap belt and the shoulder belt, and the friction between the crash occupant's legs and buttocks, and the car seat. The frictional forces due to the legs were

not considered at this time for several reasons, the foremost of which is a lack of data to drive this interaction. If considered from a theoretical standpoint, the accelerations in the direction of automotive travel reach approximately ten times the acceleration of gravity at their peak in this crash while the friction due to the seat would be driven by only a single multiple of gravity, and then mitigated by friction coefficients. This is not to say that the forces caused by the seat are truly negligible, but they are not the forces which dominate the crash at the level of the seatbelt. It is also important to consider that the twenty kilometer per hour crash considered here is not a very fast collision; at only about thirteen miles per hour this is much slower than many head on collisions. This means that many real world crashes have even greater acceleration profiles and will continue to scale as collision speed increases, while the normal force driving seat friction will not increase very much, if at all, with an increase in collision speed . For these reasons, we believe that the seatbelt conditions were appropriate and successful in our simulations. As stated there is a difference between when each of the two profiles begins to apply its effects to the crash. There was also a profile created which was averaged between the two regions as a means of simply applying the general translational motion as a simpler case. This ultimately translated into a tilting and non-tilting simulation, both of which may useful for different aspects of study or different permutations of our initial simulation. The comparison between the tilting boundary conditions, which used two separate profiles to define the seatbelt effects of the crash, and the non-tilting boundary condition approach, which used an averaged value to drive the velocity boundary conditions defining the seatbelt, indicated that the tilting boundary conditions yielded considerably more stable results. The plots stress and strain versus time in the tilting simulation were characterized

by a smooth and steady progression without abrupt transitions. These plots for both placenta and fetal head were chracterized with a fairly steep and linear increase, followed by a smooth transition towards a rounded peak, and then a steady and relatively linear decrease. In comparison, the non-tilting simulation begins with a steady a similarly steep and steady increase towards the peak, followed by a somewhat similar transition and reduction, but with many abrupt discontinuities and several somewhat subtle but very different responses in specific components of stress and strain. This more volatile material response is believed to be caused by some artifacts related to wave propagation within the model. As the model used linear elastic material models, combined with the default ABAQUS parameter for viscosity and the dissipation of momentum, there is a very real possibility that these artifacts will become negligible when more realistic material models are incorporated. Nonetheless, the current application of the non-tilting simulation appears less successful than the tilting simulation which is arguably more complex. The specific differences in stress and strain components have some very important implications. These changes in values are most likely the result of the tilting rotation of the model, which leads to a change in element orientation relative to the global coordinate system which drives the boundary condition. This means that the same elements may experience extremely different local loads due the change in orientation of the entire model. This dependency on model orientation relative to the loading direction is particularly important in placenta where the organ is essentially arranged in a disc which has been wrapped around the front and right-hand side of the uterus. If considered as separate regions, the portion on the front of the uterus would likely be pressed into the uterus under a mostly compressive load, while the portion along the right-hand side of the

uterus would be likely to experience a large shear and tensile force, compared with the compressive behavior of the front portion. This behavior is observed with differences in the dominance of the different stress components between our tilting and non-tilting simulation data. These two sets of simulation data offer some idea of the range within which these trends may lie in real world collisions, where the amount of tilt may vary greatly among passengers. For this reason, we believe the amount of tilt which occurs in different speed crashes, and the ultimate consequences of these differences, continues to be an important research question. It should also be considered that the shape, location, thickness, and distribution of the placenta are different in every pregnancy and also change throughout the pregnancy. This means that different pregnancies may be more or less susceptible to trauma due to the age of gestation or the location of the placenta. Ultimately, the data presented here concerning the tilting behavior of the collision and the resultant changes loading are an exciting observation, but much more study is needed to fully understand this highly complex behavior.

The mesh refinement study shows that there are some subtle differences between the size of the elements in our meshes. Each mesh yielded similar results, with difference of less than an order of magnitude, and very similar trends. It is worth noting that the practical level of mesh refinement has been very nearly saturated with our current fine mesh. The simulations with this mesh require a massive amount of computational time and suffer from some parallelization instabilities due to the extremely large file sizes produced. This issue highlights the continued need for improvements in the tools available to our field. As computational technologies improve, such distributed computing processes will continue to empower simulations with more detail and

accuracy. Despite the difficulties related to file sizes, we believe the finest mesh is the best one for use in future studies.

Limitations and Future Goals

There are limitations to this study, as is always the case in simulations, which are important to consider. The most obvious of these is the use of isotropic linear elastic material properties. These materials properties are known to be very useful in materials like metals, but do not capture a significant portion of the important behaviors which have been widely characterized across biological materials. The inclusion of more complex behaviors such as stress state dependency, strain rate dependency, hyperelasticity or hyperelastic-like responses, and the combined effects of viscous, plastic and elastic material responses, is a major area of research and significant progress in the modeling of biological materials. As more advanced material models become available, either through our own continued research or that of the other groups contributing to this much needed area of study, these may be incorporated and studied using the tools created through our research to date. While the ultimate goal of simulation is to exactly mimic all real world behaviors, I believe the most important material behavior to begin considering is stress state dependency. The data presented demonstrates that there is a complex trend of multiaxial loading throughout an automotive collision, and the ramifications of a stress state dependent set of material models for all tissues is extremely significant. This is especially important when contrasted with the earlier stress state dependency studies conducted on placenta, where the mechanical resistance varied by as much as orders of magnitude between stress states. Rate dependency will also become a very important aspect of simulation as the simulated collision speed increases. Beyond material models,

the lack of amniotic fluid and the use of computational fluid dynamics is a limitation concerning placental and fetal loads. The addition of the amniotic fluid is most likely the greatest anatomical limitation in our study, and will be the next major area of focus, with regards to geometry improvement, as our groups pregnant trauma simulation efforts continue. The incorporation of our pregnant abdomen into a full body simulation would also be very valuable in assuring that the context of our simulation is valid; without this it is somewhat difficult to assert that the use of just the abdomen and pelvis, essentially the fetus and surrounding anatomy, is a completely acceptable simplification.

With regards to the use of ABAQUS parameters and modeling tools which represent limitations in our current approach, the interface between different organs and tissues being defined as a tie is a major simplification. The majority of surface interfaces in the body are not well characterized by a simple tie, and such an interaction will always lack the ability to capture failure behavior at higher loads. The incorporation of frictional behaviors to capture the sliding of organs and tissues, and potentially failure behaviors to characterize things like placental abruption, are viable and important areas to study.

Another powerful aspect of the created simulation is the fact that it can be easily modified to increase crash speed. A scale-up process of increasing crash speed will be a future focus within our group. This is accomplished in ABAQUS by changing the velocity values for the predefined speed, and the coefficient term in the velocity boundary condition, to the desired collision speed. This value is then multiplied by the normalized tabular Amplitude, and mimics the twenty kilometer per hour profile at higher or lower speeds.

Conclusions

Our research indicates that the finest mesh tested, and the tilting simulation configuration, are the most effective and appropriate modeling tools available to us at this time. The data from these simulations shows that published acceleration data can be effectively incorporated into simulations and create a realistic crash behavior. The simulations here are an extremely promising initiation of a maternal simulation tool set that can be sustainably improved with future research. The potential for applications to many aspects of maternal trauma, including injury science and safety engineering, is great. Likewise, the model is capable of accommodating more complex materials, and a more refined mesh can even be created through ScanIP if the computational limitations become less serious with technological progress. This is major step forward in terms of incorporating realistic anatomy and fetal measurements in pregnant trauma. Previous state-of-the-art only included placenta and maternal organs[180].

CHAPTER VI

CONCLUSIONS AND FUTURE STUDIES

The state of the art in modeling efforts in maternal trauma has severely lagged behind that of more general trauma modeling efforts. The work presented in this study provides an essential foundation for forward progress in simulating maternal trauma. The microstructural and biomechanical analysis of placenta will allow for advanced internal state variable driven constitutive relationships to be formulated, capturing complex and previously unavailable behaviors such as stress state and rate dependencies, and damage. The anatomical geometry is more accurate than previously available meshes and can be further refined through ScanIP as is needed in future research. The simulated loading conditions reported were highly successful at recreating the crash kinematics, and can be quickly adjusted to increase or decrease the velocity of the collision. All of these results are exciting and valuable contributions to trauma simulation, but their greatest value is the opportunities they open up in future cutting-edge studies. Potential areas of future research include the following areas.

Biomechanical analysis of the Poisson's ratio of placenta under different stress states to better understand the manner in which this tissue deforms, as Poisson's ratio effects were not considered in the reported studies. Because of the biphasic nature of placenta, a comparison of Poisson's effects under confined, as well as our unconfined, compression would also be very valuable.

Evaluation of structure property data in relation to the changing frame of reference could potentially improve the value of this data. It would be particularly valuable to perform this re-analysis of the structure properties following the Poisson's ratio studies, as Poisson's ratio is the most relevant parameter when considering a deformational volume change.

Dynamic biomechanical analysis of human placenta is an important addition to the reported data. Many traumatic events occur at strain rates beyond those considered in these, or any other previously published biomechanical investigation of placenta. In particular, availability of stress state dependent data for placenta at strain rates from 1.0 to approximately 100.0 would most likely describe the majority of systems relevant to maternal trauma.

Analysis of the interface between the placenta and the uterus to characterize the actual failure event that is placental abruption is arguably the most relevant piece of data concerning the most common pathology related to trauma in pregnancy. The ethical and logistical issues concerning humans make this sample essentially impossible to obtain, but animal surrogates could be used as an alternative. It is important to note that no animal surrogate is as similar as might be expected when considering other organs, such as the heart of liver, because of the interspecies variations in reproductive anatomy. Nonetheless, lower primates and rodents possess discoid placentation which is similar to humans. Development of a method for effectively assessing this interface in any animal would at least begin to scratch the surface on this issue.

Inclusion of the amniotic fluid in the mesh would finalize the last major piece of missing anatomy. Incorporation of fluid properties through a coupled computational fluid

dynamics approach, or use of an equation of state in a traditional simulation, would be possible and hydrodynamic effects could also be incorporated.

Improvement of mesh to include smoothed geometry, especially between layers to allow for more relevant friction simulations, through the use of an alternative meshing tool such as Cubit (Sandia National Laboratories) or HyperWorks (Altair Engineering, Huntsville AL) which can be used to improve geometries and optimize elements, minimizing or possibly eliminating tetrahedral elements.

Inclusion of improved material models such as basic hyperelastic models and eventually complex models like the ISV models previously described has always been a major consideration while moving forward with this research. The placenta data has been gathered for incorporation into these types of constitutive model, but development and validation of such a model is still required.

Inclusion of more realistic properties part interfaces would greatly improve the real world value of the results in the simulation. Most of the interfaces in the body are not well simulated as a tie, and appropriate frictional or failure boundary conditions would be a major step towards accurately simulating and predicting injury scenarios.

Conversion of seatbelt boundary conditions from velocity to analogous force would most likely alleviate the local tensile artifacts at the base of the seatbelt regions caused by the model tilting. Alternatively, a script could be formulated which maintained velocity conditions, but modified them across the region so that the values adjusted for tilt.

Increase in collision velocity to study the progressive increase in severity of collisions by modifying the coefficients in the predefined fields and velocity boundary

conditions. The previously created amplitudes will support such modifications, and are still the best available indications of acceleration profiles for these anatomical regions.

REFERENCES

1. Vladutiu, C.J. and H.B. Weiss, *Motor Vehicle Safety During Pregnancy.* American Journal of Lifestyle Medicine, 2012. **6**(3): p. 241-249.

2. Weiss, H., *Hidden Epidemic of Maternal, Fetal, and Neonatal Mortality and Injury from Crashes; A Case of Societal Neglect?* Transportation Research Record: Journal of the Transportation Research Board, 2006. **1956**(-1): p. 133-140.

3. Oxford, C.M.M. and J.B. Ludmir, *Trauma in Pregnancy.* Clinical Obstetrics & Gynecology, 2009. **52**(4): p. 611-629.

4. Chames, M.C.M. and M.D.M. Pearlman, *Trauma During Pregnancy: Outcomes and Clinical Management.* Clinical Obstetrics & Gynecology, 2008. **51**(2): p. 398-408.

5. Motozawa, Y., et al., *Effects of seat belts worn by pregnant drivers during low-impact collisions.* American Journal of Obstetrics and Gynecology. **In Press, Corrected Proof**.

6. Connolly, A.M., et al., *Trauma and Pregnancy.* Amer J Perinatol, 1997. **14**(06): p. 331-336.

7. Hyde, L.K., et al., *Effect of motor vehicle crashes on adverse fetal outcomes.* Obstetrics & Gynecology, 2003. **102**(2): p. 279-286.

8. Klinich, K.D., et al., *Fetal outcome in motor-vehicle crashes: effects of crash characteristics and maternal restraint.* American Journal of Obstetrics and Gynecology, 2008. **198**(4): p. 450.e1-450.e9.

9. Aboutanos, M.B.M.D.M.P.H., et al., *Significance of Motor Vehicle Crashes and Pelvic Injury on Fetal Mortality: A Five-Year Institutional Review.* Journal of Trauma-Injury Infection & Critical Care, 2008. **65**(3): p. 616-620.

10. Brown, H.L., *Trauma in Pregnancy.* Obstetrics & Gynecology, 2009. **114**(1): p. 147-160 10.1097/AOG.0b013e3181ab6014.

11. Hitosugi, M., et al., *Traffic injuries of the pregnant women and fetal or neonatal outcomes.* Forensic Science International, 2006. **159**(1): p. 51-54.

12. Huzel, P.S. and E.A. Remsburg-Bell, *Fetal Complications Related to Minor Maternal Trauma.* Journal of Obstetric, Gynecologic, & Neonatal Nursing, 1996. **25**(2): p. 121-124.

13. Bogat, G.A., et al., *Trauma symptoms among infants exposed to intimate partner violence.* Child Abuse & Neglect, 2006. **30**(2): p. 109-125.

14. Reis, P.M., C.M. Sander, and M.D. Pearlman, *Abruptio placentae after auto accidents. A case-control study.* J Reprod Med, 2000. **45**(1): p. 6-10.

15. El KADY, D., *Perinatal Outcomes of Traumatic Injuries During Pregnancy.* Clinical Obstetrics and Gynecology, 2007. **50**(3): p. 582-591 10.1097/GRF.0b013e31811eab82.

16. Mirza, F.G., P.C. Devine, and S. Gaddipati, *Trauma in Pregnancy: A Systematic Approach.* Amer J Perinatol, 2010. **27**(EFirst): p. 579-586.

17. Bunai, Y., et al., *Fetal Death From Abruptio Placentae Associated With Incorrect Use of a Seatbelt.* The American Journal of Forensic Medicine and Pathology, 2000. **21**(3): p. 207-209.

18. Sela, H.Y. and S. Einav, *Injury in motor vehicle accidents during pregnancy: a pregnant issue.* Expert Review of Obstetrics & Gynecology, 2010. **6**(1): p. 69-84.

19. Mattox, K.L. and L. Goetzl, *Trauma in pregnancy.* Critical Care Medicine, 2005. **33**(10): p. S385-S389 10.1097/01.CCM.0000182808.99433.55.

20. Weiss, H.B., *The epidemiology of traumatic injury-related fetal mortality in Pennsylvania, 1995-1997: the role of motor vehicle crashes.* Accid Anal Prev, 2001. **33**(4): p. 449-54.

21. Metz, T.D. and J.T. Abbott, *Uterine trauma in pregnancy after motor vehicle crashes with airbag deployment: A 30-case series.* J Trauma, 2006. **61**(3): p. 658-61.

22. Weir, L.F., B.T. Pierce, and J.O. Vazquez, *Complete fetal transection after a motor vehicle collision.* Obstet Gynecol, 2008. **111**(2 Pt 2): p. 530-2.

23. Fusco, A., K. Kelly, and J. Winslow, *Uterine Rupture in a Motor Vehicle Crash with Airbag Deployment.* The Journal of Trauma and Acute Care Surgery, 2001. **51**(6): p. 1192-1194.

24. Ali, J., et al., *Predictors of Fetal Mortality in Pregnant Trauma Patients.* The Journal of Trauma and Acute Care Surgery, 1997. **42**(5): p. 782-785.

25. Wolthuis, A.M., et al., *Trauma während der Schwangerschaft.* Z Geburtshilfe Neonatol, 2005. **209**(03): p. 113-117.

26. Schiff, M.A., et al., *The Effect of Air Bags on Pregnancy Outcomes in Washington State: 2002-2005.* Obstetrics & Gynecology, 2010. **115**(1): p. 85-92 10.1097/AOG.0b013e3181c4e94f.

27. Connolly, A.M., et al., *Trauma and pregnancy.* Am J Perinatol, 1997. **14**(6): p. 331-6.

28. CHAMES, M.C. and M.D. PEARLMAN, *Trauma During Pregnancy: Outcomes and Clinical Management.* Clinical Obstetrics and Gynecology, 2008. **51**(2): p. 398-408 10.1097/GRF.0b013e31816f2aa7.

29. Ford, R.M. and R.H. Picker, *Fetal head injury following motor vehicle accident; an unusual case of intrauterine death.* Aust N Z J Obstet Gynaecol, 1989. **29**(1): p. 72-3.

30. Schiff, M.A., V.L. Holt, and J.R. Daling, *Maternal and Infant Outcomes after Injury during Pregnancy in Washington State from 1989 to 1997.* The Journal of Trauma and Acute Care Surgery, 2002. **53**(5): p. 939-945.

31. Hartl, R. and K. Ko, *In Utero Skull Fracture: Case Report.* The Journal of Trauma and Acute Care Surgery, 1996. **41**(3): p. 549-552.

32. Crosby, W.M. and J.P. Costiloe, *Safety of Lap-Belt Restraint for Pregnant Victims of Automobile Collisions.* New England Journal of Medicine, 1971. **284**(12): p. 632-636.

33. Motozawa, Y., et al., *Analysis of the kinematics of pregnant drivers during low-speed frontal vehicle collisions.* International Journal of Crashworthiness, 2010. **15**(3): p. 235-239.

34. Serpil Acar, B. and V. Esat, *Seat belt designs to protect pregnant vehicle occupants.* Recent Pat. Mech. Eng. Recent Patents on Mechanical Engineering, 2010. **3**(1): p. 1-10.

35. Serpil Acar, B. and D. van Lopik, *Computational pregnant occupant model, 'Expecting', for crash simulations.* Proceedings of the Institution of Mechanical Engineers, Part D: Journal of Automobile Engineering, 2009. **223**(7): p. 891-902.

36. Thackray, L.A. and D.M. Blackketter, *Three-point seatbelt maternal comfort and fetal safety.* Proceedings of the Institution of Mechanical Engineers, Part D: Journal of Automobile Engineering, 2002. **216**(3): p. 173-180.

37. Viano, D.C., *Restraint Effectiveness, Availability and Use in Fatal Crashes: Implications to Injury Control.* The Journal of Trauma and Acute Care Surgery, 1995. **38**(4): p. 538-546.

38. Weekes, A.M. and B.S. Acar, *Testing to Investigate the Use of Lap Belt Positioners During Pregnancy.* 2010: p. 321-328.

39. Hendey, G.W. and S.R. Votey, *Injuries in restrained motor vehicle accident victims.* Ann Emerg Med, 1994. **24**(1): p. 77-84.

40. Rupp, J.D., et al., *Development and Testing of a Prototype Pregnant Abdomen for the Small-Female Hybrid III ATD.* Stapp Car Crash J, 2001. **45**: p. 61-78.

41. Hall, D.R., *Abruptio Placentae and Disseminated Intravascular Coagulopathy.* Seminars in Perinatology, 2009. **33**(3): p. 189-195.

42. Weiss, H.B., T.J. Songer, and A. Fabio, *Fetal Deaths Related to Maternal Injury.* JAMA: The Journal of the American Medical Association, 2001. **286**(15): p. 1863-1868.

43. Ananth, C.V., et al., *Placental abruption in the United States, 1979 through 2001: Temporal trends and potential determinants.* American Journal of Obstetrics and Gynecology, 2005. **192**(1): p. 191-198.

44. Ananth, C.V., D.A. Savitz, and M.A. Williams, *Placental abruption and its association with hypertension and prolonged rupture of membranes: a methodologic review and meta-analysis.* Obstetrics and gynecology, 1996. **88**(2): p. 309-18.

45. Meroz, Y., U. Elchalal, and Y. Ginosar, *Initial Trauma Management in Advanced Pregnancy.* Anesthesiology Clinics, 2007. **25**(1): p. 117-129.

46. Daria, C.R. *Trauma Care and Managing the Injured Pregnant Patient*. Journal of Obstetric, Gynecologic, & Neonatal Nursing, 2009. 704-714 DOI: 10.1111/j.1552-6909.2009.01072.x.

47. Weir, L.F., B.T. Pierce, and J.O. Vazquez, *Complete Fetal Transection After a Motor Vehicle Collision.* Obstetrics & Gynecology, 2008. **111**(2, Part 2): p. 530-532 10.1097/01.AOG.0000290332.11576.45.

48. Baethmann, M., et al., *Fetal CNS damage after exposure to maternal trauma during pregnancy.* Acta Pædiatrica, 1996. **85**(11): p. 1331-1338.

49. Moorcroft, D.M., et al., *Computational model of the pregnant occupant: predicting the risk of injury in automobile crashes.* American Journal of Obstetrics and Gynecology, 2003. **189**(2): p. 540-544.

50. Moorcroft, D., et al., *The effects of uterine ligaments on fetal injury risk in frontal automobile crashes.* Proceedings of the Institution of Mechanical Engineers, Part D: Journal of Automobile Engineering, 2003. **217**(12): p. 1049-1055.

51. Delotte, J., et al., *Pregnant woman and road safety: experimental crash test with post mortem human subject.* Surgical and Radiologic Anatomy, 2008. **30**(3): p. 185-189.

52. Duma, S.M., *Pregnant Occupants Biomechanics: Advances in Automobile Safety Research*2010, Warrendale PA: Society of Automotive Engineers.

53. Hu, J., et al., *Quantifying dynamic mechanical properties of human placenta tissue using optimization techniques with specimen-specific finite-element models.* Journal of Biomechanics, 2009. **42**(15): p. 2528-2534.

54. Hu, J., et al., *A Stochastic Visco-hyperelastic Model of Human Placenta Tissue for Finite Element Crash Simulations.* Annals of Biomedical Engineering, 2011. **39**(3): p. 1074-1083.

55. Pearlman, M.D. and D. Viano, *Automobile crash simulation with the first pregnant crash test dummy.* American Journal of Obstetrics and Gynecology, 1996. **175**(4, Part 1): p. 977-981.

56. Manoogian, S.J., et al., *Dynamic tensile properties of human placenta.* Journal of Biomechanics, 2008. **41**(16): p. 3436-3440.

57. Strigini, F.A.L., et al., *Fetal intracranial hemorrhage: is minor maternal trauma a possible pathogenetic factor?* Ultrasound in Obstetrics and Gynecology, 2001. **18**(4): p. 335-342.

58. Karimi, P., et al., *Extensive Brain Injury in a Premature Infant Following a Relatively Minor Maternal Motor Vehicle Accident with Airbag Deployment.* J Perinatol, 0000. **24**(7): p. 454-457.

59. Piastra, M., et al., *Severe subdural hemorrhage due to minimal prenatal trauma.* Journal of Neurosurgery: Pediatrics, 2009. **4**(6): p. 543-546.

60. Damiens, R., et al., *Compressive behavior of a turtle's shell: Experiment, modeling, and simulation.* Journal of the Mechanical Behavior of Biomedical Materials, 2012. **6**(0): p. 106-112.

61. Weaver, A.A., et al., *Biomechanical modeling of eye trauma for different orbit anthropometries.* Journal of Biomechanics, 2011. **44**(7): p. 1296-1303.

62. Prabhu, R., et al., *Coupled experiment/finite element analysis on the mechanical response of porcine brain under high strain rates.* Journal of the Mechanical Behavior of Biomedical Materials, 2011. **4**(7): p. 1067-1080.

63. Lee JB, Y.K., *Development of a finite element model of the human abdomen.* Stapp Car Crash J., 2001. **45**: p. 79-100.

64. Nyein, M.K., et al., *In silico investigation of intracranial blast mitigation with relevance to military traumatic brain injury.* Proceedings of the National Academy of Sciences, 2010. **107**(48): p. 20703-20708.

65. Colgan, N.C., M.D. Gilchrist, and K.M. Curran, *Applying DTI white matter orientations to finite element head models to examine diffuse TBI under high rotational accelerations.* Progress in Biophysics and Molecular Biology, 2010. **103**(2-3): p. 304-309.

66. Begonia, M., et al., *The Influence of Strain Rate Dependency on the Structure–Property Relations of Porcine Brain.* Annals of Biomedical Engineering, 2010. **38**(10): p. 3043-3057.

67. Rupp JD, K.K., Moss S, Zhou J, Pearlman MD, Schneider LW., *Development and Testing of a Prototype Pregnant Abdomen for the Small-Female Hybrid III ATD.* Stapp Car Crash J., 2001. **45**: p. 18.

68. Yu M, M.S., Duma SM, Stitzel JD., *Finite element modeling of human placental tissue.* Ann Adv Automot Med., 2009. **53**: p. 257-70.

69. Horstemeyer, M.F., et al., *Modeling stress state dependent damage evolution in a cast Al-Si-Mg aluminum alloy.* Theoretical and Applied Fracture Mechanics. **33**(1): p. 31-47.

70. Dighe, M., A. Gokhale, and M. Horstemeyer, *Effect of loading condition and stress state on damage evolution of silicon particles in an Al-Si-Mg-Base cast alloy.* Metallurgical and Materials Transactions A, 2002. **33**(3): p. 555-565.

71. Clemmer, J., et al., *A mechanistic study for strain rate sensitivity of rabbit patellar tendon.* Journal of Biomechanics, 2010. **43**(14): p. 2785-2791.

72. Horstemeyer, M.F., S. Ramaswamy, and M. Negrete, *Using a micromechanical finite element parametric study to motivate a phenomenological macroscale model for void/crack nucleation in aluminum with a hard second phase.* Mechanics of Materials, 2003. **35**(7): p. 675-687.

73. Bernard, J.D., et al., *Structure–property relations of cyclic damage in a wrought magnesium alloy.* Scripta Materialia, 2010. **63**(7): p. 751-756.

74. Fan, J., et al., *Cyclic plasticity at pores and inclusions in cast Al–Si alloys.* Engineering Fracture Mechanics, 2003. **70**(10): p. 1281-1302.

75. Fang, H., et al., *A comparative study of metamodeling methods for multiobjective crashworthiness optimization.* Computers & Structures, 2005. **83**(25–26): p. 2121-2136.

76. Arnason, U., et al., *Mammalian mitogenomic relationships and the root of the eutherian tree.* Proceedings of the National Academy of Sciences, 2002. **99**(12): p. 8151-8156.

77. Abbassi-Ghanavati, M., et al., *Pregnancy Outcomes in Women With Thyroid Peroxidase Antibodies.* Obstetrics & Gynecology. **116**(2, Part 1): p. 381-386 10.1097/AOG.0b013e3181e904e5.

78. Manoogian, S.J., et al., *Effect of Strain Rate on the Tensile Material Properties of Human Placenta.* Journal of Biomechanical Engineering, 2009. **131**(9): p. 091008-6.

79. Yamada, H., *Strength of Biological Materials*1970: Williams and Wilkinson.

80. Gao, Z. and J.P. Desai, *Estimating zero-strain states of very soft tissue under gravity loading using digital image correlation.* Medical Image Analysis, 2010. **14**(2): p. 126-137.

81. Williams, L.N., et al., *The anisotropic compressive mechanical properties of the rabbit patellar tendon.* Biorheology, 2008. **45**(5): p. 577-586.

82. Rhee, H., et al., *A study on the structure and mechanical behavior of the Terrapene carolina carapace: A pathway to design bio-inspired synthetic composites.* Materials Science and Engineering: C, 2009. **29**(8): p. 2333-2339.

83. Wren, T.A. and D.R. Carter, *A microstructural model for the tensile constitutive and failure behavior of soft skeletal connective tissues.* J Biomech Eng, 1998. **120**(1): p. 55-61.

84. Carew, E.O., et al., *Effect of specimen size and aspect ratio on the tensile properties of porcine aortic valve tissues.* Ann Biomed Eng, 2003. **31**(5): p. 526-35.

85. Fung, Y.C., *Biomechanics: Mechanical Properties of Living Tissues*1981, New York: Springer-Verlag.

86. LaPlaca, M.C., et al., *CNS injury biomechanics and experimental models*, in *Progress in Brain Research*, T.W. John and I.R.M. Andrew, Editors. 2007, Elsevier. p. 13-26.

87. Horgan, T. and M. Gilchrist, *The creation of three-dimensional finite element models for simulating head impact biomechanics.* International Journal of Crashworthiness, 2003. **8**(4): p. 353-366.

88. Ziejewski, M., et al. *Dynamic response of head under vehicle crash loading*. in *21st International Technical Conference, On the Enhanced Safety of Vehicles, Stuttgart, Germany, Paper*. 2009.

89. Bandak, F.A., *On the mechanics of impact neurotrauma: a review and critical synthesis.* J Neurotrauma, 1995. **12**(4): p. 635-49.

90. King, A.I., *Fundamentals of impact biomechanics: Part 2--Biomechanics of the abdomen, pelvis, and lower extremities.* Annu Rev Biomed Eng, 2001. **3**(1): p. 27-55.

91. Aitokallio-Tallberg, A. and E. Halmesmaki, *Motor vehicle accident during the second or third trimester of pregnancy.* Acta Obstet Gynecol Scand, 1997. **76**(4): p. 313-7.

92. Shah, K.H., et al., *Trauma in pregnancy: maternal and fetal outcomes.* J Trauma, 1998. **45**(1): p. 83-6.

93. Pearlman, M.D., J.E. Tintinalli, and R.P. Lorenz, *Blunt trauma during pregnancy.* N Engl J Med, 1990. **323**(23): p. 1609-13.

94. Weiss, H.B., T.J. Songer, and A. Fabio, *Fetal deaths related to maternal injury.* JAMA, 2001. **286**(15): p. 1863-8.

95. Agran, P.F., et al., *Fetal death in motor vehicle accidents.* Ann Emerg Med, 1987. **16**(12): p. 1355-8.

96. Fries, M.H. and G.D. Hankins, *Motor vehicle accident associated with minimal maternal trauma but subsequent fetal demise.* Ann Emerg Med, 1989. **18**(3): p. 301-4.

97. Shah, K.H., et al., *Trauma in Pregnancy: Maternal and Fetal Outcomes.* The Journal of Trauma and Acute Care Surgery, 1998. **45**(1): p. 83-86.

98. Schiff, M.A. and V.L. Holt, *Pregnancy outcomes following hospitalization for motor vehicle crashes in Washington State from 1989 to 2001.* Am J Epidemiol, 2005. **161**(6): p. 503-10.

99. Corsi, P.R., et al., *Trauma in pregnant women: analysis of maternal and fetal mortality.* Injury, 1999. **30**(4): p. 239-43.

100. Williams, J.K., et al., *Evaluation of blunt abdominal trauma in the third trimester of pregnancy: maternal and fetal considerations.* Obstet Gynecol, 1990. **75**(1): p. 33-7.

101. Ali, J., et al., *Predictors of fetal mortality in pregnant trauma patients.* J Trauma, 1997. **42**(5): p. 782-5.

102. Pearlman, M.D., J.E. Tintinallli, and R.P. Lorenz, *A prospective controlled study of outcome after trauma during pregnancy.* Am J Obstet Gynecol, 1990. **162**(6): p. 1502-7; discussion 1507-10.

103. Van Hook, J.W., *Trauma in Pregnancy*, in *Critical Care Obstetrics*2010, Wiley-Blackwell. p. 487-507.

104. Farmer, D.L., et al., *Fetal trauma: relation to maternal injury.* J Pediatr Surg, 1990. **25**(7): p. 711-4.

105. El-Kady, D., et al., *Trauma during pregnancy: an analysis of maternal and fetal outcomes in a large population.* Am J Obstet Gynecol, 2004. **190**(6): p. 1661-8.

106. Sacks, M.S. and W. Sun, *Multiaxial mechanical behavior of biological materials.* Annu Rev Biomed Eng, 2003. **5**(1): p. 251-84.

107. Holzapfel, G.A. and R.W. Ogden, *On planar biaxial tests for anisotropic nonlinearly elastic solids. A continuum mechanical framework.* Mathematics and mechanics of solids, 2009. **14**(5): p. 474-489.

108. Sun, W., M.S. Sacks, and M.J. Scott, *Effects of boundary conditions on the estimation of the planar biaxial mechanical properties of soft tissues.* J Biomech Eng, 2005. **127**(4): p. 709-15.

109. Freed, A.D., D.R. Einstein, and M.S. Sacks, *Hypoelastic Soft Tissues: Part II: In-Plane Biaxial Experiments.* Acta Mechanica, 2010. **213**(1-2): p. 205-222.

110. Freed, A.D., *Hypoelastic soft tissues. Part I: Theory.* Acta Mechanica, 2010. **213**(1-2): p. 189-204.

111. Jones, G.W. and S.J. Chapman, *Modeling Growth in Biological Materials.* SIAM Review, 2012. **54**(1): p. 52-118.

112. Liao, J., et al., *The Intrinsic Fatigue Mechanism of the Porcine Aortic Valve Extracellular Matrix.* Cardiovascular Engineering and Technology, 2012. **3**(1): p. 62-72.

113. Joyce, E.M., J. Liao, and M.S. Sacks, *Structural and biaxial mechanical properties of decellularized aortic valve leaflets.* Journal of Biomechanics, 2006. **39**: p. S618.

114. Liao, J., E.M. Joyce, and M.S. Sacks, *Effects of decellularization on the mechanical and structural properties of the porcine aortic valve leaflet.* Biomaterials, 2008. **29**(8): p. 1065-74.

115. Tedder, M.E., et al., *Stabilized collagen scaffolds for heart valve tissue engineering.* Tissue Eng Part A, 2009. **15**(6): p. 1257-68.

116. Guan, J., et al., *The stimulation of the cardiac differentiation of mesenchymal stem cells in tissue constructs that mimic myocardium structure and biomechanics.* Biomaterials, 2011. **32**(24): p. 5568-80.

117. Merryman, W.D., et al., *Defining biomechanical endpoints for tissue engineered heart valve leaflets from native leaflet properties.* Progress in Pediatric Cardiology, 2006. **21**(2): p. 153-160.

118. Wang, B., et al., *Fabrication of cardiac patch with decellularized porcine myocardial scaffold and bone marrow mononuclear cells.* J Biomed Mater Res A, 2010. **94**(4): p. 1100-10.

119. Williams, C., et al., *Altered structural and mechanical properties in decellularized rabbit carotid arteries.* Acta Biomater, 2009. **5**(4): p. 993-1005.

120. Liao, J., et al., *Molecular orientation of collagen in intact planar connective tissues under biaxial stretch.* Acta Biomater, 2005. **1**(1): p. 45-54.

121. Liao, J., et al., *The relation between collagen fibril kinematics and mechanical properties in the mitral valve anterior leaflet.* Journal of biomechanical engineering, 2007. **129**(1): p. 78-87.

122. Stella, J.A., J. Liao, and M.S. Sacks, *Time-dependent biaxial mechanical behavior of the aortic heart valve leaflet.* J Biomech, 2007. **40**(14): p. 3169-77.

123. Grashow, J.S., et al., *Planar biaxial creep and stress relaxation of the mitral valve anterior leaflet.* Annals of Biomedical Engineering, 2006. **34**(10): p. 1509-18.

124. Vito, R.P., *The mechanical properties of soft tissues--I: a mechanical system for bi-axial testing.* J Biomech, 1980. **13**(11): p. 947-50.

125. Decraemer, W.F., et al., *A non-linear viscoelastic constitutive equation for soft biological tissues, based upon a structural model.* Journal of Biomechanics, 1980. **13**(7): p. 559-564.

126. Humphrey, J.D., *Review Paper: Continuum biomechanics of soft biological tissues.* Proceedings of the Royal Society A: Mathematical, Physical and Engineering Sciences, 2003. **459**(2029): p. 3-46.

127. Verdier, C., *Rheological Properties of Living Materials. From Cells to Tissues.* Journal of Theoretical Medicine, 2003. **5**(2): p. 67-91.

128. Haut, R.C. and R.W. Little, *A constitutive equation for collagen fibers.* J Biomech, 1972. **5**(5): p. 423-30.

129. Lanir, Y., *Constitutive equations for fibrous connective tissues.* J Biomech, 1983. **16**(1): p. 1-12.

130. Hall, C.L., *Modelling of some biological materials using continuum mechanics.* 2008.

131. Fung, Y.C., *Biomechanics : mechanical properties of living tissues / Y.C. Fung*1981, New York :: Springer-Verlag.

132. Pioletti, D.P. and L.R. Rakotomanana, *Non-linear viscoelastic laws for soft biological tissues.* EUROPEAN JOURNAL OF MECHANICS SERIES A SOLIDS, 2000. **19**(5): p. 749-760.

133. Dunn, M.G. and F.H. Silver, *Viscoelastic behavior of human connective tissues: relative contribution of viscous and elastic components.* Connect Tissue Res, 1983. **12**(1): p. 59-70.

134. Silver, F. and W. Landis, *Viscoelasticity, energy storage and transmission and dissipation by extracellular matrices in vertebrates.* Collagen: Structure and Mechanics, 2008: p. 133-154.

135. Oyen, M., *A Model for Nonlinear Viscoelastic Mechanical Responses of Collagenous Soft Tissues.* MRS Proceedings, 2011. **898**: p. null-null.

136. Bischoff, J.E., E.M. Arruda, and K. Grosh, *A rheological network model for the continuum anisotropic and viscoelastic behavior of soft tissue.* Biomechanics and Modeling in Mechanobiology, 2004. **3**(1): p. 56-65.

137. Virues-Delgadillo, J.O., et al., *Effect of deformation rate on the mechanical properties of arteries.* Journal of Biomedical Science and Engineering, 2010. **3**(2): p. 124-137.

138. Peña, J., M. Martínez, and E. Peña, *A formulation to model the nonlinear viscoelastic properties of the vascular tissue.* Acta Mechanica, 2011. **217**(1): p. 63-74.

139. Burstein, A.H. and V.H. Frankel, *The Viscoelastic Properties of Some Biological Materials.* Annals of the New York Academy of Sciences, 1968. **146**(1): p. 158-165.

140. Drozdov, A.D., *Viscoelastic structures: mechanics of growth and aging*1997: Academic press.

141. Dehoff, P.H., *On the nonlinear viscoelastic behavior of soft biological tissues.* J Biomech, 1978. **11**(1-2): p. 35-40.

142. Sanjeevi, R., *A viscoelastic model for the mechanical properties of biological materials.* J Biomech, 1982. **15**(2): p. 107-9.

143. Cowin, S.C., *Strain or deformation rate dependent finite growth in soft tissues.* J Biomech, 1996. **29**(5): p. 647-9.

144. Jager, I.L., *Viscoelastic behavior of organic materials: consequences of a logarithmic dependence of force on strain rate.* J Biomech, 2005. **38**(7): p. 1451-8.

145. Begonia, M.T., et al., *The influence of strain rate dependency on the structure-property relations of porcine brain.* Annals of Biomedical Engineering, 2010. **38**(10): p. 3043-57.

146. Weed, B.C., et al., *Stress state and strain rate dependence of the human placenta.* Annals of Biomedical Engineering, 2012. **40**(10): p. 2255-65.

147. Clemmer, J., et al., *A mechanistic study for strain rate sensitivity of rabbit patellar tendon.* J Biomech, 2010. **43**(14): p. 2785-91.

148. Williams, L.N., et al., *The anisotropic compressive mechanical properties of the rabbit patellar tendon.* Biorheology, 2008. **45**(5): p. 577-86.

149. Prabhu, R., et al., *Coupled experiment/finite element analysis on the mechanical response of porcine brain under high strain rates.* J Mech Behav Biomed Mater, 2011. **4**(7): p. 1067-80.

150. Menzel, A., *Modelling of anisotropic growth in biological tissues. A new approach and computational aspects.* Biomechanics and Modeling in Mechanobiology, 2005. **3**(3): p. 147-71.

151. Menzel, A., *Anisotropic remodelling of biological tissues.* Mechanics of Biological Tissue, 2006: p. 91-104.

152. Ehret, A.E. and M. Itskov, *Modeling of anisotropic softening phenomena: Application to soft biological tissues.* International Journal of Plasticity, 2009. **25**(5): p. 901-919.

153. Cox, M.A., et al., *Mechanical characterization of anisotropic planar biological soft tissues using large indentation: a computational feasibility study.* Journal of biomechanical engineering, 2006. **128**(3): p. 428-436.

154. Zou, Y. and Y. Zhang, *An experimental and theoretical study on the anisotropy of elastin network.* Annals of Biomedical Engineering, 2009. **37**(8): p. 1572-83.

155. Nicholls, S.P., et al., *Crimping in rat tail tendon collagen: morphology and transverse mechanical anisotropy.* International Journal of Biological Macromolecules, 1983. **5**(5): p. 283-288.

156. Gasser, T.C., R.W. Ogden, and G.A. Holzapfel, *Hyperelastic modelling of arterial layers with distributed collagen fibre orientations.* J R Soc Interface, 2006. **3**(6): p. 15-35.

157. Veis, A., *Collagen fibrillar structure in mineralized and nonmineralized tissues.* Current Opinion in Solid State and Materials Science, 1997. **2**(3): p. 370-378.

158. Chen, Q. and N.M. Pugno, *Modeling the elastic anisotropy of woven hierarchical tissues.* Composites Part B: Engineering, 2011. **42**(7): p. 2030-2037.

159. Comninou, M. and I.V. Yannas, *Dependence of stress-strain nonlinearity of connective tissues on the geometry of collagen fibres.* Journal of Biomechanics, 1976. **9**(7): p. 427-433.

160. Sacks, M.S. and W. Sun, *MULTIAXIAL MECHANICAL BEHAVIOR OF BIOLOGICAL MATERIALS.* Annual Review of Biomedical Engineering, 2003. **5**(1): p. 251-284.

161. Horstemeyer, M.F. and D.J. Bammann, *Historical review of internal state variable theory for inelasticity.* International Journal of Plasticity, 2010. **26**(9): p. 1310-1334.

162. Holzapfel, G.A., T.C. Gasser, and M. Stadler, *A structural model for the viscoelastic behavior of arterial walls: Continuum formulation and finite element analysis.* European Journal of Mechanics - A/Solids, 2002. **21**(3): p. 441-463.

163. Garikipati, K., et al., *Biological remodelling: Stationary energy, configurational change, internal variables and dissipation.* Journal of the Mechanics and Physics of Solids, 2006. **54**(7): p. 1493-1515.

164. Haslach, H., Jr., *Nonlinear viscoelastic, thermodynamically consistent, models for biological soft tissue.* Biomechanics and Modeling in Mechanobiology, 2005. **3**(3): p. 172-189.

165. Peña, E., J.A. Peña, and M. Doblaré, *On the Mullins effect and hysteresis of fibered biological materials: A comparison between continuous and discontinuous damage models.* International Journal of Solids and Structures, 2009. **46**(7–8): p. 1727-1735.

166. Peña, E., et al., *On finite-strain damage of viscoelastic-fibred materials. Application to soft biological tissues.* International Journal for Numerical Methods in Engineering, 2008. **74**(7): p. 1198-1218.

167. Jiusheng, W., L. Yuehuan, and X. Ningying, *Histological characteristics of musculus longissimus dorsi and their correlation with restriction fragment length polymorphism of the myogenin gene in JinghuaxPietrain F(2) crossbred pigs.* Meat Sci, 2009. **81**(1): p. 108-15.

168. Jansová, M. and L. Hynčík, *Biomechanical model of pregnant female for impact purposes.* Engineering Mechanics, 2008. **15**(4): p. 225-240.

169. Klinich, K.D., et al., *Effect of frozen storage on dynamic tensile properties of human placenta.* J Biomech Eng, 2012. **134**(3): p. 034501.

170. Pérès, J., et al., *Material properties of the placenta under dynamic loading conditions.* Computer Methods in Biomechanics and Biomedical Engineering, 2012: p. 1-7.

171. Tadepalli, S.C., A. Erdemir, and P.R. Cavanagh, *Comparison of hexahedral and tetrahedral elements in finite element analysis of the foot and footwear.* Journal of biomechanics, 2011. **44**(12): p. 2337-2343.

172. Ramos, A. and J.A. Simões, *Tetrahedral versus hexahedral finite elements in numerical modelling of the proximal femur.* Medical engineering & physics, 2006. **28**(9): p. 916-924.

173. Brown, R., *Trauma in pregnancy.* Trauma, 1999. **1**(3): p. 245-253.

174. Kauff, N.D. and N. Tejani, *Trauma in the obstetric patient: Evaluation and management.* Primary Care Update for OB/GYNS, 1998. **5**(1): p. 16-20.

175. Klinich, K.D., et al., *Characterization of ovine utero-placental interface tensile failure.* Placenta, 2012. **33**(10): p. 776-81.

176. Hitosugi, M., et al., *Experimental analysis of the relationship between simulated low-velocity rear-end collisions and fetal outcomes of pregnant rats.* Medicine, Science and the Law, 2009. **49**(3): p. 213-217.

177. Crosby, W.M., A.I. King, and L.C. Stout, *Fetal survival following impact: improvement with shoulder harness restraint.* Am J Obstet Gynecol, 1972. **112**(8): p. 1101-6.

178. Crosby, W.M., et al., *Impact injuries in pregnancy. I. Experimental studies.* Am J Obstet Gynecol, 1968. **101**(1): p. 100-10.

179. Manoogian, S.J., et al., *Dynamic biaxial tissue properties of pregnant porcine uterine tissue.* Stapp Car Crash J, 2008. **52**: p. 167-85.

180. Moorcroft, D.M., et al., *Computational model of the pregnant occupant: predicting the risk of injury in automobile crashes.* Am J Obstet Gynecol, 2003. **189**(2): p. 540-4.

181. Duma, S.M., et al., *Evaluating pregnant occupant restraints: the effect of local uterine compression on the risk of fetal injury.* Annu Proc Assoc Adv Automot Med, 2004. **48**: p. 103-14.

182. Agran, P.F., et al., *Fetal death in motor vehicle accidents.* Annals of Emergency Medicine, 1987. **16**(12): p. 1355-1358.

183. Klinich, K.D., et al., *Investigations of crashes involving pregnant occupants.* Annu Proc Assoc Adv Automot Med, 2000. **44**: p. 37-55.

184. Delotte, J., et al., *Does placenta position modify the risk of placental abruption in car crashes?* Computer Methods in Biomechanics and Biomedical Engineering, 2009. **12**(4): p. 399-405.

185. Jerome, D., et al., *Modeling the pregnant woman in driving position.* Surg Radiol Anat, 2006. **28**(4): p. 359-63.

186. Hu, J., et al., *Quantifying dynamic mechanical properties of human placenta tissue using optimization techniques with specimen-specific finite-element models.* J Biomech, 2009. **42**(15): p. 2528-34.

187. Yu, M., et al., *Finite element modeling of human placental tissue.* Ann Adv Automot Med, 2009. **53**: p. 257-70.

188. Acar, B.S. and D.v. Lopik, *Modelling the foetus for pregnant occupant safety.* Proceedings of the Institution of Mechanical Engineers, Part K: Journal of Multi-body Dynamics, 2012. **226**(3): p. 197-205.

189. Manoogian, S.J., S.M. Duma, and D.M. Moorcroft. *Pregnant occupant injury risk using computer simulations with NCAP vehicle crash test data*.